Vertical equilibrium models for coupled flow and transport problems

Master of Science Thesis in Applied and Computational Mathematics

Kenneth Pedersen

Department of Mathematics
University of Bergen

November 20, 2017

Acknowledgements

I would like to use the opportunity to thank my supervisor Kundan Kumar for all the help and guidance I have received. He has been great to discuss problems and solutions with, and has dedicated a big amount of time to me and my thesis. I feel lucky to have been his student, learning from his superior teaching techniques and sophisticated guidance in several subjects.

Another round of thanks goes to my family and friends, who have supported and helped me get through this enormous amount of work. Another big thanks goes out to Elise, Kristian, Marius, Martin and Zeth for doing excellent proofreading. I would also like to send some gratitude in the direction of my lunch group, for many good on- and off-topic discussions through the thesis work.

Finally, I would like to gratefully thank my loving girlfriend, who has had to stand up with a lot of frustration all the way until the end and has helped me to keep my head straight and get through the hard work. I love you.

Abstract

A better understanding of viscous fingering can help to increase the recovery of hydrocarbons. The need for modelling the impact of *viscous fingering* is great as it largely dictates the sweep quality of hydrocarbons in a porous medium [11]. In this study we will investigate the effects of viscous fingering in a porous medium by incorporating an unstable flow caused by a dynamic viscosity and gravity. Our approach will be to consider the permeability as a diagonal tensor with the permeabilities scaled as an exponent of the width of a thin-strip, where the flow is present. This thesis provides a rigorous approach towards the derivation of a 1D model and the quality of upscaling is further illustrated through an extensive study of numerical results.

Contents

Chapter 1

Motivation and outline

1.1 Introduction

Porous media research is one of the most researched areas during the past century. Considering the wide range of its uses, this can hardly come as a surprise. Porous media applications are ubiquitous in the nature ranging from the obvious fuel cells, petroleum related applications, subsurface energy storage and carbon storage (CCS) to biological applications such as tissues or bones [35, 40, 36, 24].

The petroleum related applications, such as extraction of hydrocarbons, is essentially a study of the flow and transport processes through a porous medium. A porous medium consists of a solid skeleton surrounded by a void space (such as soil). The void allows the flow to take place through this medium however the solid skeleton leads to obstruction in a freely flowing behavior. The model and behavior of the flow is intricate - and it calls for the use of a coupling of complex physics and chemistry, in order to analyze the flow process in a complex geometry due to the pore spaces interconnecting patterns.

In a study of flow and transport, there are also many other various aspects to consider. Hereunder the possible chemical dissolution of the matrix, chemical reactions between fluids, mobility differences and pressure changes. However, in this thesis, we will mainly be concerned with mobility and flow-rate differences. This can cause fluid with the highest mobility to create fingers through the column of hydrocarbons. This phenomenon is called *viscous fingering* and can occur when the interface between two fluids flows along with an uneven flow rate. This results in an uneven, or fingered, profile. This phenomenon is relatively common in reservoirs using water injection to maintain reservoir pressure. The result of this is an inefficient sweeping action which can cause significant volumes of recoverable hydrocarbons to be left behind. In severe cases it can also cause an early breakthrough of water, meaning that we end up with just water into the production wellbores.

This thesis addresses the effects of fingering happening in the flow in a porous medium. In order for the simulations to be as accurate as possible, then it is important that the model describes the physical challenges (with justified simplifications) in the best way possible.

1.2 Background

The coupling of flow and transport leads to several complexities. By flow, we mean the underlying fluid that moves whereas the transport means some of the chemical species that get transported by the underlying flow field. Possibly the simplest example is tracer transport, in which minuscule quantities of certain chemical species (e.g., dyes) are transported by the underlying flow field. This is used in several applications including underground water flow estimation, biological applications including diagnosis of diseases in our body (like in injecting a

radioactive tracer in a kidney, whereafter the kidneys efficiency and/or health can be measured by the rate of filtering) and many other applications. [26, 19, 6, 9, 7, 25, 8, 10, 15, 17]

In contrast to the passive tracer transport, the chemical species being transported may affect the flow behavior itself and examples abound. The density of the fluid may change due to the chemical species (e.g., polymers). The chemical reactions on the rock surface may reduce the space available for the flow to take place (leading to clogging). These chemical reactions are of precipitation-dissolution type. Of significance are also the coupling of the flow where a lighter fluid displaces a heavier fluid. For example, water displacing heavy oil. The instability takes place in both the cases: miscible as well as immiscible flow. In the case of later, the two fluids do not mix and behave as phases. In case of miscible flow, due to mixing, they are treated as a coupled flow and transport process. [30, 18]

This thesis deals with miscible flow process in a thin 2D domain. There are several situations in which such a geometry is encountered. In subsurface, the flow process takes place in an aquifer region that is quite thin compared to its length. A thin tube serves as a representative pore scale geometry. Thin porous media are found in several applications, including papers, filters, thin porous coatings, fuel cells, and textiles. The flow process taking place in such media experiences different flow and transport properties in the lateral and vertical directions. For example, paper formed by the fibrous materials have orientations and lead to difference in permeabilities in the lateral and vertical directions.

Performing simulations in a thin 2D channel is quite complex. The thickness being much smaller than the lateral directions, the discretization and the numerical computations for such a domain becomes challenging. Besides, we are often not interested in the full details of the solutions in the vertical direction. This is also motivated by [29, 16, 2, 34, 32]. In this case, it makes sense to identify an averaged 1D model that approximates the 2D equations with sufficiently high accuracy.

The averaging gets complicated by the complexity in the flow behavior. In the cases when concentration profile in the vertical direction does not vary much, the averaging is not difficult to understand. However, as the variation in the vertical direction increases, the average of the concentration contains lesser information regarding the profile. This becomes much worse in the case of instability known as viscous fingering [3, 39, 37, 31, 38, 24, 23, 12]. In the case of fingering, across the vertical direction, there would be oscillations in the concentration values. Thus, to capture the details, defining an appropriate 1D model becomes quite challenging. The variation in the vertical direction for the concentration is a result of competition between the diffusion and convective strengths (characterized by Peclet number). Thus, when the diffusion is of higher strength, the variation is lower. However, in the case of dominated transport, the variation may be higher. In case of coupling of the flow properties, such as viscosity dependent on the concentration, the onset of instability may make it much more complicated.

It is an important problem to identify the quantities that measure the quality of upscaling. If we would derive a 1D model from a 2D model, what would be the quantities that should be matched to give us the confidence that we have a sufficiently high accuracy. Naturally, the quantities should reflect the geometric structure of concentration profiles in the 2D geometry. Since the geometric features are part of the solution of coupled model, we need to characterize them in terms of our solution variables.

This thesis undertakes the study of upscaling of a thin 2D model to 1D model. We perform these studies when the flow and transport properties such as permeabilities and diffusion are anisotropic. Our approach is as follows: We consider permeabilities and diffusion tensor scaled with respect to the width of the strip. For example, we consider permeability to be of the form:

$$\boldsymbol{K} = \begin{bmatrix} \epsilon^{\alpha} & 0 \\ 0 & \epsilon^{\beta} \end{bmatrix}$$

The different scaling of α and β give anisotropic permeabilities. A positive α and β means that

the permeabilities are small. The higher these values are, the smaller the permeabilities are. By varying α and β we obtain the different anisotropic properties. We study for different scaling of α and β, the flow and the corresponding transport behavior. In the upscaling of transport equation, an important consideration is the relative strengths of convective and diffusive strengths. In the case of dominated transport, the vertical variation in the concentration is difficult to control. When there is a presence of gravity and viscosity depending on the concentration, then there is a possibility of instability. We study the averaging using formal asymptotic expansion in such cases.

An important part of our work has been to identify the quantities that measure the geometric features. Based on the work of Otto and Menon, we consider the quantities that measure the geometric features of the concentration profiles and use them as a measure of the quality of our upscaling. We also derive the dependence of these quantities based on the scale of diffusive and convective strengths. Extensive numerical computations illustrate the theoretical findings. Next, we discuss the contributions from this thesis.

1.3 Contributions

This thesis provides the comparison of a vertical-averaged 2D-model and a 1D-model under different scaling of flow and transport properties. An important goal of the thesis is to identify parameters that incorporate the geometric features and compare how the derived 1D model compares to the averaged 2D thin strip model.
We list our contributions as follows.

1. We provide a rigorous derivation of 1D averaged model for coupled flow and transport model starting from a 2D model in a thin strip. This derivation assumes the transport and diffusion balancing each other, however we consider different scaling of anisotropic permeability. In the derivation process, we also identify $R_L = \frac{L}{H}\left(\frac{K_v}{K_H}\right)^{1/2}$ as the parameter that governs the averaging behavior. This parameter has been used by Yortsos and collaborators [39, 37] in a formal derivation of such a model.

2. We provide a formal derivation of 1D averaged model for the coupled flow-transport model in the case when transport dominated the diffusion process. A rigorous derivation in this case is quite difficult (as undertaken by Mikelić, van Duijn, Choquet in a linear case [5, 4, 21, 22]. Since our problem is non-linear, this framework does not apply). Since we assume Darcy flow, the 1D model does not contain the Taylor dispersion terms in contrast with the Stokes flow in a thin 2D strip. The formal derivation has been performed in three cases: (a) isotropic permeability and fixed viscosity, (b) anisotropic permeability but fixed viscosity, and finally (c) viscosity depending on concentration.

3. Extensive numerical tests have been performed for the coupled model. We use dual mixed method for the flow and conformal for transport equation. We solve them iteratively at each time step. We study the number of iterations depending on the coupling strength of the model. This coupling strength is characterized by the dependence of the viscosity on the concentration making the model fully coupled. A stronger dependence on the concentration implies a higher strength of coupling and is reflected in the higher number of iterations between the two.

4. Numerical computations have been carried out for different scaling of the anisotropic permeability and for studying the convergence of averaged 2D model to 1D model. We study how the averaging behaves for different scaling of transport and diffusion dominated coupled model.

5. Motivated by the work of Otto and Menon [20], we identify quantities that incorporates the geometric features of the concentration profile. The transport of concentration is a result of balance between the diffusive processes and the convective behavior. This results in a variety of features including stable, diffused, or unstable fronts resulting in fingers. The quantities that characterize this are the length of the fronts (balance between the instability, convective and diffusive strengths), the mushy zone (characterized by entropy), and the energy. we derive the properties of these geometric quantities for a given flow model and identify the dependence of them on the diffusion term and the convective term. This derivation is new.

6. We perform numerical experiments to study the behavior of these geometric quantities with respect to the upscaling of 2D thin strip model to 1D model. We term these geometric quantities as indicators that should be used for checking if the upscaling is justified. Since the aim of our upscaling should be to capture the geometric features, we believe that these are better quantities to match when we perform the upscaling.

1.4 Outline

This thesis has the following structure.

Chapter 2 - Theory

This chapter will cover the properties of rocks, fluids and basic concepts of flow and transport in a porous medium. Hereunder we will describe the Darcy equation, which is the flow model used in this thesis. Provided is also a brief introduction to the concepts *Weak Solutions* and the *Finite Element Method/Ritz-Galerkin method*.

Chapter 3 - Theoretical Results

This chapter will present our theoretical results, using a rigorous derivation of a 1D model from a vertical-averaged 2D model. We will also present work done in the derivation of a model for a *Upscaled Reactive coupled flow-transport problem* under different regimes. In this chapter, we will also present the derivation of some limits for indicators for *viscous fingering* purposed in an article published by G. Menon and F. Otto [20]. Lastly these results will be incorporated into a formal derivation of a 1D model from a vertical-averaged 2D model.

Chapter 4 - Numerical Results

This chapter will present our numerical results from a coupled flow-transport equation. The first part will present our implementation by a reference solution. We have implemented a 2D-model, which is then averaged in the vertical direction. This vertical-averaged model is then compared to a full 1D-model to see how the 1D-model captures the different flow properties. After we will study the L_2- and L_∞-norms of the difference between the models mentioned before. Lastly the different geometrical indicators as purposed by G. Menon and F. Otto [20], applied to our numerical models, will be studied for different regimes.

Chapter 5 - Conclusion and future works

We conclude by summarizing the findings of this thesis and discuss further extensions of this work.

Chapter 2

Preliminaries

This chapter gives a brief introduction to the theory behind rock- and fluid-properties and the transport/diffusion in an porous media. Starting from the definitions and basic physics, we obtain a set of equations, which we will study in the coming chapters using numerical models.

2.1 Permeability

The permeability of a porous medium is measured by it's capability to transmit fluids through its network of pore-throats and pores. Usually this is not a homogeneous and/or isotropic property, and it will therefore depend on the direction of flow, other fluids present within the medium and the properties of the fluid(s). This results in a tensor describing the *flow potential* in all flow-directions and can only be considered constant when there is only one fluid present and there is no chemical reaction between the fluid and medium. This is called the *absolute permeability*.

The permeability will change drastically if there is more than one component or phase is present. The change is caused by the interactions between the different components and/or phases. The permeability, or *flow potential*, of two fluids within a porous media is usually not the same. The fluid with the lowest flow potential might get trapped within the pores, or even block parts of the path for the other present fluid. This leads to a new concept within permeability, which is the *relative permeability*. *Relative permeability* is the ratio between the *effective permeability* for one fluid, in the presence of another immiscible fluid, and the absolute permeability for the entire medium.

In this thesis we will study effects caused by two fluids present, with a few simplifications. One of which is that the absolute permeability is used as the effective permeability.

If the permeability is given as a scalar value instead of an tensor, then the spatial direction does not play a role and the porous medium is therefore isotropic. Due to the Onsagers principle [27], a result from thermodynamics, the permeability matrix has to be a symmetric and positive definite. The permeability is measured Darcy $[D]$, which has the dimensions of length squared (m^2), by SI-unit standards. Permeability will throughout this thesis be referred to as $\boldsymbol{K}$.

2.2 Porosity

Porosity is a measure of the void space and is a ratio between the pore-space (void space) and the bulk volume of the porous medium (the whole domain). The porosity is therefore a fraction and takes a value between 0 and 1. The formula for calculating the porosity is

$$\phi = \frac{V_v}{V_t}, \tag{2.1}$$

where ϕ is the porosity, V_v is the total void-space volume and V_t is the total volume of the porous medium. The porosity is one of the most important properties to industries working with porous media since it shows the maximum potential for storing fluids like oil, water or CO_2.

2.3 Representative Elementary Volume (REV) in Porous Media

As mentioned in earlier sections, a porous medium is not a homogeneous medium. Properties like permeability, porosity and composition of minerals varies a lot throughout the domain. This makes it difficult to measure these quantities for the entire domain. These above-mentioned parameters are usually found using a core-sample from one or multiple locations within the reservoir.

When extracting these samples, it is important that the sample(s) can represent the properties for the whole domain. If the sample size is small, then the results may be affected by microscopic effects. This can be due to a void space which is larger than average or a compact packing which makes the porosity and permeability non-representative outside that specific sample.

On the other hand, if the sample size is to large, it can be affected by macroscopic effects, such as fractures, or a layer of another medium (for instance a different rock type). Therefore the sample size must be big enough to neglect microscopic effects, but still small enough to avoid macroscopic effects. A sample size that steers clear of both of these effects are referred to as an Representative Elementary Volume (REV).

2.4 Viscosity

Viscosity is a fluids inner resistance, working against the flow. Viscosity is given in a unit called Poise [P]. The usual size of this property makes it useful to use centipoise [cP]. In standard SI-units, this resolves to the following dimensions $1\,\mathrm{cP} = 1\,m\mathrm{Pa}\,s$ (Millipascal-second). Different types of fluids have different viscosity, and as a result; different flow potentials.

2.5 Darcy's law

Henry Darcy described in 1856 a relationship for the flow of a given fluid through a porous medium. Through a series of experiments he purposed that the relationship, for flow of fluids through a porous medium, depends on the properties of the medium. His findings can in modern notation be summarized in what is known as Darcys law:

$$\underline{\mathbf{u}} = -\boldsymbol{\kappa}\,\nabla p \tag{2.2}$$

Here $\underline{\mathbf{u}}$ denotes the flux vector in the unit: volume per area per time, $\left[\frac{L^3}{L^2\,T}\right]$, which in SI-units resolves to $\left[\frac{m}{s}\right]$. Flux, in this setting, is a measure of volumetric flow through an cross-section.

The $\boldsymbol{\kappa}$ denotes the conductivity of the fluid in the porous media. The conductivity is the measure of how easily the fluid flows, or the resistance of flow, through the porous media. It is a combination of the all the properties within the porous media which influences the flow (such as porosity, the shapes of the pores, other fluids present and their level of connectedness) and the fluid properties (e.g. viscosity, density, etc).

In order to achieve a system of equations which is handleable and useful, the model will simplified from this definition. The conductivity will only include the permeability tensor and the viscosity, while the other parameters will be neglected. Therefore the definition of the flow

model becomes

$$\underline{\mathbf{u}} = -\frac{\boldsymbol{K}}{\mu} \nabla p \tag{2.3}$$

2.6 Dual-mixed weak-formulation

In the model used in the simulations, it will be used a dual-mixed formulation of the Darcy's equation with the Poisson equation to describe the flow.

Formulation 2.1. Find $u(x, y)$ and $p(x, y)$ solving the following system:

$$\begin{cases} \underline{\mathbf{u}} = -\frac{\boldsymbol{K}}{\mu} \nabla p, & \text{in } \Omega \\ \nabla \cdot \underline{\mathbf{u}} = f & \text{in } \Omega \\ f = g(x, y) & \text{in } \Omega \\ u = 0 & \text{on } \Gamma = \delta\Omega \end{cases} \tag{2.4}$$

Here $\Omega \in \mathbb{R}^2$ is the domain we will be solving the problem over and $g(x, y)$ is a source/sink term describing the flux going in/out of the domain.

We start with equation (2.3) and transform it into weak form. This is done by moving all parts over to the left side and multiplying with an test-function w and integrating over the whole domain Ω.

$$\int_\Omega \underline{\mathbf{u}} \cdot \underline{\mathbf{w}} \, dx + \int_\Omega \left(\frac{\boldsymbol{K}}{\mu} \nabla p \right) \cdot \underline{\mathbf{w}} \, dx = 0 \tag{2.5}$$

From the second part of system (2.4) we have:

$$\nabla \cdot \underline{\mathbf{u}} = f$$

Where f is a source/sink and we set this equal to 0. We then move all parts over to the left side and multiply with a test function v and integrate over Ω.

$$\int_\Omega \nabla \cdot \underline{\mathbf{u}} v \, dx = 0 \tag{2.6}$$

Integrating by part and applying boundary conditions from the system (2.4) gives us:

$$\int_\Omega \nabla \cdot \underline{\mathbf{u}} v \, dx = -\int_\Omega \underline{\mathbf{u}} \cdot \nabla v \, dx = 0 \tag{2.7}$$

Combining equation (2.5) and (2.6), with the result (2.7) we obtain

$$\int_\Omega \underline{\mathbf{u}} \cdot \underline{\mathbf{w}} \, dx + \int_\Omega \left(\frac{\boldsymbol{K}}{\mu} \nabla p \right) \cdot \underline{\mathbf{w}} \, dx - \int_\Omega \underline{\mathbf{u}} \cdot \nabla v \, dx = 0 \tag{2.8}$$

In many textbooks (such as [1]) it is proven that the functions u, p, v and w lies in Sobolev space $H_0^1(\Omega)$.

$$a_1(u, w) \equiv \int_\Omega \underline{\mathbf{u}} \cdot \underline{\mathbf{w}} \, dx \tag{2.9}$$

$$a_2(p, w) \equiv \int_\Omega \left(\frac{\boldsymbol{K}}{\mu} \nabla p \right) \cdot \underline{\mathbf{w}} \, dx \tag{2.10}$$

$$a_3(p, v) \equiv -\int_\Omega \underline{\mathbf{u}} \cdot \nabla v \, dx = 0 \tag{2.11}$$

It is easy to see that the integral on the right of equation (2.9) is a bilinear form in u and w. Equation (2.10) is bilinear in p and w while eq. (2.11) is bilinear in p and v.

2.7 Finite element method

In order to solve the system in equation (2.4), the discretization is performed using the finite element method and hereby the Ritz-Galerkin method. We then solve the mentioned system on a finite dimensional space ($V_h(\Omega)$), which is a subspace of the original solution space ($H_0^1(\Omega)$). Using the finite element method, we introduce a grid on Ω and what we will refer to as *the finite element basis functions*. An more precise mathematical definition of the finite element method is given in the book *Numerical solution of partial differential equations by the finite element method*[13]:

Definition 2.1. Let

- $K \subset \Omega$ be a geometrical domain with piecewise smooth boundary,
- P_K be a finite-dimensional linear space of functions on K,
- Σ be a set of degrees of freedom chosen for any $v \in P_K$ to be uniquely defined by it;

Given the above, the triple (K, P_K, Σ) is called a finite element. The basis associated with Σ is chosen to be a piecewise-polynomial function with support on the cells adjusted to a single grid point. In this thesis we will stick to triangular grids (so K is a triangle). Since our chosen geometry is a rectangle, then we will stick to constant triangle sizes across the domain. For other problems with a higher level of complexity, other grid-types can also be used.

This finite element basis, which we have used in our computations, is a linear basis and is constructed as such

$$\phi_i = \begin{cases} 1, & \text{if } x = x_i, \\ 0, & \text{if } x = x_j, j \neq i, \\ \text{linearly interpolated}, & \text{elsewhere} \end{cases} \tag{2.12}$$

This linear basis has two advantages; it provides enough smoothness for the solution to catch small differences in the equations and it is also a simple function. In cases with highly oscillating coefficients in the problem, higher smoothness is usually not necessary, therefore piecewise linear functions will therefore be of good use.
Having defined the basis, we can now represent any function in the finite space, V_h.

$$u = \sum_i z_i \phi_i, \tag{2.13}$$

We can illustrate this by using Poisson's equation as a starting point:

$$-\nabla \cdot \big(a(x)\nabla u(x)\big) = f(x), \quad \forall x \in \Omega \tag{2.14}$$

With zero Dirichlet boundary conditions,

$$u(x) = 0, \quad x \in \partial\Omega$$

Transforming this into a weak form,

$$\int_\Omega \Big(-\nabla \cdot \big(a(x)\nabla u(x)\big)\Big)\, v\, dx = \int_\Omega f v\, dx$$

and by using partial integration,

$$\int_\Omega a\nabla u \cdot \nabla v\, dx = \int_\Omega f v\, dx$$

Defining these parts as

$$a(u,v) = \int_\Omega a\nabla u \cdot \nabla v,$$
$$F(v) = \int_\Omega fv dx,$$

The definition for eq. (2.13) is now inserted into the equation $a(u,v) = F(v)$ and define the basis function as the test-function,

$$a\left(\sum_i z_i\phi_i, \phi_j\right) = \sum_i a(\phi_i,\phi_j)z_i = F(\phi_j) \tag{2.15}$$

If a system is constructed for all values of j from the set consisting of basis functions, we end up with a linear system of equations with respect to the vector z. This is the weight of the basis functions,

$$Az = b, \tag{2.16}$$

where $A = (a)_{i,j} = \sum_i a(\phi_i,\phi_j)$ and $b_j = F(\phi_j)$.

Solving this will give us the vector z which is needed to construct the solution.

2.8 The Thesis' Model

In this thesis we will use a coupled flow- and transport model. This means that the flow and transport will be coupled together and has to be computed together to obtain a solution. The domains which the problem will be defined on is these
The full domain, Ω, which is representing the bounds of the thin strip

$$\Omega_\epsilon := \big\{(x,y) \in \mathbb{R} | 0 < x < 1, -\epsilon < y < \epsilon\big\}$$

The boundaries of Ω_ϵ are defined by the lateral boundaries Γ_ϵ given by

$$\Gamma_\epsilon := \big\{(x,y) \in \mathbb{R} | 0 < x < 1, y \in \{-\epsilon, \epsilon\}\big\}$$

the inlet boundary Γ_i,

$$\Gamma_i := \big\{(x,y) \in \mathbb{R} | x = 0, -\epsilon < y < \epsilon\big\}$$

and the outflow boundary Γ_o

$$\Gamma_o := \big\{(x,y) \in \mathbb{R} | x = 1, -\epsilon < y < \epsilon\big\}$$

The Darcy equation (2.3) will be coupled together with

$$\partial_t c - \nabla \cdot (D\nabla c + \underline{\mathbf{u}} c) = f, \in \Omega$$

In this thesis, the following system will make up all the equation used:

$$\underline{\mathbf{u}} = -\frac{\boldsymbol{K}}{\mu} \nabla p + \frac{1}{10} c(x,y,t) \underline{\mathbf{g}} \text{ in } \Omega \tag{2.17}$$

$$\nabla \cdot \underline{\mathbf{u}} = 0, \text{ in } \Omega \tag{2.18}$$

$$p = p_{b_i}, \text{ on } \Gamma_i \tag{2.19}$$

$$p = p_{b_o}, \text{ on } \Gamma_o \tag{2.20}$$

$$\partial_t c = \nabla \cdot (D\nabla c + \underline{\mathbf{u}} c) + f, \text{ in } \Omega \tag{2.21}$$

$$c = 1, \text{ on } \Gamma_i \tag{2.22}$$

$$c = 0, \text{ on } \Gamma_o \tag{2.23}$$

$$\tag{2.24}$$

With the following parameters:

$$\mu(c) = f(y,c) \tag{2.25}$$

$$\boldsymbol{K} = \begin{bmatrix} \epsilon^\alpha & 0 \\ 0 & \epsilon^\beta \end{bmatrix} \tag{2.26}$$

$$\underline{\mathbf{g}} = \begin{bmatrix} 10 \\ 0 \end{bmatrix}, \tag{2.27}$$

This will be incorporated in different regimes and for different values of ϵ, α and β and different functions $\mu(c) = f$. In some of the regimes, there will also be included a gravity term in the flow equation. We will now summarize the usage of this model throughout the thesis, with each of the uses described.

2.8.1 Without gravity

If there is no gravity present, equation (2.17) reduces to

$$\underline{\mathbf{u}} = -\frac{\boldsymbol{K}}{\mu}\nabla p, \text{ in } \Omega \tag{2.28}$$

2.8.1.1 Isotropic permeability and fixed viscosity

This thesis provides a study of numerous cases where there is an isotropic permeability and the viscosity is fixed. In section (3.1.1) there is a rigorous derivation for isotropic permeability and a fixed viscosity of 1. The approach is to have a flow model given and assuming that the diffusion and convection are both of order 1 and therefore balancing each-other. This rigorous derivation is new and has not been studied before.

In section (3.2.1) a formal derivation of effective 1D-model derived from a vertical-averaged 2D-model is provided. As mentioned in the remark in the end, this case does not give raise to a Taylor Dispersion type term. As presented in the section, this is due to the use of Darcy equation as flow-model as opposed to the Stoke-model used in [14]. This formal derivation of an effective system of equation for this case is not been done for this setting before.

In the numerical results we have have studied different aspects of this case. Section (4.3.1.1) present a plot of the difference between the indicator $P(t)$ for the vertical-averaged 2D model and 1D-model while section (4.3.1.2) shows the indicator $H(t)$ for the same comparison as previous, and also here the difference is negligible. Lastly, section (4.3.1.4) show the difference when the diffusion in the 1D-model is slightly increased. The magnitude of the increase is studied based on the permeability tensor.

2.8.1.2 Anisotropic permeability and fixed viscosity

This thesis also provides a study of numerous cases where there is an anisotropic permeability and the viscosity is again fixed. In section (3.1.2) and (3.1.2) there is a rigorous derivation for anisotropic permeability. Again the viscosity is fixed 1 and the same approach as for the isotropic permeability is used. However, having an anisotropic permeability have some challenges and therefore this sets some additional assumtions. These are explicitly mentioned in the sections.

In section (3.2.2) a similar formal derivation, as in the previous section for isotropic permeability, of effective 1D-model derived from a vertical-averaged 2D-model is provided. However, this section uses a anisotropic permeability instead. This case does not give raise to a Taylor Dispersion type term either.

In the numerical results we have have studied different aspects of this case. Section (4.3.1.1) does also present a plot of the difference for the indicator $P(t)$, now for anisotropic permeability, and (4.3.1.2) for indicator $H(t)$. Section (4.3.1.4) show the difference when the diffusion in the 1D-model is slightly to compensate for the difference in the indicators. The magniture of the increase is studied based on the permeability tensor.

2.8.1.3 Isotropic permeability and viscosity depending on concentration

Of the parts excluding gravity, this thesis will briefly study the case when there is a dependence of concentration within the viscosity. In our derivation chapter, the section (3.2.3) is dedicated to the case when we have a non-constant viscosity. As for the fixed viscosity cases, our approach is to start with the flow model. The Darcy equation is asymptotically expanded to derive the relationship for flow. This is then inserted into the convection-diffusion equation and again asymptotically expanded. This does neither give rise to a Taylor Dispersion type term, which is in compliance with the other cases.

2.8.2 With gravity

2.8.2.1 Isotropic permeability and viscosity depending on concentration

This thesis has numerical results of the model with gravity considering an isotropic permeability and a viscosity depending on the concentration. In section (4.4.2) the case considered has a small difference in concentration in the y-direction and therefore there is some turbulence present.

2.8.2.2 Anisotropic permeability and viscosity depending on concentration

This thesis also includes numerical studies of the model with gravity considering an anisotropic permeability and again a viscosity depending on the concentration. In section (4.4.1) a low flux is considered and we consider a high flux in section (4.4.3). The difference between these cases is large because with a low flux, there is not much difference in concentration in the y-direction and therefore there is not much turbulence present. However in the high flux case, there is mush more turbulence and therefore the indicators in this section is also more interesting.

Chapter 3

Upscaling Of A Thin Strip 2D-Model

In this chapter, different aspects of the upscaling of a thin strip 2D-model will be covered. The first section (3.1) is *Rigorous derivation of 1D-model*. This will start by stating the regime and equations. The approach here is to have a flow model given and assuming that the diffusion and convection are both of order 1 and therefore balancing each-other. We provide a proof of convergence for three cases $\alpha = 0$, $\alpha > 0$ and $-1 < \alpha < 0$. This rigorous derivation is new and has not been studied before.

The second section (3.2) is *Upscaled reactive flow-transport problem*. This section will cover the formal derivation of an upscaled coupled flow-transport model. This will cover the derivation from a full system to a system which will be asymptotically expanded. First the Darcy equation is asymptotically expanded to derive the relationship for flow. This is then inserted into the convection-diffusion equation and again asymptotically expanded. This is again done for three cases: (a) isotropic permeability and fixed viscosity, (b) anisotropic permeability and fixed viscosity and (c) isotropic permeability and viscosity depending on concentration. For each of this cases we end up with a system of effective equation in 1D. As mentioned in the remark in the end, none of this cases gives raise to a Taylor Dispersion type term. This is due to the Darcy equation as flow-model as opposed to the Stoke-model used in [14]. This formal derivation of an effective system of equation for this case is not been done for this setting before.

The third section (3.3) is *Flow problem*. This section will consider an anisotropic permeability and fixed viscosity equal to 1. This section will start with the Darcy equation and derives a weak formulation of this which is then vertically averaged. This result is then used to give an requirement for boundedness, which then is used to prove the existence and boundedness of the solution of an coupled flow and transport problem.

The forth and last section (3.4) in this chapter is *Indicators*. This derivation is motivated by the work of Otto and Menon in [20] and use the identified quantities which incorporates the geometric features of the concentration profile. These indicators is then used to formally derive and identify the dependence of them on the diffusion- and the convective-term. All of these indicators are studied within this section with our model and thereafter derived using the relationship of the indicators themself, to the diffusion of our model. This derivation is new.

3.1 Rigorous derivation of 1D model

In this section we will perform a rigorous derivation of a 1D model from a 2D model. A formal derivation has previously been published by Z. Yang and Y. C. Yortsos in Asymptotic Regimes in Miscible Displacements in Random Poreous Media [37].

We consider a miscible flow in a 2D heterogeneous porous medium (a rectangular geometry). The fluids we are considering are incompressible and the mixing do not cause any change in

volume. All parameters are non-dimensional. The rectangular domain is defined as

$$\Omega = (0,1) \times (-\epsilon, \epsilon)$$

Given a diffusion coefficient, $D \sim \mathcal{O}(1)$, the following equation can be derived:

$$\partial_t c^\epsilon - \nabla \cdot (D \nabla c^\epsilon + q^\epsilon c^\epsilon) = f, \in \Omega \tag{3.1}$$

Assuming a parabolic flow profile of the following form,

$$q^\epsilon = \frac{3}{2} Q \left(1 - \frac{y^2}{\epsilon^2}\right) \tag{3.2}$$

Thereafter integrating q^ϵ in y from $-\epsilon$ to ϵ.

$$\int_{-\epsilon}^{\epsilon} q^\epsilon dy = \int_{-\epsilon}^{\epsilon} \frac{3}{2} Q \left(1 - \frac{y^2}{\epsilon^2}\right) dy \tag{3.3}$$

$$= \frac{3}{2} Q \int_{-\epsilon}^{\epsilon} \left(1 - \frac{y^2}{\epsilon^2}\right) dy \tag{3.4}$$

$$= \frac{3}{2} Q \left[y - \frac{y^3}{3\epsilon^2} \right]_{-\epsilon}^{\epsilon} \tag{3.5}$$

$$= 2\epsilon Q \tag{3.6}$$

Which results in the following relation

$$\frac{1}{2\epsilon} \int_{-\epsilon}^{\epsilon} q^\epsilon \, dy = Q \tag{3.7}$$

The average of a function, $f = f(x)$, is defined as the following

$$\bar{f} = \frac{1}{b-a} \int_a^b f(\psi) \, d\psi \tag{3.8}$$

Using that definition from eq. (3.8) on the concentration where $c = c(x, y)$, taking the average in the y-direction

$$\bar{c}^\epsilon(x) = \frac{1}{2\epsilon} \int_{-\epsilon}^{\epsilon} c^\epsilon(x, y) dy \tag{3.9}$$

$$\begin{aligned} \int_0^1 \int_{-\epsilon}^{\epsilon} \partial_t c^\epsilon \varphi \, dy \, dx + \int_0^1 \int_{-\epsilon}^{\epsilon} D \partial_x c^\epsilon \partial_x \varphi \, dy dx + \int_0^1 \int_{-\epsilon}^{\epsilon} D \partial_y c^\epsilon \partial_y \varphi \, dy dx \\ + \int_0^1 \int_{-\epsilon}^{\epsilon} q_1^\epsilon c^\epsilon \partial_x \varphi \, dy dx + \int_0^1 \int_{-\epsilon}^{\epsilon} q_1^\epsilon c^\epsilon \partial_y \varphi \, dy dx = 0 \end{aligned} \tag{3.10}$$

Choose φ to be $\varphi(x)$. Then the equation can be simplified to the following

$$\int_0^1 \int_{-\epsilon}^{\epsilon} \partial_t c^\epsilon \varphi \, dy \, dx + \int_0^1 \int_{-\epsilon}^{\epsilon} D \partial_x c^\epsilon \partial_x \varphi \, dy dx + \int_0^1 \int_{-\epsilon}^{\epsilon} q_1^\epsilon c^\epsilon \partial_x \varphi \, dy \, dx = 0 \tag{3.11}$$

Dividing by 2ϵ

$$\frac{1}{2\epsilon} \int_0^1 \partial_t \left[\int_{-\epsilon}^{\epsilon} c^\epsilon dy \right] \varphi \, dx + \frac{1}{2\epsilon} \int_0^1 D \partial_x \left[\int_{-\epsilon}^{\epsilon} c^\epsilon dy \right] \partial_x \varphi \, dx + \frac{1}{2\epsilon} \int_0^1 \int_{-\epsilon}^{\epsilon} q_1^\epsilon c^\epsilon \partial_x \varphi \, dy \, dx = 0 \tag{3.12}$$

Using eq. (3.9) will lead to

$$\int_0^1 \partial_t \bar{c}^\epsilon \varphi \, dx + \int_0^1 D\partial_x \bar{c}^\epsilon \partial_x \varphi \, dx + \int_0^1 \left[\frac{1}{2\epsilon} \int_{-\epsilon}^{\epsilon} q_1^\epsilon c^\epsilon dy \right] \partial_x \varphi \, dx = 0 \tag{3.13}$$

Whereafter it is needed to show that

$$\frac{1}{2\epsilon} \int_{-\epsilon}^{\epsilon} q_1^\epsilon c^\epsilon dy \to Q\bar{c}^\epsilon \tag{3.14}$$

In order for that to be valid; the following must hold

$$\begin{aligned} &\int_0^1 \frac{1}{2\epsilon} \int_{-\epsilon}^{\epsilon} \left(q_1^\epsilon - Q\right) \left(c^\epsilon - \bar{c}^\epsilon\right) \partial_x \varphi \, dy \, dx \\ &\leq \int_0^1 \left(\frac{1}{2\epsilon} \left(\int_{-\epsilon}^{\epsilon} \left(q_1^\epsilon - Q\right) \left(c^\epsilon - \bar{c}^\epsilon\right) \, dy \right)^2 \right)^{\frac{1}{2}} \left(\int_{-\epsilon}^{\epsilon} \left(\partial_x \varphi\right)^2 dy \right)^{\frac{1}{2}} \, dx \end{aligned} \tag{3.15}$$

In eq. (3.15) we use the Cauchy-Schwarz inequality. In the relation, q_1^ϵ is not given. So we have from Darcy's equation

$$q_1^\epsilon = -\epsilon^\alpha \partial_x p^\epsilon \sim \mathcal{O}\left(\frac{1}{\epsilon}\right) \tag{3.16}$$

3.1.1 For $\alpha = 0$

$$\begin{aligned} \|q_1^\epsilon - Q\|_{L^\infty} &\leq C, \\ \Rightarrow \|c^\epsilon - \bar{c}\| &\leq \epsilon C \end{aligned} \tag{3.17}$$

The inequality (3.17) holds as long as

$$\|\partial_x p^\epsilon\|_{L_\infty} \leq C \tag{3.18}$$

Which means that if $\alpha = 0$, then the norm of $c^\epsilon - \bar{c}$ is less then ϵC. From this it can be concluded that as $\epsilon \to 0$, the norm goes to 0. And thus we have a proof of convergence.

3.1.2 For $0 < \alpha$

When $\alpha > 0$, $q^\epsilon \to 0$ as $\epsilon \to 0$. The following weak form can be concluded from eq. (3.1)

$$(\epsilon^\alpha \partial_x p^\epsilon, \partial_x \varphi) + \left(\epsilon^\beta \partial_y p^\epsilon, \partial_y \varphi\right) = (f, \varphi) \tag{3.19}$$

A test-function is then chosen φ to be $\varphi(x)$

$$(\epsilon^\alpha \partial_x p^\epsilon, \partial_x \varphi) = (f, \varphi) \tag{3.20}$$

Again choosing $\varphi(x) = \bar{p}^\epsilon$, leads to

$$\begin{aligned} \int_0^1 \epsilon^\alpha \left(\partial_x \bar{p}^\epsilon\right)^2 dx &= \int_0^1 f \bar{p}^\epsilon dx \\ \left\| \epsilon^{\frac{\alpha}{2}} \partial_x \bar{p}^\epsilon \right\|^2_{L_{\infty(\Omega)}} &\leq \|f\|^2_{L_{\infty(\Omega)}} \end{aligned}$$

This is bounded as long as $\|f\|^2_{L_{\infty(\Omega)}}$ is balanced by term $\epsilon^{\frac{\alpha}{2}}$, and by this we have proof of convergence.

3.1.3 For $-1 < \alpha < 0$

For starters it is assumed that the following inequality holds

$$\|\partial_x p^\epsilon\| \leq C \tag{3.21}$$

In the case that this assumption does not hold, there is an infinite pressure difference in the x-direction and hence an infinite flux. Therefore this assumption should be well justified.
By definition, that leaves the following

$$\left\|q^{(1)\epsilon}\right\|_{L_2} = \|\epsilon^\alpha \partial_x p^\epsilon\|_{L_2} \leq C\epsilon^\alpha \tag{3.22}$$

We want to estimate the difference

$$\int_0^\epsilon q^{(1)\epsilon} c^\epsilon \, dy - \int_0^\epsilon \bar{q}^{(1)\epsilon} \bar{c}^\epsilon \, dy \tag{3.23}$$

By definition of the vertical average, this is given

$$\int_0^\epsilon \left(\bar{q}^{(1)\epsilon} - q^{(1)\epsilon}\right) \bar{c}^\epsilon \, dy = 0 \tag{3.24}$$

Thus by adding eq. (3.23) and eq. (3.24) then this can be concluded

$$\int_0^\epsilon q^{(1)\epsilon} c^\epsilon \, dy - \int_0^\epsilon \bar{q}^{(1)\epsilon} \bar{c}^\epsilon \, dy - \int_0^\epsilon \left(\bar{q}^{(1)\epsilon} + q^{(1)\epsilon}\right) \bar{c}^\epsilon \, dy \tag{3.25}$$

$$\int_0^\epsilon q^{(1)\epsilon} \left(c^\epsilon - \bar{c}^\epsilon\right) \, dy \tag{3.26}$$

From eq. (3.22) it is known that $q^{(1)\epsilon}$ is bounded, which leaves this to be proved

$$\|c^\epsilon - \bar{c}^\epsilon\| \leq C\epsilon \tag{3.27}$$

Assuming that the following holds for all time

$$\|\nabla c^\epsilon\|_{L_2(0,T,L^2)} \leq C \tag{3.28}$$

Inserting this into the following equation

$$(\partial_t c^\epsilon, \varphi) + (D\nabla c^\epsilon, \nabla\varphi) + (q^\epsilon c^\epsilon, \nabla\varphi) = (f, \varphi)$$

and choosing the test-function, φ to be c^ϵ which leads to

$$\int_\Omega \frac{1}{2} \nabla \cdot \left(q^\epsilon \left(c^\epsilon\right)^2\right) = \int_\Omega \left(\left(\nabla \cdot q^\epsilon\right) c^\epsilon + q^\epsilon c^\epsilon \nabla c^\epsilon\right) \tag{3.29}$$

Applying the divergence theorem

$$\int_{\partial\Omega} \underline{\mathbf{n}} \cdot \left(q^\epsilon \left(c^\epsilon\right)^2\right) = 0 \tag{3.30}$$

Having the boundary value $q^\epsilon|_{\partial\Omega} = 0$, so Grönwall's inequality can be used. Since the gradient is bounded by eq. (3.28), then this lead to the following

$$\|c^\epsilon\| \leq C\|\nabla c^\epsilon\| \leq \tilde{C} \tag{3.31}$$

Which means that this holds

$$\|c^\epsilon - \bar{c}^\epsilon\| \leq C\left\|\partial_y c^\epsilon\right\| \tag{3.32}$$

Again, by using the result from eq. (3.32) in eq. (3.26), this results in a bound and thus proof of convergence.

3.2 Upscaled reactive coupled flow-transport problem

This section will give a derivation of an upscaled reactive coupled flow-transport equation where the pore-scale geometry is not influenced by the chemical reactions taking place. Formal homogenization techniques are used to obtain the upscaled equation. In the later part of this section, the impact of having a non-constant viscosity is studied which is dependent on the local concentration.

3.2.1 Case 1: $\alpha = 0, \beta = 0$ and constant viscosity

We will first consider the case when $\alpha = 0, \beta = 0$ and a constant viscosity. The two dimensional bounded domain representing the strip is given by:

$$\Omega_\epsilon := \left\{(x, y) \in \mathbb{R} | 0 < x < 1, -\epsilon < y < \epsilon\right\}$$

The boundaries of Ω_ϵ are defined by the lateral boundary Γ_ϵ given by

$$\Gamma_\epsilon := \left\{(x, y) \in \mathbb{R} | 0 < x < 1, y \in \{-\epsilon, \epsilon\}\right\}$$

the inlet boundary Γ_i,

$$\Gamma_i := \left\{(x, y) \in \mathbb{R} | x = 0, -\epsilon < y < \epsilon\right\}$$

and the outflow boundary Γ_o

$$\Gamma_o := \left\{(x, y) \in \mathbb{R} | x = 1, -\epsilon < y < \epsilon\right\}$$

For modelling the reactive coupled flow-transport, the following dimensionless system of equations are considered, describing the flow of the solutes in a fixed geometry

$$c_t^\epsilon = \nabla \cdot \left(\epsilon D \nabla c^\epsilon - q^\epsilon c^\epsilon\right), \text{ in } \Omega_\epsilon, \tag{3.33}$$

$$q^\epsilon = -\left(\frac{K^\epsilon}{\mu\left(c^\epsilon\right)}\right) \nabla p^\epsilon, \text{ in } \Omega_\epsilon, \tag{3.34}$$

$$\nabla \cdot q^\epsilon = 0, \text{ in } \Omega_\epsilon, \tag{3.35}$$

$$v_t^\epsilon = \epsilon f(c^\epsilon, v^\epsilon), \text{ on } \Gamma_\epsilon, \tag{3.36}$$

$$-\nu^\epsilon \cdot \epsilon D \nabla c^\epsilon = v_t^\epsilon, \text{ on } \Gamma_\epsilon, \tag{3.37}$$

$$q^\epsilon = 0, \text{ on } \Gamma_\epsilon, \tag{3.38}$$

$$c^\epsilon = c_{b_i}, \text{ on } \Gamma_i, \tag{3.39}$$

$$p^\epsilon = p_{b_i}, \text{ on } \Gamma_i, \tag{3.40}$$

$$\nu \cdot \nabla c^\epsilon = 0, \text{ on } \Gamma_o, \tag{3.41}$$

$$p^\epsilon = p_{b_o}, \text{ on } \Gamma_o, \tag{3.42}$$

$$c^\epsilon(x, y, 0) = c_0(x, y), \tag{3.43}$$

$$v^\epsilon(x, 0) = v_0(x), \tag{3.44}$$

$$K^\epsilon = \begin{bmatrix} \epsilon^\alpha & 0 \\ 0 & \epsilon^\beta \end{bmatrix} \tag{3.45}$$

Since the pore geometry is fixed; another variable, v, is needed to take the thickness of the deposition into account for the reactant/product on the lateral boundaries. Then a coordinate-transformation is performed:

$$x := x \quad \eta := \frac{y}{\epsilon}$$

The domain then changes to

$$\Omega_\epsilon := \left\{(x,\eta) \in \mathbb{R} | 0 < x < 1, -1 < \eta < 1\right\} \tag{3.46}$$

From this, we obtain a system of equations needed for the further calculations:

$$c_t^\epsilon + \nabla \cdot (q^\epsilon c^\epsilon) = \epsilon D \left(\partial_{xx} c^\epsilon + \epsilon^{-2} \partial_{\eta\eta} c^\epsilon\right), \text{ in } \Omega_\epsilon \tag{3.47}$$

$$\left(q^{(1)\epsilon}, q^{(2)\epsilon}\right)^T = -\left(\epsilon^\alpha \left(\mu^{-1}(c^\epsilon)\right) \partial_x p^\epsilon, \ \epsilon^{\beta-1} \left(\mu^{-1}(c^\epsilon)\right) \partial_\eta p^\epsilon\right)^T, \text{ in } \Omega_\epsilon \tag{3.48}$$

$$\partial_x q^{(1)\epsilon} + \epsilon^{-1} \partial_\eta q^{(2)\epsilon} = 0, \text{ in } \Omega_\epsilon \tag{3.49}$$

$$v_t^\epsilon = f(c^\epsilon, v^\epsilon), \text{ on } \Gamma_\epsilon \tag{3.50}$$

$$-\nu^\epsilon \cdot \epsilon D \left(\partial_x c^\epsilon, \epsilon^{-1} \partial_\eta c^\epsilon\right) = \epsilon v_t^\epsilon, \text{ on } \Gamma_\epsilon \tag{3.51}$$

$$q^\epsilon = 0, \text{ on } \Gamma_\epsilon \tag{3.52}$$

Since the geometry is fixed, then the Darcy/Poisson equations (3.47 and 3.48) can be solved as one, with the no-slip boundary condition (3.52). Then an asymptotic expansion of eq. (3.49) is performed to leading order

$$-\partial_x \left(\epsilon^\alpha \left(\mu^{-1}\left(c^\epsilon\right)\right) \partial_x p^\epsilon\right) - \partial_\eta \left(\epsilon^{\beta-2} \left(\mu^{-1}\left(c^\epsilon\right)\right) \partial_\eta p^\epsilon\right) = 0$$

Assuming that these variables have asymptotic expansions as such:

$$c^\epsilon = c_0 + \epsilon c_1 + \epsilon^2 c_2 + \mathcal{O}(\epsilon^3), \tag{3.53}$$

$$p^\epsilon = p_0 + \epsilon p_1 + \epsilon^2 p_2 + \mathcal{O}(\epsilon^3), \tag{3.54}$$

Inserting the expansion of p^ϵ into $\mu^{-1}\left(c^\epsilon\right)$ gives:

$$\mu^{-1}\left(c^\epsilon\right) = \mu^{-1}\left(c_0 + \epsilon c_1 + \epsilon^2 c_2\right)$$

Taylor expanding $\mu^{-1}\left(c^\epsilon\right)$ around c_0 results in

$$\begin{aligned}
&\mu^{-1}\left(c^\epsilon\right) = \mu^{-1}\left(c_0\right) + \epsilon \partial_1 \mu^{-1}\left(c_0\right) c_1 + \epsilon^2 \partial_{11} \mu^{-1}\left(c_0\right) c_2 + \mathcal{O}(\epsilon^3) \\
&-\partial_x \Big(\epsilon^\alpha \left(\mu^{-1}\left(c_0\right) + \epsilon \partial_1 \mu^{-1}\left(c_0\right) c_1 + \epsilon^2 \partial_{11} \mu^{-1}\left(c_0\right) c_2\right) \\
&\quad \partial_x \left(p_0 + \epsilon p_1 + \epsilon^2 p_2\right)\Big) - \\
&\partial_\eta \Big(\epsilon^{\beta-2} \left(\mu^{-1}\left(c_0\right) + \epsilon \partial_1 \mu^{-1}\left(c_0\right) c_1 + \epsilon^2 \partial_{11} \mu^{-1}\left(c_0\right) c_2\right) \\
&\quad \partial_\eta \left(p_0 + \epsilon p_1 + \epsilon^2 p_2\right)\Big) \\
&= 0
\end{aligned} \tag{3.55}$$

Fully expanding the equation yields

$$\begin{aligned}
&-\partial_x\Big(\epsilon^{\alpha}\Big(\mu^{-1}\left(c_0\right)\partial_x p_0+\epsilon\mu^{-1}\left(c_0\right)\partial_x p_1+\epsilon^2\mu^{-1}\left(c_0\right)\partial_x p_2+\\
&\qquad\epsilon\partial_1\mu^{-1}\left(c_0\right)c_1\partial_x p_0+\epsilon^2\partial_1\mu^{-1}\left(c_0\right)c_1\partial_x p_1+\epsilon^2\partial_{11}\mu^{-1}\left(c_0\right)c_2\partial_x p_0\Big)\Big)\\
&-\partial_\eta\Big(\epsilon^{\beta-2}\Big(\mu^{-1}\left(c_0\right)\partial_\eta p_0+\epsilon\mu^{-1}\left(c_0\right)\partial_\eta p_1+\epsilon^2\mu^{-1}\left(c_0\right)\partial_\eta p_2+\\
&\qquad\epsilon\partial_1\mu^{-1}\left(c_0\right)c_1\partial_\eta p_0+\epsilon^2\partial_1\mu^{-1}\left(c_0\right)c_1\partial_\eta p_1+\epsilon^2\partial_{11}\mu^{-1}\left(c_0\right)c_2\partial_\eta p_0+\\
&\qquad\epsilon^3\partial_1\mu^{-1}\left(c_0\right)c_1\partial_\eta p_2+\epsilon^3\partial_{11}\mu^{-1}\left(c_0\right)c_2\partial_\eta p_1\Big)\Big)\\
&\qquad=0
\end{aligned}\tag{3.56}$$

Collecting the terms based on the power of ϵ:

$$\begin{aligned}
&-\partial_x\Big(\epsilon^{\alpha}\left(\mu^{-1}\left(c_0\right)\partial_x p_0\right)+\\
&\qquad\epsilon^{\alpha+1}\left(\mu^{-1}\left(c_0\right)\partial_x p_1+\partial_1\mu^{-1}\left(c_0\right)c_1\partial_x p_0\right)+\\
&\qquad\epsilon^{\alpha+2}\left(\mu^{-1}\left(c_0\right)\partial_x p_2+\partial_1\mu^{-1}\left(c_0\right)c_1\partial_x p_1+\partial_{11}\mu^{-1}\left(c_0\right)c_2\partial_x p_0\right)\Big)\\
&-\partial_\eta\Big(\epsilon^{\beta-2}\left(\mu^{-1}\left(c_0\right)\partial_\eta p_0\right)+\\
&\qquad\epsilon^{\beta-1}\left(\mu^{-1}\left(c_0\right)\partial_\eta p_1+\partial_1\mu^{-1}\left(c_0\right)c_1\partial_\eta p_0\right)+\\
&\qquad\epsilon^{\beta}\left(\mu^{-1}\left(c_0\right)\partial_\eta p_2+\partial_1\mu^{-1}\left(c_0\right)c_1\partial_\eta p_1+\partial_{11}\mu^{-1}\left(c_0\right)c_2\partial_\eta p_0\right)+\\
&\qquad\epsilon^{\beta+1}\left(\partial_1\mu^{-1}\left(c_0\right)c_1\partial_\eta p_2+\partial_{11}\mu^{-1}\left(c_0\right)c_2\partial_\eta p_1\right)\Big)\\
&\qquad=0
\end{aligned}\tag{3.57}$$

For $\alpha=0,\beta=0$, the above is reduced to the following equation:

$$\begin{aligned}
&-\partial_x\Big(\left(\mu^{-1}\left(c_0\right)\partial_x p_0\right)+\\
&\qquad\epsilon\left(\mu^{-1}\left(c_0\right)\partial_x p_1+\partial_1\mu^{-1}\left(c_0\right)c_1\partial_x p_0\right)+\\
&\qquad\epsilon^2\left(\mu^{-1}\left(c_0\right)\partial_x p_2+\partial_1\mu^{-1}\left(c_0\right)c_1\partial_x p_1+\partial_{11}\mu^{-1}\left(c_0\right)c_2\partial_x p_0\right)\Big)\\
&-\partial_\eta\Big(\epsilon^{-2}\left(\mu^{-1}\left(c_0\right)\partial_\eta p_0\right)+\\
&\qquad\epsilon^{-1}\left(\mu^{-1}\left(c_0\right)\partial_\eta p_1+\partial_1\mu^{-1}\left(c_0\right)c_1\partial_\eta p_0\right)+\\
&\qquad\left(\mu^{-1}\left(c_0\right)\partial_\eta p_2+\partial_1\mu^{-1}\left(c_0\right)c_1\partial_\eta p_1+\partial_{11}\mu^{-1}\left(c_0\right)c_2\partial_\eta p_0\right)+\\
&\qquad\epsilon\left(\partial_1\mu^{-1}\left(c_0\right)c_1\partial_\eta p_2+\partial_{11}\mu^{-1}\left(c_0\right)c_2\partial_\eta p_1\right)\Big)\\
&\qquad=0
\end{aligned}\tag{3.58}$$

Collecting terms of order $\mathcal{O}(\epsilon^{-2})$

$$\begin{aligned} -\partial_\eta \left(\mu^{-1}\left(c_0\right)\partial_\eta p_0\right) &= 0, \\ M\partial_{\eta\eta} p_0 &= 0, \\ \partial_\eta p_0 &= A_0(x) \end{aligned} \tag{3.59}$$

Here $A_0(x)$ and $A_1(x)$ are generic constants possibly dependent of x. Firstly the case is considered, the viscosity, $M = \mu^{-1}\left(c_0\right)$, is constant. Meaning that the change of p_0 in the η-direction is constant. Or that

$$p_0(x,\eta) = A_0(x)\eta + A_1(x) \tag{3.60}$$

Using equation (3.38) we see that at when $\eta = \{-1, 1\}$, so $\partial_\eta p_0(x,\eta) = 0$. Thus

$$p_0(x) = A_1(x) \tag{3.61}$$

This means that p_0 is independent of η.

Collecting terms of order $\mathcal{O}(\epsilon^{-1})$

$$\begin{aligned} -\partial_\eta \left(\mu^{-1}\left(c_0\right)\partial_\eta p_1 + \partial_1\mu^{-1}\left(c_0\right)\partial_\eta p_0\right) &= 0, \\ -M\partial_{\eta\eta} p_1(x,\eta) &= 0, \\ \partial_\eta p_1(x,\eta) &= A_2(x), \\ p_1(x,\eta) &= A_2(x)\eta + A_3(x) \end{aligned} \tag{3.62}$$

Initially it is observed that $\partial_1\mu^{-1}\left(c_0\right) = 0$ because the viscosity is constant. Both A_2 and A_3 is generic constants depending only on x. Again using equation (3.38) it is reduced to

$$p_1(x) = A_2(x) \tag{3.63}$$

Again, in compliance with the previous order of ϵ, it is shown that p_1 is independent of η.

Collecting terms of order $\mathcal{O}(\epsilon^{0})$

$$\begin{aligned} -\partial_x \left(\mu^{-1}\left(c_0\right)\partial_x p_0\right) - \partial_\eta \left(\mu^{-1}\left(c_0\right)\partial_\eta p_2\right) &= 0, \\ -M\partial_{xx} p_0 - M\partial_{\eta\eta} p_2 &= 0, \\ \partial_{xx} p_0 + \partial_{\eta\eta} p_2 &= 0 \end{aligned}$$

Integrating over η, the following equation is obtained

$$\int_{-1}^{1} \partial_{xx} p_0 \, d\eta + \int_{-1}^{1} \partial_{\eta\eta} p_2 \, d\eta = 0 \tag{3.64}$$

$$2\partial_{xx} p_0 + \partial_\eta p_2|_{\eta=1} - \partial_\eta p_2|_{\eta=-1} = 0 \tag{3.65}$$

$$\Rightarrow \partial_{xx} p_0 = 0 \tag{3.66}$$

Which results in the following p_0:

$$p_0(x) = A_0 x + A_1 \tag{3.67}$$

At $x = 0, p^\epsilon = p_{b_i}$:

$$p_0(x=0) = A_1 = p_{b_i}$$

At $x = 1, p^\epsilon = p_{b_o}$:

$$\begin{aligned} p_0(x=1) &= A_0 + p_{b_i} = p_{b_0} \\ &\Rightarrow A_0 = p_{b_0} - p_{b_i} \\ p_0(x) &= \left(p_{b_0} - p_{b_i}\right) x + p_{b_i} \end{aligned}$$

Ending up with the following form, for p^ϵ

$$p^\epsilon = \left(p_{b_0} - p_{b_i}\right) x + p_{b_i} \tag{3.68}$$

Inserting this result into eq. (3.48) the following can be obtained:

$$\begin{aligned} q^{(1)\epsilon} &= -\mu^{-1}(c^\epsilon)\partial_x p^\epsilon && (3.69)\\ &= -\left(\mu^{-1}(c_0) + \epsilon\partial_1\mu^{-1}(c_0)c_1 + \epsilon^2\partial_{11}\mu^{-1}(c_0)c_2\right)\partial_x\left(\left(p_{b_0} - p_{b_i}\right)x + p_{b_i}\right) \\ &= -M\left(p_{b_0} - p_{b_i}\right) && (3.70) \end{aligned}$$

We then start collecting terms for each of the orders of ϵ in eq. (3.70).

Collecting terms of order $\mathcal{O}(\epsilon^0)$

$$q_0^{(1)} = -M\left(p_{b_0} - p_{b_i}\right)$$

For both $\mathcal{O}(1)$ and $\mathcal{O}(\epsilon)$ we get their value to be zero

$$\begin{aligned} q_1^{(1)} &= 0 \\ q_2^{(1)} &= 0 \end{aligned}$$

Shifting to $q^{(2)\epsilon}$ and repeating the procedure:

$$\begin{aligned} q^{(2)\epsilon} &= -\epsilon^{-1}\mu^{-1}(c^\epsilon)\partial_\eta p^\epsilon && (3.71)\\ &= -\left(\mu^{-1}(c_0) + \epsilon\partial_1\mu^{-1}(c_0)c_1 + \epsilon^2\partial_{11}\mu^{-1}(c_0)c_2\right)\partial_\eta\left(\left(p_{b_0} - p_{b_i}\right)x + p_{b_i}\right) \\ &= 0 && (3.72) \end{aligned}$$

From this, a flux can be deducted which can be written with this form:

$$q^\epsilon = \begin{bmatrix} q^{(1)\epsilon} \\ q^{(2)\epsilon} \end{bmatrix} = -M \begin{bmatrix} p_{b_0} - p_{b_i} \\ 0 \end{bmatrix} \tag{3.73}$$

The following asymptotic expansion for v^ϵ is (also) assumed:

$$v^\epsilon = v_0 + \epsilon v_1 + \epsilon^2 v_2 + \mathcal{O}(\epsilon^3), \tag{3.74}$$

Using the expansions, in the convection-diffusion equation (3.47) with the boundary condition (3.51), the following equation is obtained

$$\begin{aligned} \partial_t c_0 + \epsilon\partial_t c_1 + \epsilon^2\partial_t c_2 =& \epsilon D\partial_{xx}c_0 + \epsilon^2 D\partial_{xx}c_1 + \epsilon^{-1}D\partial_{\eta\eta}c_0 + \\ & D\partial_{\eta\eta}c_1 + \epsilon D\partial_{\eta\eta}c_2 - \\ & q^{(1)\epsilon}\partial_x c_0 - \epsilon q^{(1)\epsilon}\partial_x c_1 - \epsilon^2 q^{(1)\epsilon}\partial_x c_2 \end{aligned} \tag{3.75}$$

$$D\left(\partial_\eta c_0 + \epsilon\partial_\eta c_1 + \epsilon^2\partial_\eta c_2\right) = \epsilon\partial_t v_0 + \epsilon^2\partial_t v_1 + \mathcal{O}(\epsilon^3), \text{ on } \Gamma_\epsilon \times \{\eta = -1\} \tag{3.76}$$

$$-D\left(\partial_\eta c_0 + \epsilon\partial_\eta c_1 + \epsilon^2\partial_\eta c_2\right) = \epsilon\partial_t v_0 + \epsilon^2\partial_t v_1 + \mathcal{O}(\epsilon^3), \text{ on } \Gamma_\epsilon \times \{\eta = 1\} \tag{3.77}$$

$$\tag{3.78}$$

The terms are then collected, based on their power of ϵ.

ϵ^{-1} terms:

$$\partial_{\eta\eta} c_0 = 0, \text{ in } \Omega_\epsilon$$

From this the following can be concluded

$$c_0(x, \eta, t) = A_0(x, t)\eta + A_1(x, t), \tag{3.79}$$

where A_0 and A_1 are constants depending only on x and t.

ϵ^0 terms:

$$\partial_t c_0 = D\partial_{\eta\eta} c_1 - q^{(1)\epsilon}\partial_x c_0 \tag{3.80}$$

$$\partial_\eta c_0 = 0, \text{ at } \eta = \{-1, 1\} \tag{3.81}$$

Equation (3.81) combined with (3.79) the final relation for c_0 can be written as such

$$c_0(x, \eta, t) = A_1(x, t) = c_0(x, t), \tag{3.82}$$

Starting by integrating eq. (3.80) over η.

$$\int_{-1}^{1} \partial_t c_0 d\eta = D\int_{-1}^{1} \partial_{\eta\eta} c_1 d\eta - \int_{-1}^{1} q^{(1)\epsilon}\partial_x c_0 d\eta$$

$$2\partial_t c_0 = D\left(\partial_\eta c_1|_{\eta=1} - \partial_\eta c_1|_{\eta=-1}\right) + 2M\left(p_{b_0} - p_{b_i}\right)\partial_x c_0 \tag{3.83}$$

ϵ^1 terms:

$$\partial_t c_1 = D\partial_{xx} c_0 + D\partial_{\eta\eta} c_2 - q^{(1)\epsilon}\partial_x c_1 \tag{3.84}$$

$$\partial_\eta c_1 = \frac{1}{D}\partial_t v_0, \text{ at } \eta = -1 \tag{3.85}$$

$$\partial_\eta c_1 = -\frac{1}{D}\partial_t v_0, \text{ at } \eta = 1 \tag{3.86}$$

ϵ^2 terms:

$$\partial_\eta c_2 = \frac{1}{D}\partial_t v_1, \text{ at } \eta = -1 \tag{3.87}$$

$$\partial_\eta c_2 = -\frac{1}{D}\partial_t v_1, \text{ at } \eta = 1 \tag{3.88}$$

Using eq. (3.85) and (3.86) in eq. (3.83) gives

$$\partial_t c_0 + \partial_t v_0 - M\left(p_{b_0} - p_{b_i}\right)\partial_x c_0 = 0 \tag{3.89}$$

As observed in the simulations, when going from 2D to 1D, the effective diffusion will be higher than in 2D. So as seen in eq. (3.89); there is no diffusion term. Therefore another expansion term is included, namely c_1.
In order to obtain an equation for c1, then eq. (3.89) is subtracted from (3.80).

$$\partial_t c_0 - D\partial_{\eta\eta} c_1 - M\left(p_{b_0} - p_{b_i}\right)\partial_x c_0 - \partial_t c_0 - \partial_t v_0 + M\left(p_{b_0} - p_{b_i}\right)\partial_x c_0 = 0$$

$$\partial_{\eta\eta} c_1 = -\frac{1}{D}\partial_t v_0 \tag{3.90}$$

Successfully integrating the equation above with respect to η, then the following can be concluded for $c_1(x,\eta,t)$:

$$c_1 = -\frac{1}{2D}\partial_t v_0\,\eta^2 + A_1(x,t)\,\eta + A_2(x,t) \tag{3.91}$$

where A_1 and A_2 are constants of integration. It follows by the boundary terms from eq. (3.85) that $A_1 = 0$. As will be shown later, there is no need to explicitly expressing A_2 functions, since its effect will get canceled in the averaging process later on.

Integrating eq. (3.84) from $\eta = -1$ to $\eta = 1$

$$\partial_t \int_{-1}^{1} c_1 d\eta = D\partial_{xx} c_0 \int_{-1}^{1} d\eta + \int_{-1}^{1} D\partial_{\eta\eta} c_2 d\eta + M\left(p_{b_o} - p_{b_i}\right)\partial_x \int_{-1}^{1} c_1 d\eta \tag{3.92}$$

Defining

$$\bar{c}_1 = \frac{1}{2}\int_{-1}^{1} c_1 d\eta$$

and using in eq. (3.92)

$$2\partial_t \bar{c}_1 - 2D\partial_{xx} c_0 - \left[D\partial_\eta c_2\right]_{\eta=-1}^{\eta=1} - 2M\left(p_{b_o} - p_{b_i}\right)\partial_x \bar{c}_1 = 0 \tag{3.93}$$

$$\partial_t \bar{c}_1 - D\partial_{xx} c_0 + \partial_t v_1 - M\left(p_{b_o} - p_{b_i}\right)\partial_x \bar{c}_1 = 0 \tag{3.94}$$

Adding eq. (3.94) times ϵ and (3.89)

$$\epsilon\partial_t \bar{c}_1 - \epsilon D\partial_{xx} c_0 + \epsilon\partial_t v_1 - \epsilon M\left(p_{b_o} - p_{b_i}\right)\partial_x \bar{c}_1 + \partial_t c_0 + \partial_t v_0 - M\left(p_{b_0} - p_{b_i}\right)\partial_x c_0 = 0$$

$$\partial_t\left(c_0 + \epsilon\bar{c}_1\right) - \epsilon D\partial_{xx}\left(c_0 + \epsilon\bar{c}_1\right) + \partial_t\left(v_0 + \epsilon v_1\right) - M\left(p_{b_o} - p_{b_i}\right)\partial_x\left(c_0 + \epsilon\bar{c}_1\right) = -\epsilon^2 D\partial_{xx}\bar{c}_1 \tag{3.95}$$

Thereafter defining the following

$$c_e = c_0 + \epsilon\bar{c}_1 \tag{3.96}$$

$$v_e = v_0 + \epsilon v_1 \tag{3.97}$$

Taking base in the definitions (3.96) and (3.97), then the following can be obtained

$$\partial_t\left(c_e + v_e\right) - \epsilon D\partial_{xx} c_e - M\left(p_{b_o} - p_{b_i}\right)\partial_x c_e = -\epsilon^2 D\partial_{xx}\bar{c}_1 \tag{3.98}$$

For v_e it can be shown formally by Taylor expansion of $f(c^\epsilon, v^\epsilon)$ around (c_e, v_e),

$$\begin{aligned}\partial_t v_e &= f(c^\epsilon, v^\epsilon) = f(c_0 + \epsilon\bar{c}_1, v_0 + \epsilon v_1) + \epsilon\left(c_1|_{\eta=1} - \bar{c}_1\right)\partial_1 f(c_0 + \epsilon\bar{c}_1, v_0 + \epsilon v_1) + \mathcal{O}(\epsilon^2)\\ &= f(c_e, v_e) + \epsilon\left(c_1|_{\eta=1} - \bar{c}_1\right)\partial_1 f(c_e, v_e) + \mathcal{O}(\epsilon^2)\end{aligned} \tag{3.99}$$

From eq. (3.91) it is obtained

$$c_1|_{\eta=1} - \bar{c}_1 = -\frac{1}{3D}\partial_t v_0$$

Which results in the final equation for $\partial_t v_e$:

$$\partial_t v_e = f(c_e, v_e) - \frac{\epsilon}{3D}\partial_t v_0 \partial_1 f(c_e, v_e) \tag{3.100}$$

Summarizing: The set of effective equations up to $\mathcal{O}(\epsilon^2)$ are obtained.

$$\begin{aligned} \partial_t \left(c_e + v_e\right) &= \partial_x \left\{ \epsilon D \partial_x c_e + M \left(p_{b_o} - p_{b_i}\right) c_e - \epsilon^2 D \partial_x \bar{c}_1 \right\} \\ \partial_t v_e &= f(c_e, v_e) - \frac{\epsilon}{3D}\partial_t v_0 \partial_1 f(c_e, v_e) \end{aligned} \tag{3.101}$$

3.2.2 Case 2: $\alpha = 1, \beta = 2$ and constant viscosity

Secondly we will consider the case when $\alpha = 1, \beta = 2$. The same computations is applicable up until eq. (3.57). The viscosity will again be held constant, so $M = \mu^{-1}(c_0)$ and $\partial_1 \mu^{-1}(c_0) = 0$. Eq. (3.57) reduces to

$$\begin{aligned} -\partial_x \Big(& \epsilon \left(M \partial_x p_0\right) + \\ & \epsilon^2 \left(M \partial_x p_1\right) + \\ & \epsilon^3 \left(M \partial_x p_2\right) \Big) \\ -\partial_\eta \Big(& \left(M \partial_\eta p_0\right) + \\ & \epsilon \left(M \partial_\eta p_1\right) + \\ & \epsilon^2 \left(M \partial_\eta p_2\right) \Big) \\ & = 0 \end{aligned} \tag{3.102}$$

Collecting terms of order $\mathcal{O}(\epsilon^0)$

$$\begin{aligned} -M \partial_{\eta\eta} p_0 &= 0 \\ p_0(x, \eta) &= A_0(x)\eta + A_1(x) \end{aligned} \tag{3.103}$$

Using equation (3.38) it is clear that for $\eta = \{-1, 1\}$, $\partial_\eta p_0(x, \eta) = 0$. Thus

$$p_0(x, \eta) = p_0(x) = A_1(x) \tag{3.104}$$

Again, p_0 is independent of η.

Collecting terms of order $\mathcal{O}(\epsilon^1)$

$$-M \partial_{xx} p_0 - M \partial_{\eta\eta} p_1 = 0 \tag{3.105}$$

Integrating over η from -1 to 1

$$\begin{aligned} -M \partial_{xx} p_0 \int_{-1}^{1} d\eta - M \int_{-1}^{1} \partial_{\eta\eta} p_1 d\eta &= 0 \\ -2M \partial_{xx} p_0 - M \left[\partial_\eta p_1\right]_{\eta=-1}^{\eta=1} &= 0 \end{aligned}$$

Again, by using the equation (3.38) from the boundary, it is clear that $\partial_\eta p_1(x, \eta)|_{\eta=\{-1,1\}} = 0$. Thus

$$\begin{aligned} \partial_{xx} p_0 &= 0 \\ \partial_{xx} A_1(x) &= 0 \\ A_1(x) &= Ax + B \\ p_0(x) &= Ax + B \end{aligned}$$

Using boundary data:

$$p_0(x=0) = p_{b_i}$$
$$p_0(x=1) = p_{b_o}$$

Thus

$$p_0(x) = \left(p_{b_o} - p_{b_i}\right) x + p_{b_i} \tag{3.106}$$

Inserting this result into eq. (3.48):

$$\begin{aligned} q^{(1)\epsilon} &= -\epsilon\mu^{-1}(c^\epsilon)\partial_x p^\epsilon \\ &= -\epsilon\left(\mu^{-1}(c_0) + \epsilon\partial_1\mu^{-1}(c_0)c_1 + \epsilon^2\partial_{11}\mu^{-1}(c_0)c_2\right)\partial_x\left(\left(p_{b_0} - p_{b_i}\right)x + p_{b_i}\right) \\ &= -\epsilon M\left(p_{b_0} - p_{b_i}\right) \end{aligned} \tag{3.107}$$

$$\begin{aligned} q^{(2)\epsilon} &= -\epsilon\left(\mu^{-1}(c_0) + \epsilon\partial_1\mu^{-1}(c_0)c_1 + \epsilon^2\partial_{11}\mu^{-1}(c_0)c_2\right)\partial_\eta\left(\left(p_{b_0} - p_{b_i}\right)x + p_{b_i}\right) \\ &= -\epsilon M\partial_\eta\left(\left(p_{b_0} - p_{b_i}\right)x + p_{b_i}\right) \\ &= 0 \end{aligned} \tag{3.108}$$

Again using the expansions, in the convection-diffusion equation (3.47) with the boundary condition (3.51), the following equation is obtained:

$$\begin{aligned} \partial_t c_0 + \epsilon\partial_t c_1 + \epsilon^2\partial_t c_2 =& \epsilon D\partial_{xx}c_0 + \epsilon^2 D\partial_{xx}c_1 + \epsilon^3 D\partial_{xx}c_2 + \\ & \epsilon^{-1}D\partial_{\eta\eta}c_0 + D\partial_{\eta\eta}c_1 + \epsilon D\partial_{\eta\eta}c_2 + \\ & \epsilon M\left(p_{b_o} - p_{b_i}\right)\left(\partial_x c_0 + \epsilon\partial_x c_1 + \epsilon^2\partial_x c_2\right) \end{aligned} \tag{3.109}$$

$$D\left(\partial_\eta c_0 + \epsilon\partial_\eta c_1 + \epsilon^2\partial_\eta c_2\right) = \epsilon\partial_t v_0 + \epsilon^2\partial_t v_1 + \mathcal{O}(\epsilon^3), \text{ on } \Gamma_\epsilon \times \{\eta = -1\} \tag{3.110}$$

$$-D\left(\partial_\eta c_0 + \epsilon\partial_\eta c_1 + \epsilon^2\partial_\eta c_2\right) = \epsilon\partial_t v_0 + \epsilon^2\partial_t v_1 + \mathcal{O}(\epsilon^3), \text{ on } \Gamma_\epsilon \times \{\eta = 1\} \tag{3.111}$$

Collecting terms of order $\mathcal{O}(\epsilon^{-1})$

$$D\partial_{\eta\eta}c_0 = 0$$
$$D\partial_\eta c_0 = 0, \text{ at } \eta = \{-1, 1\}$$

From this it can be concluded that

$$c_0(x,t) = A_0(x,t) \tag{3.112}$$

Where A_0 is some integration constant depending on x and t.

Collecting terms of order $\mathcal{O}(\epsilon^0)$

$$\partial_t c_0 = D\partial_{\eta\eta}c_1 \tag{3.113}$$
$$D\partial_\eta c_1 = \partial_t v_0, \text{ at } \eta = -1 \tag{3.114}$$
$$-D\partial_\eta c_1 = \partial_t v_0, \text{ at } \eta = 1 \tag{3.115}$$

Integrating over η from 0 to 1,

$$\begin{aligned}\partial_t c_0 \int_{-1}^{1} d\eta &= D \int_{-1}^{1} \partial_{\eta\eta} c_1 \\ 2\partial_t c_0 &= \left[D\partial_\eta c_1\right]_{\eta=-1}^{\eta=1} \\ \partial_t c_0 &= -\partial_t v_0 \end{aligned} \tag{3.116}$$

Inserting back into eq. (3.113) the following result is given for c_1

$$\begin{aligned} D\partial_{\eta\eta} c_1 &= -\partial_t v_0 \\ c_1 &= -\frac{1}{2D}\partial_t v_0\, \eta^2 + A_0(x,t)\,\eta + A_1(x,t) \end{aligned} \tag{3.117}$$

where A_0 and A_1 are constants of integration. Using boundary terms, eq. (3.114) and (3.115), we see that $A_1 = 0$. As will be shown later, there is no need to express A_0 function explicitly, since its effect will get canceled in the averaging process later on.

Collecting terms of order $\mathcal{O}(\epsilon^1)$

$$\partial_t c_1 = D\partial_{xx} c_0 + D\partial_{\eta\eta} c_2 + M\left(p_{b_o} - p_{b_i}\right)\partial_x c_0 \tag{3.118}$$

Integrating over η from -1 to 1:

$$\begin{aligned} \int_{-1}^{1} \partial_t c_1 d\eta &= D\int_{-1}^{1} \partial_{xx} c_0 d\eta + D\int_{-1}^{1} \partial_{\eta\eta} c_2 d\eta + M\left(p_{b_o} - p_{b_i}\right)\int_{-1}^{1} \partial_x c_0 d\eta \\ \partial_t \int_{-1}^{1} c_1 d\eta &= 2D\partial_{xx} c_0 + \left[D\partial_\eta c_2\right]_{\eta=-1}^{\eta=1} + 2M\left(p_{b_o} - p_{b_i}\right)\partial_x c_0 \end{aligned}$$

Using the definition of the average of c_1 from previous section,

$$2\partial_t \bar{c}_1 = 2D\partial_{xx} c_0 + \left[D\partial_\eta c_2\right]_{\eta=-1}^{\eta=1} + 2M\left(p_{b_o} - p_{b_i}\right)\partial_x c_0 \tag{3.119}$$

Collecting terms of order $\mathcal{O}(\epsilon^2)$

$$D\partial_\eta c_2 = \partial_t v_1, \text{ at } \eta = -1 \tag{3.120}$$

$$-D\partial_\eta c_2 = \partial_t v_1, \text{ at } \eta = 1 \tag{3.121}$$

Inserting these boundary terms into eq. (3.119),

$$\partial_t \bar{c}_1 = D\partial_{xx} c_0 - \partial_t v_1 + M\left(p_{b_o} - p_{b_i}\right)\partial_x c_0 \tag{3.122}$$

Adding eq. (3.122) times ϵ and (3.116) results in

$$\epsilon\partial_t \bar{c}_1 - \epsilon D\partial_{xx} c_0 + \epsilon\partial_t v_1 - \epsilon M\left(p_{b_o} - p_{b_i}\right)\partial_x c_0 + \partial_t c_0 + \partial_t v_0 = 0 \tag{3.123}$$

$$\partial_t\left(c_0 + \epsilon\bar{c}_1\right) - D\partial_{xx}\left(c_0 + \epsilon\bar{c}_1\right) + \partial_t\left(v_0 + \epsilon v_1\right) - \epsilon M\left(p_{b_o} - p_{b_i}\right)\partial_x c_0 = -\epsilon D\partial_{xx}\bar{c}_1 \tag{3.124}$$

With the same definitions of c_e and v_e as in the previous section,

$$\partial_t\left(c_e + v_e\right) - D\partial_{xx} c_e - \epsilon M\left(p_{b_o} - p_{b_i}\right)\partial_x c_0 = -\epsilon D\partial_{xx}\bar{c}_1 \tag{3.125}$$

For v_e it can be shown formally by Taylor expansion of $f(c^\epsilon, v^\epsilon)$ around (c_e, v_e),

$$\begin{aligned} \partial_t v_e &= f(c^\epsilon, v^\epsilon) = f(c_0 + \epsilon\bar{c}_1, v_0 + \epsilon v_1) + \epsilon\left(c_1|_{\eta=1} - \bar{c}_1\right)\partial_1 f(c_0 + \epsilon\bar{c}_1, v_0 + \epsilon v_1) + \mathcal{O}(\epsilon^2) \\ &= f(c_e, v_e) + \epsilon\left(c_1|_{\eta=1} - \bar{c}_1\right)\partial_1 f(c_e, v_e) + \mathcal{O}(\epsilon^2) \end{aligned} \tag{3.126}$$

From eq. (3.117) we get that

$$c_1|_{\eta=1} - \bar{c}_1 = -\frac{1}{3D}\partial_t v_0$$

This results in the final equation for $\partial_t v_e$:

$$\partial_t v_e = f(c_e, v_e) - \frac{\epsilon}{3D}\partial_t v_0 \partial_1 f(c_e, v_e) \tag{3.127}$$

To summarize, the set of effective equations up to $\mathcal{O}(\epsilon^2)$ can be obtained.

$$\begin{aligned} \partial_t \left(c_e + v_e\right) &= \partial_x \left\{ D\partial_x c_e + \epsilon M \left(p_{b_o} - p_{b_i}\right) c_e - \epsilon D \partial_x \bar{c}_1 \right\} \\ \partial_t v_e &= f(c_e, v_e) - \frac{\epsilon}{3D}\partial_t v_0 \partial_1 f(c_e, v_e) \end{aligned} \tag{3.128}$$

3.2.3 Case 3: $\alpha = 0, \beta = 0$ and non-constant viscosity

Lastly we will consider the case when $\alpha = 0$ and $\beta = 0$, but now the viscosity is no longer held constant. The same computations is again applicable up until eq. (3.57). The viscosity function will be refered to as $M(c) = \mu^{-1}(c)$. Equation (3.57) then becomes

$$\begin{aligned}
&-\partial_x\Big(\big(M\left(c_0\right)\partial_x p_0\big) + \\
&\quad \epsilon\left(M(c_0)\partial_x p_1 + \partial_1 M(c_0)c_1\partial_x p_0\right) + \\
&\quad \epsilon^2\left(M(c_0)\partial_x p_2 + \partial_1 M(c_0)c_1\partial_x p_1 + \frac{1}{2}\partial_{11}M(c_0)c_1^2\partial_x p_0\right)\Big) \\
&-\partial_\eta\Big(\epsilon^{-2}\left(M(c_0)\partial_\eta p_0\right) + \\
&\quad \epsilon^{-1}\left(M(c_0)\partial_\eta p_1 + \partial_1 M(c_0)c_1\partial_\eta p_0\right) + \\
&\quad \left(M(c_0)\partial_\eta p_2 + \partial_1 M(c_0)c_1\partial_\eta p_1 + \partial_{11}M(c_0)c_2\partial_\eta p_0\right) + \\
&\quad \epsilon\left(\partial_1 M(c_0)c_1\partial_\eta p_2 + \frac{1}{2}\partial_{11}M(c_0)c_1^2\partial_\eta p_1\right)\Big) \\
&\quad = 0
\end{aligned} \tag{3.129}$$

Collecting terms of order $\mathcal{O}(\epsilon^{-2})$

$$\begin{aligned}
-\partial_\eta\left(M(c_0)\partial_\eta p_0\right) &= 0 \\
M(c_0)\partial_\eta p_0 &= A_0(x,t)
\end{aligned}$$

Using equation (3.38) it can be seen that when $\eta = \{-1, 1\}$, then $\partial_\eta p_0(x,\eta) = 0$. Thus,

$$p_0(x,\eta,t) = p_0(x,t) \tag{3.130}$$

Collecting terms of order $\mathcal{O}(\epsilon^{-1})$

$$\begin{aligned}
-\partial_\eta\left(M(c_0)\partial_\eta p_1 + \partial_1 M(c_0)c_1\partial_\eta p_0\right) &= 0 \\
M(c_0)\partial_\eta p_1 &= A_0(x,t)
\end{aligned}$$

From last order of ϵ, it can be seen that $\partial_\eta p_0 = 0$. Using same boundary as previous order, then $A_0(x,t) = 0$ and therefore

$$p_1(x,\eta,t) = p_1(x,t) \tag{3.131}$$

Collecting terms of order $\mathcal{O}(\epsilon^0)$

$$\begin{aligned}
-\partial_x\left(M(c_0)\partial_x p_0\right) - \partial_\eta\left(M(c_0)\partial_\eta p_2 + \partial_1 M(c_0)c_1\partial_\eta p_1 + \frac{1}{2}\partial_{11}M(c_0)c_1^2\partial_\eta p_0\right) &= 0 \\
-\partial_x\left(M(c_0)\partial_x p_0\right) - \partial_\eta\left(M(c_0)\partial_\eta p_2\right) &= 0
\end{aligned}$$

Integrating over η from -1 to 1

$$\begin{aligned}
-\partial_x \int_{-1}^{1} \left(M(c_0)\partial_x p_0\right) d\eta - \int_{-1}^{1} \partial_\eta \left(M(c_0)\partial_\eta p_2\right) d\eta &= 0 \\
-2\partial_x \left(M(c_0)\partial_x p_0\right) - M(c_0) \int_{-1}^{1} \partial_{\eta\eta} p_2 d\eta &= 0 \\
-2\partial_x \left(M(c_0)\partial_x p_0\right) - M(c_0) \left[\partial_\eta p_2\right]_{\eta=-1}^{\eta=1} &= 0 \\
\partial_x \left(M(c_0)\partial_x p_0\right) &= 0 \\
M(c_0)\partial_x p_0 &= A_0(t) \\
\partial_x p_0 &= \frac{A_0(t)}{M(c_0)}
\end{aligned}$$

Using the boundary data, which is not dependent on t, we get

$$\partial_x p_0 = \frac{A_0}{M(c_0)} \tag{3.132}$$

Collecting terms of order $\mathcal{O}(\epsilon)$

$$-\partial_x \left(M(c_0)\partial_x p_1 + \partial_1 M(c_0) c_1 \partial_x p_0\right) - \partial_\eta \left(\partial_1 M(c_0) c_1 \partial_\eta p_2 + \frac{1}{2}\partial_{11} M(c_0) c_1^2 \partial_\eta p_1\right) = 0$$

Integrating over η from -1 to 1

$$\begin{aligned}
&- \partial_x \int_{-1}^{1} \left(M(c_0)\partial_x p_1 + \partial_1 M(c_0) c_1 \partial_x p_0\right) d\eta \\
&- \int_{-1}^{1} \partial_\eta \left(\partial_1 M(c_0) c_1 \partial_\eta p_2 + \frac{1}{2}\partial_{11} M(c_0) c_1^2 \partial_\eta p_1\right) d\eta = 0
\end{aligned}$$

$$\begin{aligned}
-\partial_x \int_{-1}^{1} \left(M(c_0)\partial_x p_1 + \partial_1 M(c_0) c_1 \partial_x p_0\right) d\eta &= 0 \\
M(c_0)\partial_x p_1 + \partial_1 M(c_0) c_1 \partial_x p_0 &= A_1(t)
\end{aligned}$$

$$\begin{aligned}
M(c_0)\partial_x p_1 &= -\partial_1 M(c_0) c_1 \partial_x p_0 + A_1(t) \\
M(c_0)\partial_x p_1 &= -\partial_1 M(c_0) c_1 \frac{A_0}{M(c_0)} + A_1(t) \\
\partial_x p_1 &= -\frac{A_0 c_1}{M(c_0)^2}\partial_1 M(c_0) + \frac{1}{M(c_0)} A_1(t)
\end{aligned}$$

As before, using the boundary condition which is time-independent,

$$\partial_x p_1 = -\frac{A_0 c_1}{M(c_0)^2}\partial_1 M(c_0) + \frac{A_1}{M(c_0)} \tag{3.133}$$

Going to the flux,

$$\begin{aligned}
q^{(1)\epsilon} &= -M(c_0)\partial_x p^\epsilon \\
&= -M(c_0)\left(\partial_x p_0 + \epsilon \partial_x p_1\right) && (3.134) \\
&= -M(c_0)\left(\frac{A_0}{M(c_0)} - \epsilon\frac{A_0 c_1}{M(c_0)^2}\partial_1 M(c_0) - \epsilon\frac{1}{M(c_0)} A_1\right) && (3.135) \\
&= A_0\left(\frac{\epsilon c_1}{M(c_0)}\partial_1 M(c_0) - 1\right) + \epsilon A_1 && (3.136)
\end{aligned}$$

and

$$\begin{aligned} q^{(2)\epsilon} &= -M(c_0)\partial_\eta p^\epsilon \\ &= 0 \end{aligned} \tag{3.137}$$

Both $\partial_x p_0$ and $\partial_x p_1$ are independent of η and, because the boundary is also independent of η, the integration constant from integrating p_0 and p_1 itself are independent of η. And because of this, then it can be concluded that $q^{(2)\epsilon} = 0$.

Inserting this into our transport equation, the following can be obtained:

$$\partial_t c^\epsilon = \epsilon D\left(\partial_{xx} c_0 + \epsilon^{-2}\partial_{\eta\eta} c^\epsilon\right) - \partial_x\left(q^{(1)\epsilon} c^\epsilon\right)$$

$$\begin{aligned} \partial_t c_0 + \epsilon\partial_t c_1 + \epsilon^2\partial_t c_2 =& \epsilon D\partial_{xx} c_0 + \epsilon^2 D\partial_{xx} c_1 + \epsilon^3 D\partial_{xx} c_2 + \\ & \epsilon^{-1} D\partial_{\eta\eta} c_0 + D\partial_{\eta\eta} c_1 + \epsilon D\partial_{\eta\eta} c_2 - \\ & \partial_x\left(\left(A_0\left(1 - \frac{\epsilon c_1}{M(c_0)}\partial_1 M(c_0)\right) - \epsilon A_1\right)\left(c_0 + \epsilon c_1 + \epsilon^2 c_2\right)\right) \end{aligned} \tag{3.138}$$

$$\begin{aligned} \partial_t c_0 + \epsilon\partial_t c_1 + \epsilon^2\partial_t c_2 =& \epsilon D\partial_{xx} c_0 + \epsilon^2 D\partial_{xx} c_1 + \epsilon^3 D\partial_{xx} c_2 + \\ & \epsilon^{-1} D\partial_{\eta\eta} c_0 + D\partial_{\eta\eta} c_1 + \epsilon D\partial_{\eta\eta} c_2 - \\ & \partial_x\left(\left(A_0\left(1 - \frac{\epsilon c_1}{M(c_0)}\partial_1 M(c_0)\right) - \epsilon A_1\right)\left(c_0 + \epsilon c_1 + \epsilon^2 c_2\right)\right) \end{aligned} \tag{3.139}$$

$$\begin{aligned} \partial_t c_0 + \epsilon\partial_t c_1 + \epsilon^2\partial_t c_2 =& \epsilon D\partial_{xx} c_0 + \epsilon^2 D\partial_{xx} c_1 + \epsilon^3 D\partial_{xx} c_2 + \\ & \epsilon^{-1} D\partial_{\eta\eta} c_0 + D\partial_{\eta\eta} c_1 + \epsilon D\partial_{\eta\eta} c_2 - \\ & \partial_x\Bigg(A_0 c_0 + \epsilon\left[-\frac{A_1 c_1}{M(c_0)}\partial_1 M(c_0) c_0 - A_1 c_0 + A_0 c_1\right] \\ & + \epsilon^2\left[-\frac{A_1 c_1}{M(c_0)}\partial_1 M(c_0) c_1 - A_1 c_1 + A_0 c_2\right] \\ & + \epsilon^3\left[-\frac{A_1 c_1}{M(c_0)}\partial_1 M(c_0) c_2 - A_1 c_2\right]\Bigg) \end{aligned} \tag{3.140}$$

The boundaries (3.76) and (3.77) remains the same:

$$\begin{aligned} D\left(\partial_\eta c_0 + \epsilon\partial_\eta c_1 + \epsilon^2\partial_\eta c_2\right) &= \epsilon\partial_t v_0 + \epsilon^2\partial_t v_1 + \mathcal{O}(\epsilon^3), \text{ on } \Gamma_\epsilon \times \{\eta = -1\} \\ -D\left(\partial_\eta c_0 + \epsilon\partial_\eta c_1 + \epsilon^2\partial_\eta c_2\right) &= \epsilon\partial_t v_0 + \epsilon^2\partial_t v_1 + \mathcal{O}(\epsilon^3), \text{ on } \Gamma_\epsilon \times \{\eta = 1\} \end{aligned}$$

Collecting terms of order $\mathcal{O}(\epsilon^{-1})$

$$D\partial_{\eta\eta} c_0 = 0$$

This results in the following c_0:

$$c_0(x, \eta, t) = A_2(x, t)\eta + A_3(x, t) \tag{3.141}$$

Collecting terms of order $\mathcal{O}(\epsilon^0)$

$$\begin{aligned} \partial_t c_0 &= D\partial_{\eta\eta} c_1 + A_0 \partial_x c_0 \\ D\partial_\eta c_0 &= 0, \text{ at } \eta = \{-1, 1\} \end{aligned} \tag{3.142}$$

Using the boundary term from here, it can be seen that $c_0(x, \eta, t) = c_0(x, t)$. The first equation (3.142) is then integrated:

$$\begin{aligned} \partial_t c_0 \int_{-1}^{1} d\eta &= D \int_{-1}^{1} \partial_{\eta\eta} c_1 d\eta + A_0 \partial_x c_0 \int_{-1}^{1} d\eta \\ 2\partial_t c_0 &= \left[D\partial_\eta c_1 \right]_{\eta=-1}^{\eta=1} + 2A_0 \partial_x c_0 \end{aligned} \tag{3.143}$$

Collecting terms of order $\mathcal{O}(\epsilon^1)$

$$\partial_t c_1 = D\partial_{xx} c_0 + D\partial_{\eta\eta} c_2 - A_1 \partial_x \left(\frac{c_1}{M(c_0)} \partial_1 M(c_0) c0 \right) - A_1 \partial_x c_0 + A_0 \partial_x c_1 \tag{3.144}$$

$$\begin{aligned} D\partial_\eta c_1 &= \partial_t v_0, \text{ at } \eta = -1 \\ -D\partial_\eta c_1 &= \partial_t v_0, \text{ at } \eta = 1 \end{aligned}$$

Inserting these boundary terms into eq. (3.143) enables the final equation to be obtained:

$$\partial_t c_0 + \partial_t v_0 - A_0 \partial_x c_0 = 0 \tag{3.145}$$

Further inserting eq. (3.145) into (3.142):

$$\begin{aligned} \partial_{\eta\eta} c_1 &= -\frac{1}{D} \partial_t v_0 \\ c_1 &= -\frac{1}{2D} \partial_t v_0 \eta^2 + A_2(x,t)\eta + A_3(x,t) \end{aligned}$$

Using the boundary $D\partial_\eta c_1 = \partial_t v_0, \text{ at } \eta = -1$,

$$c_1 = -\frac{1}{2D} \partial_t v_0 \eta^2 + A_3(x,t) \tag{3.146}$$

Like in the previous sections, the value of A_3 will not make any influence due to averaging, so this does not need to be explicitly expressed.

Collecting terms of order $\mathcal{O}(\epsilon^2)$

$$\partial_t c_2 = D\partial_{xx} c_1 - A_1 \partial_x \left(\frac{c_1}{M(c_0)} \partial_1 M(c_0) c1 \right) - A_1 \partial_x c_1 + A_0 \partial_x c_2$$

$$\begin{aligned} D\partial_\eta c_2 &= \partial_t v_1, \text{ at } \eta = -1 \\ -D\partial_\eta c_2 &= \partial_t v_1, \text{ at } \eta = 1 \end{aligned}$$

Integrating eq. (3.144) over η,

$$\begin{aligned} \partial_t c_1 \int_{-1}^{1} d\eta &= D\partial_{xx} c_0 \int_{-1}^{1} d\eta + D \int_{-1}^{1} \partial_{\eta\eta} c_2 d\eta \\ &\quad - A_1 \partial_x \left(\frac{\int_{-1}^{1} c_1 d\eta}{M(c_0)} \partial_1 M(c_0) c0 \right) - A_1 \partial_x c_0 \int_{-1}^{1} d\eta + A_0 \partial_x c_1 \int_{-1}^{1} d\eta \\ 2\partial_t \bar{c}_1 &= 2D\partial_{xx} c_0 + \left[D\partial_\eta c_2 \right] - 2A_1 \partial_x \left(\frac{\bar{c}_1}{M(c_0)} \partial_1 M(c_0) c0 \right) - 2A_1 \partial_x c_0 + A_0 \partial_x \bar{c}_1 \end{aligned}$$

$$\partial_t \bar{c}_1 - D\partial_{xx} c_0 + \partial_t v_1 + A_1 \partial_x \left(\frac{\bar{c}_1}{M(c_0)} \partial_1 M(c_0) c0 \right) + A_1 \partial_x c_0 + A_0 \partial_x \bar{c}_1 = 0 \tag{3.147}$$

Adding ϵ times eq. (3.147) to eq. (3.145)

$$\begin{aligned} &\epsilon \partial_t \bar{c}_1 - \epsilon D \partial_{xx} c_0 + \epsilon \partial_t v_1 + \epsilon A_1 \partial_x \left(\frac{\bar{c}_1}{M(c_0)} \partial_1 M(c_0) c0 \right) \\ &+ \epsilon A_1 \partial_x c_0 + A_0 \partial_x \bar{c}_1 + \partial_t c_0 + \partial_t v_0 - A_0 \partial_x c_0 = 0 \end{aligned} \tag{3.148}$$

$$\begin{aligned} &\partial_t \left(c_0 + \epsilon \bar{c}_1 \right) - \epsilon D \partial_{xx} c_0 + \partial_t \left(v_0 + \epsilon v_1 \right) + \epsilon A_1 \partial_x \left(\frac{\bar{c}_1}{M(c_0)} \partial_1 M(c_0) c0 \right) \\ &- \left(A_0 - \epsilon A_1 \right) \partial_x c_0 + \epsilon A_0 \partial_x \bar{c}_1 = 0 \end{aligned} \tag{3.149}$$

The definitions of c_e and v_e remains that same as in the previous sections:

$$\begin{aligned} &\partial_t \left(c_e + v_e \right) - \epsilon D \partial_{xx} c_e + \epsilon A_1 \partial_x \left(\frac{\bar{c}_1}{M(c_0)} \partial_1 M(c_0) c0 \right) \\ &+ A_0 \partial_x c_e = - \left(2A_0 - \epsilon A_1 \right) \partial_x c_0 - \epsilon^2 D \partial_{xx} \bar{c}_1 \end{aligned} \tag{3.150}$$

For v_e it can be shown formally by Taylor expansion of $f(c^\epsilon$ around (c_e, v_e),

$$\begin{aligned} \partial_t v_e &= f(c^\epsilon, v^\epsilon) = f(c_0 + \epsilon \bar{c}_1, v_0 + \epsilon v_1) + \epsilon \left(c_1|_{\eta=1} - \bar{c}_1 \right) \partial_1 f(c_0 + \epsilon \bar{c}_1, v_0 + \epsilon v_1) + \mathcal{O}(\epsilon^2) \\ &= f(c_e, v_e) + \epsilon \left(c_1|_{\eta=1} - \bar{c}_1 \right) \partial_1 f(c_e, v_e) + \mathcal{O}(\epsilon^2) \end{aligned} \tag{3.151}$$

From eq. (3.146) we get that

$$c_1|_{\eta=1} - \bar{c}_1 = -\frac{1}{3D} \partial_t v_0$$

Which results in the final equation for $\partial_t v_e$:

$$\partial_t v_e = f(c_e, v_e) - \frac{\epsilon}{3D} \partial_t v_0 \partial_1 f(c_e, v_e) \tag{3.152}$$

Summarizing: The set of effective equations up to $\mathcal{O}(\epsilon^2)$ are obtained (as such):

$$\begin{aligned} \partial_t \left(c_e + v_e \right) =& \partial_x \Bigg\{ \epsilon D \partial_x c_e - \epsilon A_1 \left(\frac{\bar{c}_1}{M(c_0)} \partial_1 M(c_0) c_0 \right) \\ &- A_0 c_e - \left(2A_0 - \epsilon A_1 \right) c_0 - \epsilon^2 D \partial_x \bar{c}_1 \Bigg\} \\ \partial_t v_e =& f(c_e, v_e) - \frac{\epsilon}{3D} \partial_t v_0 \partial_1 f(c_e, v_e) \end{aligned} \tag{3.153}$$

3.2.4 Remark

None of the results listed in this chapter gives rise to a Taylor Dispersion term, like seen in [14]. This is somehow contradicting the numerical results in this thesis, which shows a smaller difference when a Taylor Dispersion term is included. This is mainly due to our model uses a Darcy type flow, while in the cited article the flow is gotten from a Stoke flow. While it is possible to obtain a parabolic flow profile, which again gives raise to a Taylor Dispersion type term, it is not possible without introducing a source term and possibly introducing a η-dependency within the other parameters such as boundary concentrations or so. This is outside the scope of this thesis.

3.3 Flow problem

In this section we will prove the existence and boundedness of a solution an coupled flow and transport problem. We start off with our equation for flow (Darcy)

$$\nabla \cdot (-\boldsymbol{K}^\epsilon \nabla p^\epsilon) = f \tag{3.154}$$

where,

$$\boldsymbol{K}^\epsilon = \begin{bmatrix} \epsilon^\alpha & 0 \\ 0 & \epsilon^\beta \end{bmatrix}$$

We will then study what happens to the solution when ϵ, the thickness of the strip, goes to zero. We then transform eq. (3.154) from a differential equation into a weak formulation

$$(\epsilon^\alpha \partial_x p^\epsilon, \partial_x \varphi)_{\Omega^\epsilon} + \left(\epsilon^\beta \partial_y p^\epsilon, \partial_y \varphi\right)_{\Omega^\epsilon} = (f, \varphi)_{\Omega^\epsilon} \tag{3.155}$$

where φ is a test-function and the domain is defined as

$$\Omega^\epsilon = (0,1) \times (0,\epsilon) \tag{3.156}$$

Then we do a coordinate transformation, where we define

$$x := x, \quad \eta := \frac{y}{\epsilon}$$

This transforms our domain to

$$\Omega^\epsilon = (0,1) \times (0,1) \tag{3.157}$$

Take a test-function such that $\varphi = \varphi(x)$, which means it is independent of η. This gives us

$$(\epsilon^\alpha \partial_x p^\epsilon, \partial_x \varphi)_{\Omega^\epsilon} = (f, \varphi)_{\Omega^\epsilon} \tag{3.158}$$

$$\int_0^1 \int_0^1 (\epsilon^\alpha \partial_x p^\epsilon \partial_x \varphi)\, d\eta\, dx = \int_0^1 \int_0^1 f\varphi\, d\eta\, dx \tag{3.159}$$

$$\int_0^1 \epsilon^\alpha \left(\int_0^1 \partial_x p^\epsilon d\eta \right) \partial_x \varphi\, dx = \int_0^1 \int_0^1 f\varphi d\eta\, dx \tag{3.160}$$

Which in it's strong form corresponds to the following:

$$\partial_x \left(-\epsilon^\alpha \int_0^1 \partial_x p^\epsilon d\eta \right) = \int_0^1 f d\eta \tag{3.161}$$

We define the average of p^ϵ as

$$\bar{p}^\epsilon = \int_0^1 p^\epsilon d\eta$$

From eq. (3.160) we use the definition of the average of p^ϵ and get the following

$$\int_0^1 \epsilon^\alpha \left(\partial_x \int_0^1 p^\epsilon d\eta \right) \partial_x \varphi dx = \int_0^1 \int_0^1 f\varphi\, d\eta\, dx \tag{3.162}$$

$$\int_0^1 \epsilon^\alpha \partial_x \bar{p}^\epsilon \partial_x \varphi\, dx = \int_0^1 \int_0^1 f\varphi\, d\eta\, dx \tag{3.163}$$

Again, we choose a test-function satisfying the previous choice

$$\varphi = \bar{p}^{\epsilon}$$

This gives

$$\int_0^1 \epsilon^{\alpha} \partial_x \bar{p}^{\epsilon} \partial_x \bar{p}^{\epsilon} dx = \int_0^1 f \bar{p}^{\epsilon} dx \tag{3.164}$$

$$\int_0^1 |\partial_x \bar{p}^{\epsilon}|^2 \, dx = \int_0^1 \epsilon^{-\alpha} f \bar{p}^{\epsilon} \, dx \tag{3.165}$$

$$\leq \left\| \epsilon^{-\alpha} f \right\|_{L^2(\Omega^{\epsilon})} \|\bar{p}^{\epsilon}\|_{L^2(\Omega^{\epsilon})} \tag{3.166}$$

Required that the following holds

$$\left\| \epsilon^{-\alpha} f \right\|_{L^2(\Omega^{\epsilon})} \leq C$$

where C is an generic constant, gives us the following

$$\int_0^1 |\partial_x \bar{p}^{\epsilon}|^2 \, dx \leq C \left\| \epsilon^{-\alpha} f \right\|_{L^2(\Omega^{\epsilon})} \|\bar{p}^{\epsilon}\|_{L^2(\Omega^{\epsilon})} \tag{3.167}$$

Applying Poincare inequality theorem to the previous result, we get

$$\left\| \bar{p}^{\epsilon}(x) \right\|_{L^2(\Omega^{\epsilon})} \leq C \left\| \nabla \bar{p}^{\epsilon}(x) \right\|_{L^2(\Omega^{\epsilon})} \tag{3.168}$$

Since $\bar{p}^{\epsilon}$ is only a function of x, this means that

$$\left\| \partial_x \bar{p}^{\epsilon}(x) \right\|_{L^2(\Omega^{\epsilon})} \leq \left\| \partial_x \bar{p}^{\epsilon}(x) \right\|^2_{L^2(\Omega^{\epsilon})} \leq C \left\| \epsilon^{-\alpha} f \right\|_{L^2(\Omega^{\epsilon})} \leq C \tag{3.169}$$

Thus, this stays bounded as long as

$$\left\| \epsilon^{-\alpha} f \right\|_{L^2(\Omega^{\epsilon})} \leq C$$

is true.

From the Poincare inequality, where C is a generic constant, we get

$$\|\bar{p}^{\epsilon}\| \leq C \|\partial_x \bar{p}^{\epsilon}\| \tag{3.170}$$

From this we can conclude that $\bar{p}^{\epsilon}$ converges strongly to $\bar{p}$ when ϵ goes to zero, as well as $\partial_x \bar{p}^{\epsilon}$ converges weakly to $\partial_x \bar{p}$.

From the equation for $\bar{p}^{\epsilon}$:

$$\int_0^1 \left[\partial_x \bar{p}^{\epsilon} \right] \partial_x \varphi \, dx = \int_0^1 \epsilon^{-\alpha} f \varphi \, dx \tag{3.171}$$

For $\alpha > 0$:

For an $\alpha > 0$, we have the following relation:

$$\int_0^1 [\partial_x \bar{p}]\, \partial_x \varphi \, dx = \int_0^1 \epsilon^{-\alpha} f \varphi \, dx \tag{3.172}$$

Which in its strong form is

$$\Rightarrow -\partial_{xx} \bar{p} = \epsilon^{-\alpha} f$$

As we see from the strong form, this is stays bounded for all values of ϵ as that term goes to zero.

$$\bar{p} = p_D, \text{ at Dirichlet boundaries} \tag{3.173}$$

$$q_1^\epsilon = -\epsilon^\alpha \partial_x p^\epsilon \tag{3.174}$$

$$q_2^\epsilon = -\epsilon^\beta \partial_\eta p^\epsilon \tag{3.175}$$

To obtain information about q_1^ϵ:

$$\|\partial_x \bar{p}^\epsilon\| \leq C$$

$$\bar{q}_1^\epsilon = -\epsilon^\alpha \partial_x \bar{p}^\epsilon$$

$$\Rightarrow \bar{q}_1^\epsilon \to 0 \text{ as } \epsilon \to 0 \text{ for any } \alpha > 0.$$

For $0 > \alpha > -1$

$$\nabla \cdot \left(-\frac{K^\epsilon}{\mu(c^\epsilon)} \nabla p^\epsilon \right) = f$$

$$\Rightarrow \nabla \cdot \left(-\lambda(c^\epsilon) \nabla p^\epsilon \right) = f \tag{3.176}$$

We define $\lambda(c^\epsilon)$ in the following way

$$\lambda(c^\epsilon) = \begin{bmatrix} \epsilon^\alpha & 0 \\ 0 & \epsilon^\beta \end{bmatrix} \mu^{-1}(c^\epsilon) = \tilde{\mu}(c^\epsilon) \begin{bmatrix} \epsilon^\alpha & 0 \\ 0 & \epsilon^\beta \end{bmatrix} \tag{3.177}$$

Let c^ϵ be given and that the following holds

$$0 < \tilde{\mu}_1 \leq \mu^{-1}(c^\epsilon) \leq \tilde{\mu}_0$$

Using eq. (3.177) we transform eq. (3.176) info weak formulation:

$$\left(\tilde{\mu}(c^\epsilon) \partial_x p^\epsilon, \partial_x \varphi \right) + \left(\epsilon^{\beta-\alpha} \partial_\eta p^\epsilon, \partial_\eta \varphi \right) = (f, \varphi) \tag{3.178}$$

Let $\varphi = \varphi(x)$ and

$$\bar{f} = \int_0^1 f \, d\eta$$

$$\int_0^1 \left(\int_0^1 \tilde{\mu}(c^\epsilon) \partial_x p^\epsilon \, d\eta \right) \partial_x \varphi \, dx = \int_0^1 \epsilon^{-\alpha} \bar{f} \varphi \, dx \tag{3.179}$$

$$\varphi = \bar{p}^\epsilon$$

$$\Rightarrow \int_0^1 \left(\int_0^1 \tilde{\mu}(c^\epsilon) \partial_x p^\epsilon \, d\eta \right) \partial_x \bar{p}^\epsilon \, dx = \int_0^1 \epsilon^{-\alpha} \bar{f} \bar{p}^\epsilon \, dx \tag{3.180}$$

$$\int_0^1 \int_0^1 \tilde{\mu}(c^\epsilon) \partial_x p^\epsilon \partial_x \bar{p}^\epsilon \, dx \, d\eta =$$
$$\int_0^1 \int_0^1 \bar{\tilde{\mu}}(c^\epsilon) \partial_x p^\epsilon \partial_x \bar{p}^\epsilon \, dx \, d\eta + \int_0^1 \int_0^1 \left(\tilde{\mu}(c^\epsilon) - \bar{\tilde{\mu}}(c^\epsilon) \right) \partial_x p^\epsilon \partial_x \bar{p}^\epsilon \, dx \, d\eta$$

$$\int_0^1 \bar{\tilde{\mu}}(c^\epsilon) \left(\partial_x \bar{p}^\epsilon \right)^2 \, dx + \int_0^1 \int_0^1 \left(\tilde{\mu}(c^\epsilon) - \bar{\tilde{\mu}}(c^\epsilon) \right) \partial_x p^\epsilon \partial_x \bar{p}^\epsilon \, dx \, d\eta \tag{3.181}$$

Here we assume the following

- $\left\| \tilde{\mu}(c^\epsilon) - \bar{\tilde{\mu}}(c^\epsilon) \right\|_{L^\infty} \to 0$ as $\epsilon \to 0$
- $\| c^\epsilon - \bar{c}^\epsilon \|_{L^\infty} \to 0$
- $\tilde{\mu}$ is a smooth function (upscaled).

This reduces to c^ϵ being bounded.

$$\| \partial_x \bar{p}^\epsilon \| \leq C$$
$$\| \bar{p}^\epsilon \| \leq C$$

$$\Rightarrow \bar{p}^\epsilon \to \bar{p} \text{ (strongly)}$$
$$\Rightarrow \partial_x \bar{p}^\epsilon \to \partial_x \bar{p} \text{ (weakly)}$$

$$\int_0^1 \int_0^1 \tilde{\mu}(c^\epsilon) \partial_x \bar{p}^\epsilon \partial_x \varphi \to \int_0^1 \tilde{\mu}(\bar{c}) \partial_x \bar{p} \partial_x \varphi \tag{3.182}$$

$$\Rightarrow \tilde{\mu}(c^\epsilon) \to \tilde{\mu}(\bar{c})$$
$$\Rightarrow \partial_x \bar{p}^\epsilon \to \partial_x \bar{p} \text{ (weakly)}$$

We then take $\alpha = -\frac{1}{2}$ and obtain the following

$$\bar{q}_1^\epsilon = -\epsilon^\alpha \partial_x \bar{p}^\epsilon \sim -\epsilon^{-\frac{1}{2}} \tag{3.183}$$

$$\| q_1^\epsilon - \bar{q}_1 \| \sim -\epsilon^{-\frac{1}{2}} \tag{3.184}$$

$$\| c^\epsilon - \bar{c} \| \sim \epsilon \tag{3.185}$$

3.4 Indicators

From the paper of G. Menon, F. Otto, Dynamic Scaling in Miscible Viscous Fingering [20], they purpose a few indicators of viscous fingering. These indicators we will show that be used to test the relationship between a vertical-averaged 2D-model and a full 1D model. We will start by defining the different indicators.

The first of these is the measure the width of fingers. Therefore they define the mean perimeter, $E(t)$, as the following

$$P(t) = \fint \left|\nabla c(x,y,t)\right| dx = \int_{\mathbb{R}} \frac{1}{\epsilon} \int_0^\epsilon \sqrt{\left(\partial_x c(x,y,t)\right)^2 + \left(\partial_y c(x,y,t)\right)^2} dy\, dx \tag{3.186}$$

where $c(x,y,t)$ is the local concentration at time t and position (x,y). The next indicator is what the cited paper defines as the *gravitational potential energy*

$$E(t) = \fint \left[c(x,y,t) - c_0(x)\right] x dx = \int_{\mathbb{R}} \frac{1}{\epsilon} \int_0^\epsilon \left[c(x,y,t) - c_0(x)\right] x\, dy\, dx \tag{3.187}$$

The two next equations are two so called *entropy* functions. These functions is a measure of the zone of the domain which, by the paper is called "*mushy zone*", has the following: $0 < c(x,t) < 1$

$$H(t) = \fint c(1-c) dx = \int_{\mathbb{R}} \frac{1}{\epsilon} \int_0^\epsilon c(x,y,t)(1 - c(x,y,t)) dy\, dx \tag{3.188}$$

$$S(t) = -\fint \left(c\, log(c) + (1-c)\, log(1-c)\right) dx = \int_{\mathbb{R}} \frac{1}{\epsilon} \int_0^\epsilon \left(c\, log(c) + (1-c)\, log(1-c)\right) dy\, dx \tag{3.189}$$

We will now prove the relationship between the parameters to understand the measures. We will use this on the system

$$\begin{aligned} \partial_t c + \underline{\mathbf{u}} \cdot \nabla c - D\Delta c &= 0 \\ \nabla \cdot \underline{\mathbf{u}} &= 0 \end{aligned} \tag{3.190}$$

Let the flux, $\underline{\mathbf{u}}$ be given. We then differentiate the equation (3.187) with respect to time, t. We then get

$$\frac{\partial E}{\partial t} = -\int_{\mathbb{R}} \frac{1}{\epsilon} \int_0^\epsilon \frac{\partial c}{\partial t}\, dy\, dx \tag{3.191}$$

Going back to the system (3.190) we get

$$\frac{\partial c}{\partial t} + \underline{\mathbf{u}} \cdot \nabla c - D\Delta c = 0$$

We multiply through the equation by x

$$\frac{\partial c}{\partial t} x + \underline{\mathbf{u}} \cdot \nabla c\, x - D\Delta c\, x = 0 \tag{3.192}$$

Integrating over the domain and using partial integration we get

$$\int_{\mathbb{R}} \frac{1}{\epsilon} \int_0^\epsilon \frac{\partial c}{\partial t} x\, dy\, dx - \int_{\mathbb{R}} \frac{1}{\epsilon} \int_0^\epsilon \underline{\mathbf{u}} \cdot \nabla x\, c\, dy\, dx + \int_{\mathbb{R}} \frac{1}{\epsilon} \int_0^\epsilon D\nabla c \cdot \nabla x\, dy\, dx = 0 \tag{3.193}$$

$$\int_{\mathbb{R}} \frac{1}{\epsilon} \int_0^\epsilon \frac{\partial c}{\partial t} x\, dy\, dx = \int_{\mathbb{R}} \frac{1}{\epsilon} \int_0^\epsilon \underline{\mathbf{u}} \cdot \nabla x\, c - \int_{\mathbb{R}} \frac{1}{\epsilon} \int_0^\epsilon D\nabla c \cdot \nabla x\, dy\, dx \tag{3.194}$$

$$\int_{\mathbb{R}} \frac{1}{\epsilon} \int_0^\epsilon \frac{\partial c}{\partial t} x\, dy\, dx = I_1 + I_2 \tag{3.195}$$

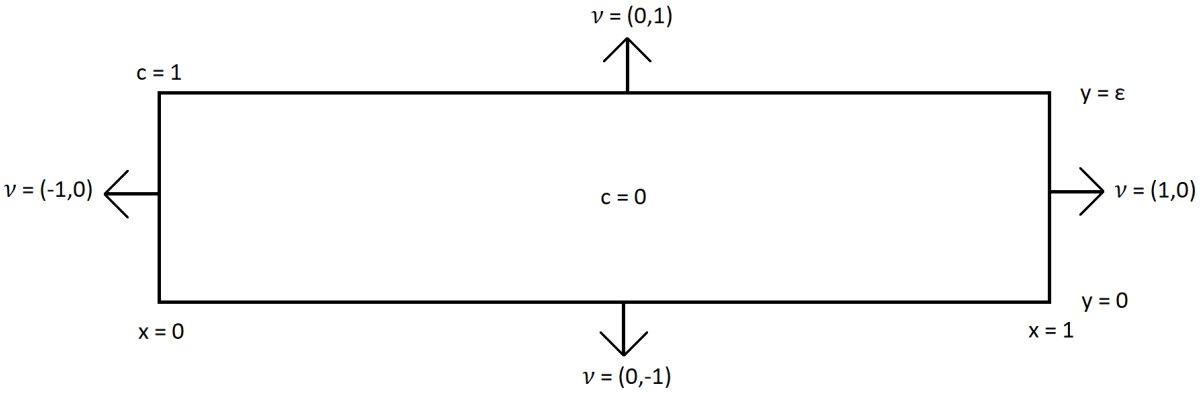

Figure 3.1: The bondaries and its values for eq. (3.197)

where

$$I_1 = \int_{\mathbb{R}} \frac{1}{\epsilon} \int_0^{\epsilon} \underline{\mathbf{u}} \cdot \nabla x \, c \, dy \, dx = \int_{\mathbb{R}} \frac{1}{\epsilon} \int_0^{\epsilon} \left(\underline{\mathbf{u}} \cdot \underline{\hat{\mathbf{e}_1}} \right) \, c \, dy \, dx = \int_{\mathbb{R}} \frac{1}{\epsilon} \int_0^{\epsilon} u_1 \, c \, dy \, dx \tag{3.196}$$

$$I_2 = -\int_{\mathbb{R}} \frac{1}{\epsilon} \int_0^{\epsilon} D \nabla c \cdot \nabla x \, dy \, dx = -\int_{\mathbb{R}} \frac{1}{\epsilon} \int_0^{\epsilon} D \nabla c \cdot \underline{\hat{\mathbf{e}_1}} \, dy \, dx = -D \int_{\partial\Omega} c \, \underline{\hat{\mathbf{e}_1}} \cdot \underline{\hat{\nu}} \tag{3.197}$$

Using the boundary data visualized in the figure above, we get the following for eq. (3.197)

$$I_2 = -D \int_{\partial\Omega} c \, \underline{\hat{\mathbf{e}_1}} \cdot \underline{\hat{\nu}} = D \tag{3.198}$$

Thus

$$\frac{\partial E}{\partial t} = -\int_{\mathbb{R}} \frac{1}{\epsilon} \int_0^{\epsilon} u_1 \, c \, dy \, dx + D \tag{3.199}$$

We assume that the following holds,

$$-\int_{\mathbb{R}} \frac{1}{\epsilon} \int_0^{\epsilon} u_1 \, c \, dy \, dx \leq C \, E^{\alpha}, \alpha > 0 \tag{3.200}$$

where C depends on assumption of u_1. Thus we can bound the growth rate of E

$$\frac{\partial E}{\partial t} \leq C \, E^{\alpha} + D \tag{3.201}$$

We then turn to indicator $H(t)$

$$H(t) = \int_{\mathbb{R}} \frac{1}{\epsilon} \int_0^{\epsilon} c(1-c) \, dy \, dx$$

Again using system (3.190) and multiply by $g'(c)$ we get

$$\frac{\partial c}{\partial t} g'(c) + \underline{\mathbf{u}} \cdot \nabla c \, g'(c) - D \Delta c \, g'(c) = 0 \tag{3.202}$$

Integrating over the domain, using partial integration on all terms and applying the boundary conditions we have

$$\frac{d}{dt} \int g(c) dx + \int_{\mathbb{R}} \frac{1}{\epsilon} \int_0^{\epsilon} \underline{\mathbf{u}} \cdot \nabla g(c) \, dy \, dx + \int_{\mathbb{R}} \frac{1}{\epsilon} \int_0^{\epsilon} D |\nabla c|^2 \, g''(c) \, dy \, dx = 0 \tag{3.203}$$

However, by using partial integration once more on the transport term

$$\int_{\mathbb{R}} \frac{1}{\epsilon} \int_0^\epsilon \underline{\mathbf{u}} \cdot \nabla g \, dy = \int_{\mathbb{R}} \frac{1}{\epsilon} \int_0^\epsilon \nabla \cdot (\underline{\mathbf{u}} g) \, dy \, dx$$

Applying the divergence theorem to this term, choosing $g(c) = c(1-c)$ and evaluating at the boundary, we get

$$\int_{\mathbb{R}} \frac{1}{\epsilon} \int_0^\epsilon \nabla \cdot (\underline{\mathbf{u}} g) \, dy \, dx = \int_{\partial\Omega} g \underline{\mathbf{u}} \cdot \nu = 0$$

Thus equation (3.203) reduces to

$$\frac{d}{dt} \fint g(c) dx = 2D \int_{\mathbb{R}} \frac{1}{\epsilon} \int_0^\epsilon |\nabla c|^2 \, dy \, dx \tag{3.204}$$

$$\frac{d}{dt} \fint c(1-c) dx = 2D \int_{\mathbb{R}} \frac{1}{\epsilon} \int_0^\epsilon |\nabla c|^2 \, dy \, dx \tag{3.205}$$

Using system (3.190) again and multiplying by c we get

$$\frac{\partial c}{\partial t} c + \underline{\mathbf{u}} \cdot \nabla c \, c - D \Delta c \, c = 0 \tag{3.206}$$

Integrating over the domain and using partial integration we obtain

$$\frac{d}{dt} \fint |c|^2 + \fint D |\Delta c|^2 \, c + \fint u \cdot \nabla c \, c = 0 \tag{3.207}$$

Using the chain rule,

$$\fint u \cdot \nabla c \, c = \frac{1}{2} \fint \left(\nabla \cdot (\underline{\mathbf{u}} c^2) \right)$$

Since $g(c)$ is a concave function ($g''(c) = -2$, we have for $x_1 \leq x_2$:

$$g\left(\frac{x_1 + x_2}{2} \right) \geq \frac{1}{2} g(x_1) + \frac{1}{2} g(x_2)$$

Thus

$$H(t) \leq \frac{1}{2} \int_{\mathbb{R}} \frac{1}{\epsilon} \int_0^\epsilon c(1-\bar{c}) \, dy \, dx + \frac{1}{2} \int_{\mathbb{R}} \frac{1}{\epsilon} \int_0^\epsilon \bar{c}(1-c) \, dy \, dx = \int_{\mathbb{R}} \bar{c}(1-\bar{c}) \, dx \tag{3.208}$$

We then consider

$$\begin{aligned} \int_{\mathbb{R}} \frac{1}{\epsilon} \int_0^\epsilon (c-\bar{c})^2 \, dy \, dx &= \int_{\mathbb{R}} \frac{1}{\epsilon} \int_0^\epsilon c^2 - 2c\bar{c} + \bar{c}^2 \, dy \, dx \\ &= \int_{\mathbb{R}} \frac{1}{\epsilon} \int_0^\epsilon c^2 - 2\bar{c}^2 + \bar{c}^2 \, dy \, dx \\ &= \int_{\mathbb{R}} \frac{1}{\epsilon} \int_0^\epsilon c^2 - \bar{c}^2 \, dy \, dx \end{aligned}$$

Adding and subtracting c in the equation above, we have

$$\begin{aligned} \int_{\mathbb{R}} \frac{1}{\epsilon} \int_0^\epsilon c^2 + c - c - \bar{c}^2 \, dy \, dx &= \int_{\mathbb{R}} \frac{1}{\epsilon} \int_0^\epsilon c^2 - c \, dy \, dx + \int_{\mathbb{R}} \bar{c} - \bar{c}^2 \, dx \\ &= \int_{\mathbb{R}} \frac{1}{\epsilon} \int_0^\epsilon c(c-1) \, dy \, dx + \int_{\mathbb{R}} \bar{c}(1-\bar{c}) \, dx \\ &= -H(t) + \int_{\mathbb{R}} \bar{c}(1-\bar{c}) \geq 0 \end{aligned}$$

Thus

$$H(t) \leq \int_{\mathbb{R}} \bar{c}(1-\bar{c}) \tag{3.209}$$

Using the proofs from the paper [20], we know that

$$\int_{\mathbb{R}} \bar{c}(1-\bar{c}) \leq C\, E(t)^{\frac{1}{2}}$$

Therefore

$$H(t) \leq C\, E(t)^{\frac{1}{2}} \tag{3.210}$$

$$\begin{aligned} P(t) = \int_{\mathbb{R}} \frac{1}{\epsilon} \int_0^{\epsilon} |\nabla c| &= \int_{\mathbb{R}} \frac{1}{\epsilon} \int_0^{\epsilon} \frac{|\nabla c|\, c^{\frac{1}{2}}(1-c^{\frac{1}{2}})}{c^{\frac{1}{2}}(1-c^{\frac{1}{2}})} \\ &\leq \left(\int_{\mathbb{R}} \frac{1}{\epsilon} \int_0^{\epsilon} \frac{|\nabla c|}{c^{\frac{1}{2}}(1-c^{\frac{1}{2}})} \right)^{\frac{1}{2}} \left(c^{\frac{1}{2}} \int_{\mathbb{R}} \frac{1}{\epsilon} \int_0^{\epsilon} (1-c^{\frac{1}{2}}) \right)^{\frac{1}{2}} \\ &= \left(\frac{dS(t)}{dt} \right)^{\frac{1}{2}} H(t)^{\frac{1}{2}} \end{aligned}$$

Integrating $P(t)$ from $t = 0$ to $t = t$

$$\int_0^t P(\tau) d\tau \leq \int_0^t \left(\frac{dS(\tau)}{dt} \right)^{\frac{1}{2}} H(\tau)^{\frac{1}{2}} d\tau \leq H(t)^{\frac{1}{2}} S(t)^{\frac{1}{2}} \tag{3.211}$$

This comes from the monotonicity of $H(t)$. Therefore we have the following relations

$$\frac{dE(t)}{dt} \leq Ct^{\alpha} \tag{3.212}$$

$$\frac{dH(t)}{dt} \leq CE^{\frac{1}{2}}, \quad \rightarrow H \sim t^{\beta} \tag{3.213}$$

$$\frac{dS(t)}{dt} \leq CE^{\frac{1}{2}}, \quad \rightarrow S \sim t^{\beta} \tag{3.214}$$

$$P(t) \leq \left(\frac{dS(t)}{dt} \right)^{\frac{1}{2}} H(t)^{\frac{1}{2}}, \quad \rightarrow P \sim t^{\beta} \tag{3.215}$$

From eq. (X.X) and if we assume $u_1 \sim \epsilon^{\alpha}$, this gives $C = \epsilon^{\alpha}\tilde{C}$

$$\frac{dE(t)}{dt} \leq \epsilon^{\alpha} C E^{\frac{1}{2}} + \epsilon^{\gamma} D$$

$$\int \frac{dE}{\epsilon^{\alpha} C E^{\frac{1}{2}} + \epsilon^{\gamma} D} \leq \int dt \tag{3.216}$$

Where the first part is due to the flow velocity and the other is due to the diffusion coefficient. Using substitution, long division we end up with the final relation which is an implicit function in E

$$\frac{2\epsilon C E^{\frac{1}{2}} - 2\epsilon^{\gamma} D ln(\epsilon^{\alpha} C E^{\frac{1}{2}} + \epsilon^{\alpha} D)}{\epsilon^{2\alpha} C^2} \leq t + C_2 \tag{3.217}$$

Chapter 4

Numerical Results

In this chapter, a study of different numerical results will be covered. The first section (4.1) we will provide the numerical results for a constructed solution utilized on our implementation. The approach is to consider a known solution of pressure and concentration. This is then used to calculate the exact flux and concentration profile. These are then used to study the performance of the FEniCS implementation. The convergence rates and error-norms are presented in the later part of this section.

In section (4.2) we study the impact on the solution of different parameters in our model. Subsection (4.2.1) presents numbers of difference between the the vertical-averaged 2D model and 1D model for different step-sizes, where the step-size is the length of the hypotenuse of the triangular grid-cells. This is again shown for five different lengths for three different cases, (a) $\alpha = 0$, $\beta = 0$ and $D = 0.05$ (diffusion), (b) $\alpha = 0$, $\beta = 0$ and $D = 0.1$ and (c) $\alpha = 1$, $\beta = 2$ and $D = 0.05$.

The next subsection (4.2.2) cover the dependence of ϵ in our model. ϵ is the width of the thin strip and is also controlling the permeability (see equation 2.26). Here the l_2- and l_∞-norms, for the difference in the two models we consider, are presented for again three cases; (a) $\alpha = -1$, $\beta = -1$ and $D = 0.05$ (diffusion), (b) $\alpha = 0$, $\beta = 0$ and $D = 0.05$ and (c) $\alpha = 1$, $\beta = 2$ and $D = 0.05$.

The third subsection (4.2.3) cover the strength of coupling of our coupled flow- and transport model. A higher iteration count means that there is a stronger coupling. The approach here is to use up to 5 different function for viscosity; $exp(-c)$, $exp(-2c)$, $exp(-3c)$, $exp(-4c)$ and $exp(-5c)$. These has an increasing negative steepness and results in more changes for a changed concentration. For the case when $\alpha = \beta = 0$ the model did not converge for any functions steeper than $exp(-2c)$, so these have been omitted in the plots. All plots of the iteration-counts are plotted with the iteration count on the vertical axis and time on the horizontal axis. For the divergent simulations, the series plot has been set to dashed. The cases studied is (a) $\alpha = -1$, $\beta = -1$ and $D = 0.05$, (b) $\alpha = 1$, $\beta = 2$ and $D = 0.05$ and (c) $\alpha = 0$, $\beta = 0$ and $D = 0.05$.

The last of the subsections under this section is the (4.2.4) which covers the impact of ϵ on the magnitude of the flow. This shows briefly that for a smaller ϵ, strip width, the magnitude of the flow decreases and the differences between the two models does also decrease until some limit. When this limit is reached (in this case it is for $\epsilon = 0.05$) the error increases again.

The third section (4.3) of this chapter, the quantities porposed by G. Menon, F. Otto in *Dynamic Scaling in Miscible Viscous Fingering* [20] are considered. These incorporates the geometric features of the concentration profile and are compared for the vertical-averaged 2D- and 1D-model. These indicators are studied for a isotropic and anisotropic permeability. The section focuses on the differences of the vertical-averaged 2D- and 1D-model and tries to minimize this difference by adjusting the diffusion for the 1D-model. The magnitude of the diffusion for 1D-model will be investigated together with the permeability values to check if this adjustment is due to a Taylor Dispersion term missing.

The last section (4.4) of this chapter is *Indicators of comparison for a turbulent flow with gravity of vertical-averaged 2D- and 1D-model*. This section compares the different indicators from [20] with the dependence on the diffusion coefficient, D, and on the width of the thin strip, ϵ. All cases is considered with the presence of gravity and a viscosity which depends on the local concentration. The permeability is in the first of the cases (4.4.1) considered anisotropic with a low flux and almost no difference of concentration in the y-direction. The next case (4.4.2) considers isotropic permeability a medium flux with a small difference of concentration in the y-direction. This causes some turbulence which is reflected in the results and it is clear that there is more difference here. Finally, the last case (4.4.3) again considers an anisotropic permeability, but with a high flux. This case also features a larger difference of concentration in the y-direction. This case causes more turbulence than Case 2 which results in even more fluctuations in the indicators. As expected the first case shows little variation in terms of instability while the two last cases features more instability and therefore more fluctuations.

4.1 Reference solution

The implementation has been implemented using the Dual-Mixed formulation by FEniCS [28]. The reference solution is used on the system of equations mentioned in the Preliminaries, section (2.8). The model studied is reduced to the following:

$$\begin{aligned} \underline{\mathbf{u}} + \boldsymbol{K}\nabla p = 0, &\quad \text{in } \Omega \\ \nabla \cdot \underline{\mathbf{u}} = f, &\quad \text{in } \Omega \end{aligned}$$

with the following boundary conditions

$$\underline{\mathbf{u}} = \underline{\mathbf{u_0}}, \text{ on } \Gamma \tag{4.1}$$

$$-\underline{\mathbf{u}} \cdot \hat{\underline{\mathbf{n}}} = f, \text{ on } \Gamma \tag{4.2}$$

where f is a given function. The domain, Ω, is defined as the following

$$\Omega = [0, 5] \times [0, 1]$$

and the boundary

$$\Gamma = \partial\Omega$$

This is then solved using the *Finite element method* through the *FEniCS*-framework. It is therefore needed to transform equation (4.1) into a variational formulation. Initially, a derivation of the weak formulation of the equation is performed:

$$\int_\Omega \underline{\mathbf{u}} \cdot w \, dx + \int_\Omega \boldsymbol{K}\nabla p \cdot w \, dx = 0 \tag{4.3}$$

$$\int_\Omega \nabla \cdot \underline{\mathbf{u}} \, v \, dx = \int_\Omega f \, v \, dx \tag{4.4}$$

where the spaces for the test-functions are defined like

$$V_1 = \left\{ v : v \text{ is continuous on } \Omega, \frac{\partial v}{\partial x_1} \text{ and } \frac{\partial v}{\partial x_2} \text{ are piecewise continuous on } \Omega \text{ and } v = 0 \text{ on } \Gamma \right\}$$

$$V_2 = \left\{ w : w \text{ is continuous on } \Omega, \frac{\partial w}{\partial x_1} \text{ and } \frac{\partial w}{\partial x_2} \text{ are piecewise continuous on } \Omega \text{ and } w = 0 \text{ on } \Gamma \right\}$$

Seeking a solution u which satisfies eq. (4.1), in addition to the problem:

Find $u \in V$ such that $a(u, v) = L(v) \quad \forall v \in V$ where

$$a(u, v) = \int_\Omega \underline{\mathbf{u}} \cdot w \, dx + \int_\Omega \boldsymbol{K} \nabla p + \int_\Omega \nabla \cdot \underline{\mathbf{u}} \, v \, dx \tag{4.5}$$

and

$$L(v) = \int_\Omega f \, v \, dx \tag{4.6}$$

A reference solution is then constructed to be able to calculate the errors. The pressure will be given by the following function:

$$p(x, y) = x(x - 5)y(y - 1) \tag{4.7}$$

The following boundary conditions are also added to the model:

$$p_0 = \begin{cases} 1 & : x = 0 \\ 0 & : x = 5 \end{cases} \tag{4.8}$$

Where the permeability tensor, $\boldsymbol{K}$, is of the following form:

$$\boldsymbol{K} = \begin{bmatrix} 2 & 0 \\ 0 & 1 \end{bmatrix}$$

Combining eq. (4.1) and (4.7) into eq. (2.3) will result in the following equation for the flux:

$$\underline{\mathbf{u}}(x, y) = \begin{bmatrix} 2(5 - 2x)y(x - 1) \\ (1 - 2y)x(x - 5) \end{bmatrix} \tag{4.9}$$

Furthermore, a reference solution for the concentration is constructed

$$c(x, y, t) = (5 - x)y(1 - y)t \tag{4.10}$$

with the following boundary- and initial-values:

$$c_0 = \begin{cases} 1 & : x = 0 \\ 0 & : x \neq 0, t = 0 \end{cases} \tag{4.11}$$

This was solved using a mesh with the following domain-size:

$$(x, y) = [0, 5] \times [0, 1]$$

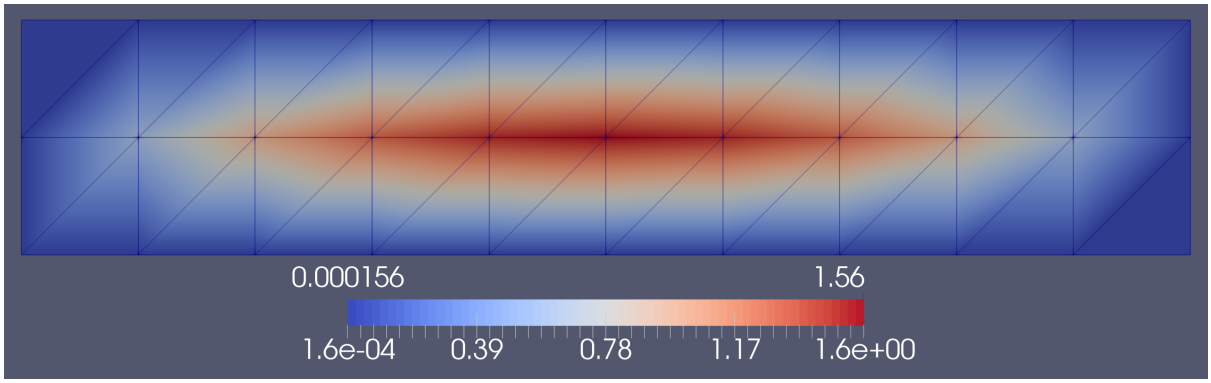

Figure 4.1: The computed reference solution for pressure

As can be seen in this plot, the pressure has a maximum in the middle of the domain, where it reaches around $p(2.5, 0.5) = 1.56$. This has the associated flux profiles which can be seen on fig. (4.2) and (4.3).

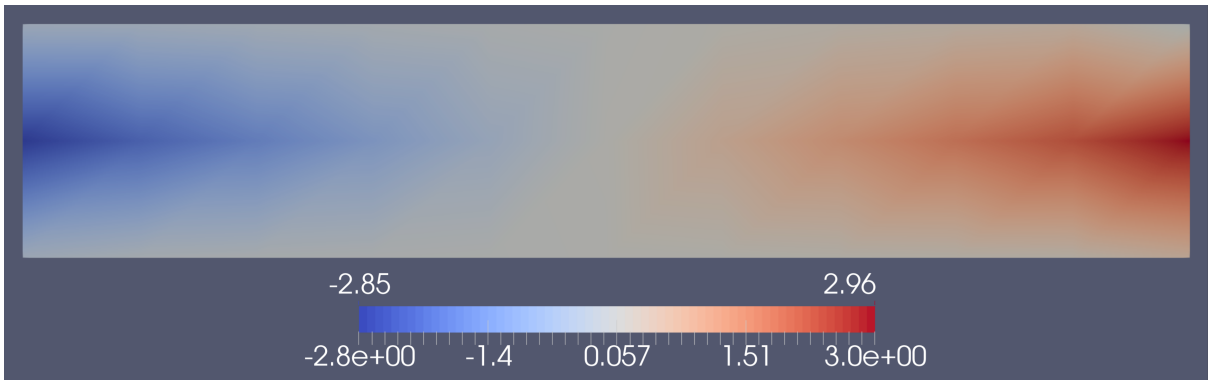

Figure 4.2: Magnitude of flux in x-direction

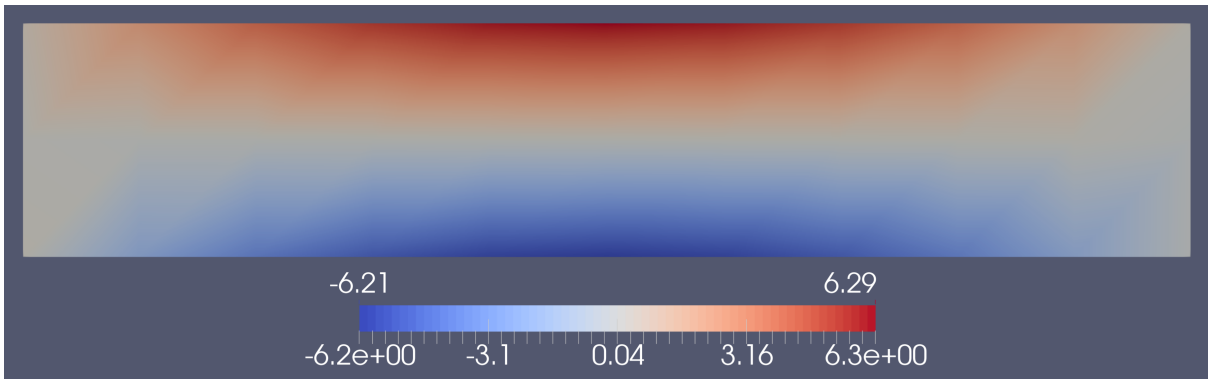

Figure 4.3: Magnitude of flux in y-direction

The plots below shows the concentration profile for propagation, at 3 different points in time, t.

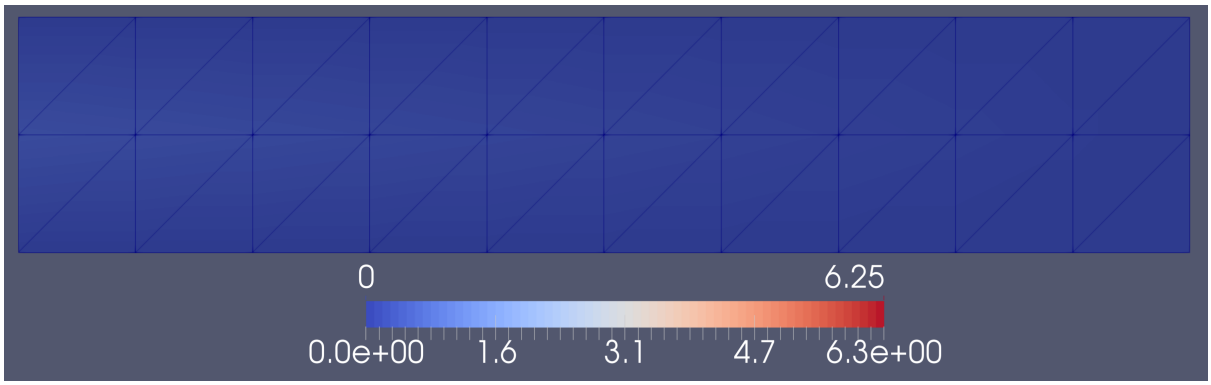

Figure 4.4: Computed concentration at $t = 0.25$

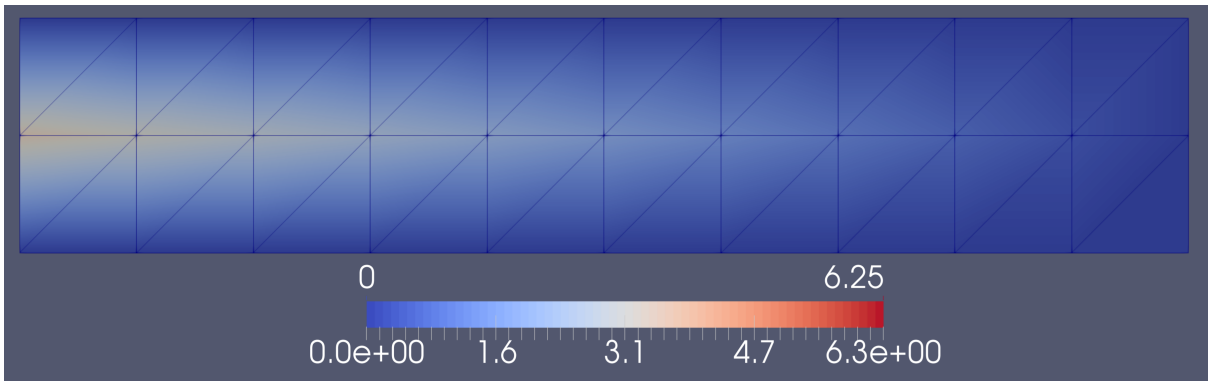

Figure 4.5: Computed concentration at $t = 2.75$

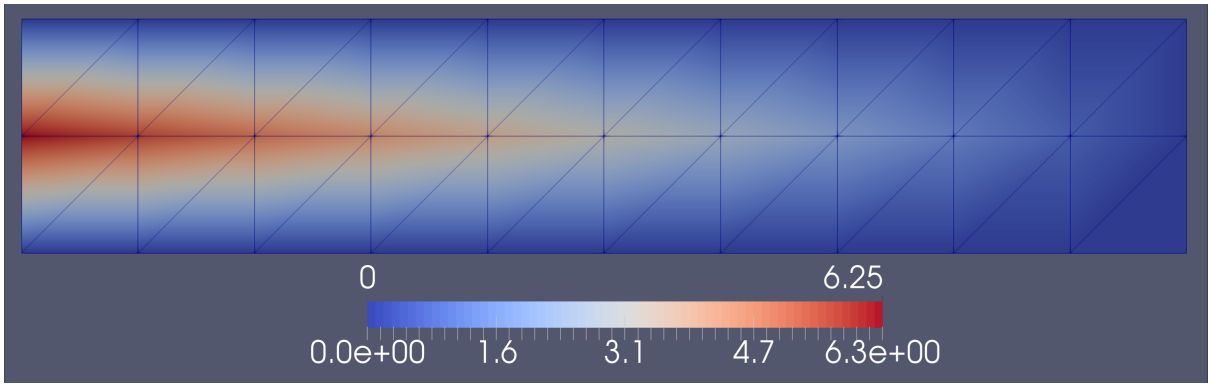

Figure 4.6: Computed concentration at $t = 5.0$

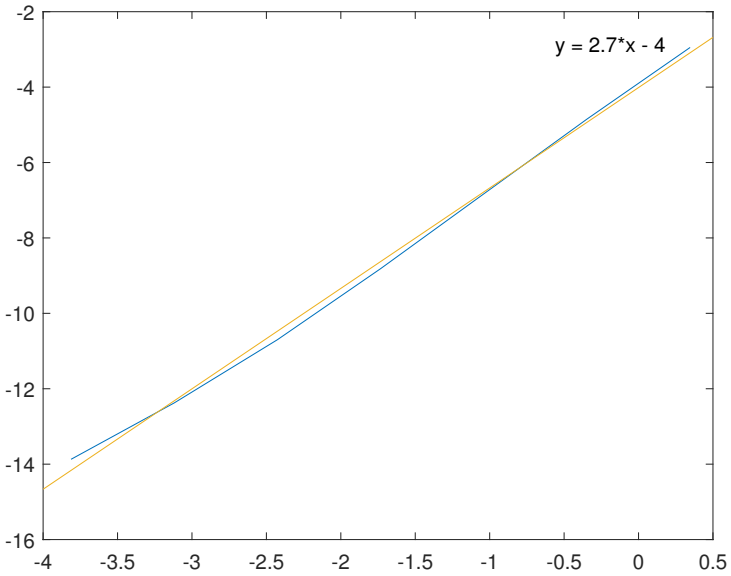

Figure 4.7: Logarithmic plot for error in flux against step-size, h

In figure (4.7) the logarithm of the error in flux (vertical axis) is plotted against the logarithm of step-size, h (horizontal axix). The blue line is the error series and the yellow line is the linear regression, which show that the convergence in error is 2.7. This means that the error decreases more than quadratically for decreasing step-size (fining of the mesh-size).

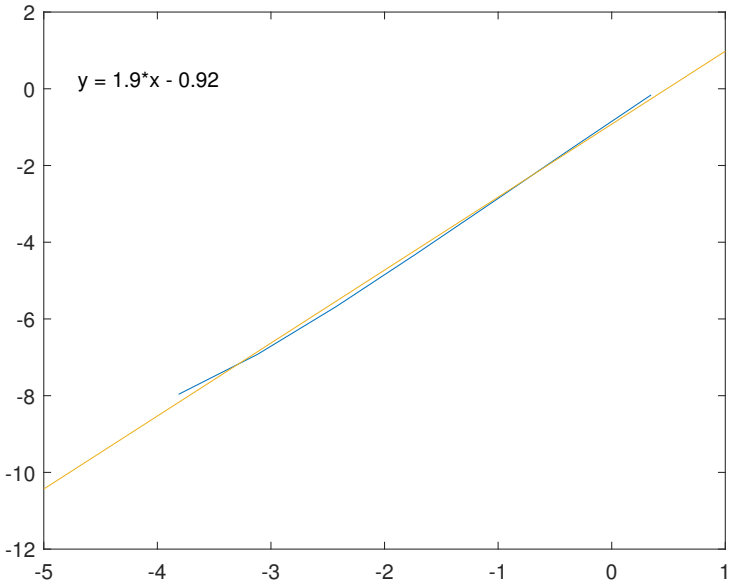

Figure 4.8: Logarithmic plot for error in pressure against step-size, h

In figure (4.8) the logarithm of the error in pressure (vertical axis) is plotted against the logarithm of step-size, h (horizontal axix). The blue line is the error series and the yellow line is the linear regression, which show that the convergence in error for pressure is 1.9. This means that the error in pressure decreases slightly less than quadratically for decreasing step-size (fining of the mesh-size).

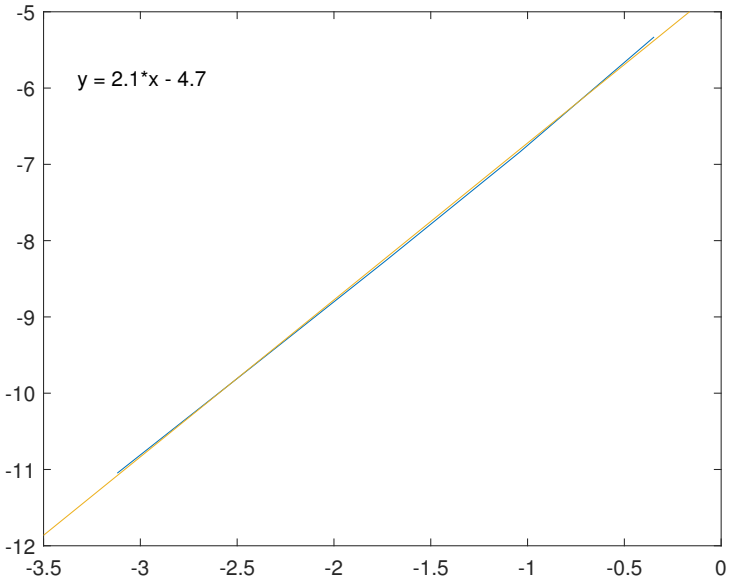

Figure 4.9: Logarithmic plot for error in concentration against step-size, h

In figure (4.9) the logarithm of the error in concentration (vertical axis) is plotted against the logarithm of step-size, h (horizontal axix). The blue line is the error series and the yellow line is the linear regression, which show that the convergence in error for concentration is 2.1. This means again that the error in concentration also decreases more than quadratically for decreasing step-size (fining of the mesh-size), like the flux.

When decreasing the time-step parameter, the simulations seems to have no significant difference in errors. This means that the errors in the simulations is dominated by the spacial and/or discretization error.

	1	2	3	4	5	6	7
h	1.414	$7.071 \cdot 10^{-1}$	$3.536 \cdot 10^{-1}$	$1.768 \cdot 10^{-1}$	$8.839 \cdot 10^{-2}$	$4.419 \cdot 10^{-2}$	$2.210 \cdot 10^{-2}$
l_2	$5.242 \cdot 10^{-2}$	$7.838 \cdot 10^{-3}$	$1.079 \cdot 10^{-3}$	$1.484 \cdot 10^{-4}$	$2.256 \cdot 10^{-5}$	$4.220 \cdot 10^{-6}$	$9.460 \cdot 10^{-7}$
l_∞	$6.801 \cdot 10^{-2}$	$1.320 \cdot 10^{-3}$	$1.916 \cdot 10^{-3}$	$2.807 \cdot 10^{-4}$	$4.667 \cdot 10^{-5}$	$1.173 \cdot 10^{-5}$	$2.937 \cdot 10^{-6}$
p	–	2.74	2.86	2.86	2.72	2.42	2.16

h: Step-size (length of hypotenuse in triangles in mesh)
l_2: l_2-norm of the error
l_∞: l_∞-norm of the error
p: The computed convergence rate

Table 4.1: Numbers for the convergence for flux

4.2 Comparing the vertical-averaged 2D-model with the 1D-model

4.2.1 Analyses of the errors due to the step-size

The convergence rate was studied by running simulations and measuring the errors at a fixed time, $t = 0.5$ (halfway through the simulation). The following results were obtained from the simulations:

	1	2	3	4	5
h	$1.005 \cdot 10^{-1}$	$5.099 \cdot 10^{-2}$	$2.695 \cdot 10^{-2}$	$1.601 \cdot 10^{-2}$	$1.179 \cdot 10^{-2}$
l_2	$1.255 \cdot 10^{-1}$	$1.253 \cdot 10^{-1}$	$1.224 \cdot 10^{-1}$	$1.207 \cdot 10^{-1}$	$1.202 \cdot 10^{-1}$
l_∞	$2.449 \cdot 10^{-1}$	$2.388 \cdot 10^{-1}$	$2.325 \cdot 10^{-1}$	$2.292 \cdot 10^{-1}$	$2.283 \cdot 10^{-1}$

h: Step-size (length of hypotenuse in triangles in mesh)
l_2: l_2-norm of the error
l_∞: l_∞-norm of the error

Table 4.2: Comparing the errors between the vertical-averaged 2D-model and the 1D-model for $\alpha = 0, \beta = 0$ and $D = 0.05$

	1	2	3	4	5
h	$1.005 \cdot 10^{-1}$	$5.099 \cdot 10^{-2}$	$2.695 \cdot 10^{-2}$	$1.601 \cdot 10^{-2}$	$1.179 \cdot 10^{-2}$
l_2	$9.528 \cdot 10^{-2}$	$9.447 \cdot 10^{-2}$	$9.338 \cdot 10^{-2}$	$9.272 \cdot 10^{-2}$	$9.249 \cdot 10^{-2}$
l_∞	$1.565 \cdot 10^{-1}$	$1.542 \cdot 10^{-1}$	$1.527 \cdot 10^{-1}$	$1.516 \cdot 10^{-1}$	$1.513 \cdot 10^{-1}$

h: Step-size (length of hypotenuse in triangles in mesh)
l_2: l_2-norm of the error
l_∞: l_∞-norm of the error

Table 4.3: Comparing the errors between the vertical-averaged 2D-model and the 1D-model for $\alpha = 0, \beta = 0$ and $D = 0.1$

	1	2	3	4	5
h	$1.005 \cdot 10^{-1}$	$5.099 \cdot 10^{-2}$	$2.695 \cdot 10^{-2}$	$1.601 \cdot 10^{-2}$	$1.179 \cdot 10^{-2}$
l_2	$1.523 \cdot 10^{-2}$	$1.227 \cdot 10^{-2}$	$1.199 \cdot 10^{-2}$	-	$1.287 \cdot 10^{-2}$
l_∞	$3.102 \cdot 10^{-2}$	$2.460 \cdot 10^{-2}$	$2.435 \cdot 10^{-2}$	-	$2.615 \cdot 10^{-2}$

h: Step-size (length of hypotenuse in triangles in mesh)
l_2: l_2-norm of the error
l_∞: l_∞-norm of the error

Table 4.4: Comparing the errors between the vertical-averaged 2D-model and the 1D-model for $\alpha = 1, \beta = 2$ and $D = 0.1$

As can be seen in the tables (4.2), (4.3) and (4.4), when $\alpha = 0, \beta = 0$, the decreasing of the mesh-size barely influences the magnitute of the errors. This is because the errors are not caused by the mesh-size and, but rather the low diffusion coefficients used in these examples. In the following section, the errors caused by the width of the strip, ϵ, are studied in greater detail. The ϵ controls the width of the thin strip and the permeability tensor.

4.2.2 Analysis of the errors due to the width of the thin strip, ϵ

The three tables below shows the l_2- and l_∞ errors for the vertical-averaged 2D-model compared to the 1D-model. All calculations are performed with $n_x = 40$, $n_y = 10$, $\mu(c) = exp(-c)$ and the errors are measured at time $t = 0.5$.

	1	2	3	4
ϵ	0.4	0.2	0.1	0.05
h	$4.717 \cdot 10^{-2}$	$3.202 \cdot 10^{-2}$	$2.693 \cdot 10^{-2}$	$2.550 \cdot 10^{-2}$
l_2	$2.160 \cdot 10^{-2}$	$5.447 \cdot 10^{-1}$	$7.729 \cdot 10^{-1}$	-
l_∞	$5.515 \cdot 10^{-1}$	$8.042 \cdot 10^{-1}$	$9.542 \cdot 10^{-1}$	-

ϵ: Width of the thin strip
h: Step-size (length of hypotenuse in triangles in mesh)
l_2: l_2-norm of the error
l_∞: l_∞-norm of the error

Table 4.5: Comparing the errors between the vertical-averaged 2D-model and the 1D-model for $\alpha = -1, \beta = -1$ and $D = 0.05$

	1	2	3	4
ϵ	0.4	0.2	0.1	0.05
h	$4.717 \cdot 10^{-2}$	$3.202 \cdot 10^{-2}$	$2.693 \cdot 10^{-2}$	$2.550 \cdot 10^{-2}$
l_2	$1.283 \cdot 10^{-1}$	$1.245 \cdot 10^{-1}$	$1.224 \cdot 10^{-1}$	$1.233 \cdot 10^{-1}$
l_∞	$2.451 \cdot 10^{-1}$	$2.368 \cdot 10^{-1}$	$2.325 \cdot 10^{-1}$	$2.337 \cdot 10^{-1}$

ϵ: Width of the thin strip
h: Step-size (length of hypotenuse in triangles in mesh)
l_2: l_2-norm of the error
l_∞: l_∞-norm of the error

Table 4.6: Comparing the errors between the vertical-averaged 2D-model and the 1D-model for $\alpha = 0, \beta = 0$ and $D = 0.05$

	1	2	3	4
ϵ	0.4	0.2	0.1	0.05
h	$4.717 \cdot 10^{-2}$	$3.202 \cdot 10^{-2}$	$2.693 \cdot 10^{-2}$	$2.550 \cdot 10^{-2}$
l_2	$4.642 \cdot 10^{-2}$	$2.351 \cdot 10^{-2}$	$1.199 \cdot 10^{-2}$	$5.956 \cdot 10^{-3}$
l_∞	$9.229 \cdot 10^{-2}$	$4.748 \cdot 10^{-2}$	$2.425 \cdot 10^{-2}$	$1.210 \cdot 10^{-2}$

ϵ: Width of the thin strip
h: Step-size (length of hypotenuse in triangles in mesh)
l_2: l_2-norm of the error
l_∞: l_∞-norm of the error

Table 4.7: Comparing the errors between the vertical-averaged 2D-model and the 1D-model for $\alpha = 1, \beta = 2$ and $D = 0.05$

It can be seen in table (4.5) and (4.6) that errors is either steady or increases when ϵ decreases. This is due to the scenario where $\alpha, \beta \leq 0$, which means that the permeability increases and the concentration will differ more in the y-direction and therefore result in larger errors.

4.2.3 Strength of coupling

The strength of the coupling between the pressure/flux-calculations and the transport-equation is now studied. More iterations means that the system is more stiff and responds rapidly to changes. Three cases are studied:

- $\alpha = 1, \beta = 2$
- $\alpha = -1, \beta = -1$
- $\alpha = 0, \beta = 0$

All cases will be using the same values for the other parameters, $D_{2D} = 0.1$, $D_{1\mathrm{D}} = 0.5$ (diffusion coefficients), $\epsilon = 0.1$, $nx = 40$, $ny = 20$, $\Delta t = 0.025$.

With the following permeability tensor for the 2D-model,

$$\boldsymbol{K} = \begin{bmatrix} \epsilon^{\alpha} & 0 \\ 0 & \epsilon^{\beta} \end{bmatrix}$$

and $K = \epsilon^{\alpha}$ in the 1D-model.

The plots will be solid for convergent simulations and a dashed line if the simulation was canceled due to the solver not converging. This could either be because it did not reach the desired tolerance within our preset maximum iteration count or within the PETc-solver in the FEniCS-core itself.

4.2.3.1 Case 1: $\alpha = -1, \beta = -1$

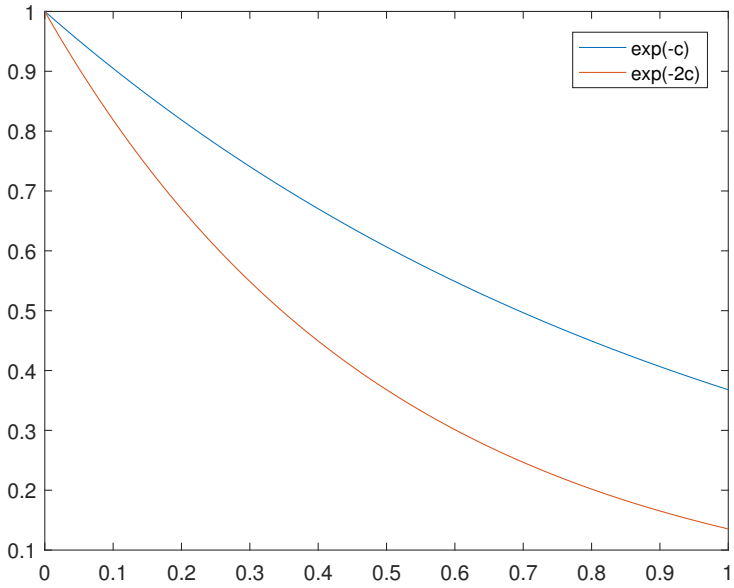

Figure 4.10: The profiles of the viscosities, μ, used in the calculations. The vertical axis is the value, for example $\mu = exp(-c)$, and the horizontal axis is the concentration

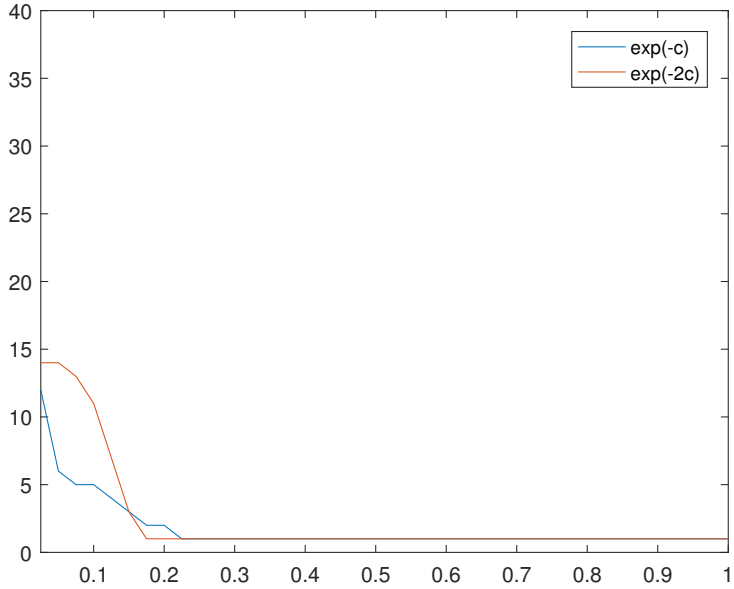

Figure 4.11: $\alpha = -1$, $\beta = -1$

Fig. (4.11) shows the iteration count for each time-step, where $\alpha = -1, \beta = -1$ and μ is a function of c. A steeper curve for the μ, see fig. (4.10), results a higher number of iterations in the early timesteps. As it is shown in the fig. (4.11), number of iterations reaches a maximum of 12 and 14 for $\mu(c) = exp(-c)$ and $\mu(c) = exp(-2c)$, respectively. For any steeper curve of μ than $\mu(c) = exp(-2c)$, the simulation fails to converge from the first timestep.

4.2.3.2 Case 2: $\alpha = 1, \beta = 2$

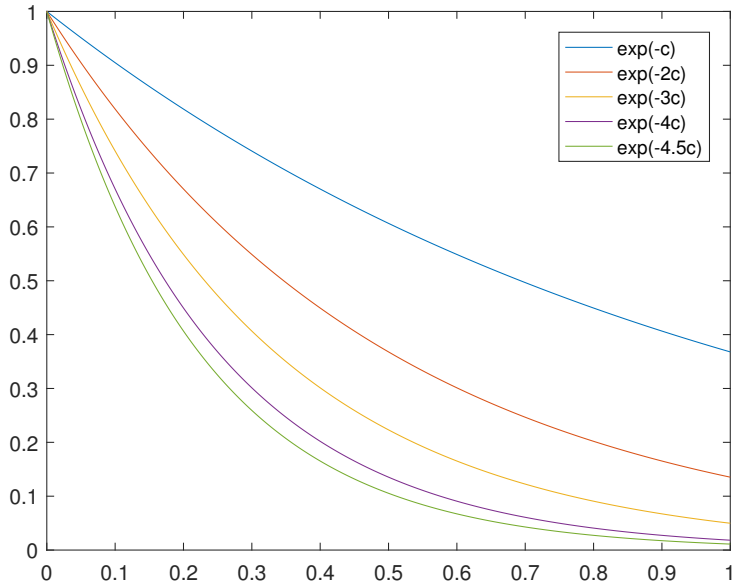

Figure 4.12: The profiles for each of the values of μ, in the case where $\alpha = 1$ and $\beta = 2$

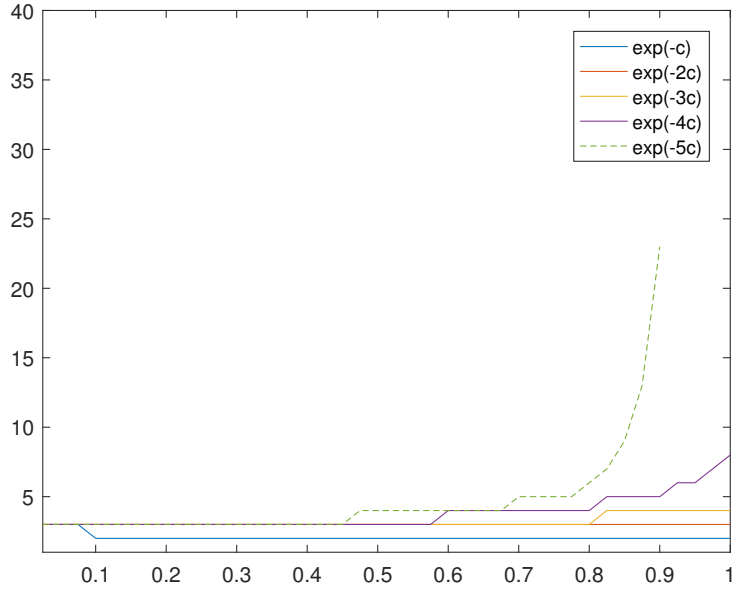

Figure 4.13: $\alpha = 1$, $\beta = 2$

Again, fig. (4.13) shows the iteration count for each time-step, where $\alpha = 1, \beta = 2$ and μ is a function of c, where the profile is showed in fig. (4.12). In contrary to the first case [section (4.2.3.1)], this case shows little to no impact on the early time-steps but shows an bigger impact on the later time-steps. As the fig. (4.13) shows an higher impact occurs starting from about $t = 0.8$ and beyond. The maximum for the convergent simulations are the last time-step, $t = 1.0$ where the number of iterations reaches 8. A single case was also tested outside these values, namely $\mu(c) = exp(-4.5c)$. This was still convergent, but the maximum shifted to one time-step earlier, $t = 0.975$ where it reached 16 iterations and then went down to 13 at the last time-step.

4.2.3.3 Case 3: $\alpha = 0, \beta = 0$

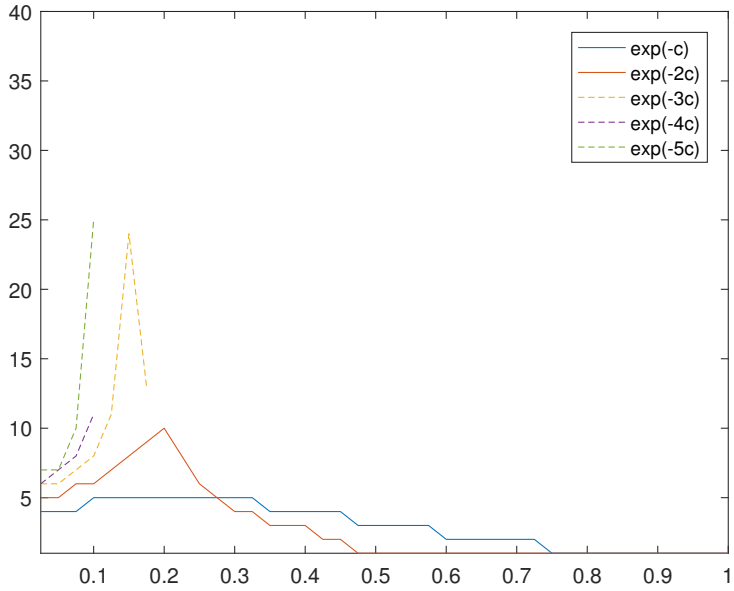

Figure 4.14: $\alpha = 0$, $\beta = 0$

Fig. (4.14) shows the iteration count for each time-step, for $\alpha = 0, \beta = 0$ and μ is a function of c, profile showed in (fig. 4.10). The maximum iteration count for this simulation occurs when $\mu(c) = exp(-c)$ in the area $t \in (0.1, 0.3)$. As $\mu(c)$ becomes steeper, this maximum seem to shift to the left and it gets steeper. This means that when $\mu(c)$ has a steeper curve, the maximum value increases.

4.2.3.4 Conclusions

From these three cases, it can be seen that the maximum in the first case (section 4.2.3.1) the maximum moves to the right, while in both second (section 4.2.3.2) and third case (section 4.2.3.3) the maximum shifts towards earlier time-steps.
Later on, it was attempted to lower the iterative tolerance from 10^{-6} to 10^{-3}. A change in iterations for $\mu(c) = exp(-c)$ and $\mu(c) = exp(-2c)$ did not appear before timestep $t = 0.75$. The order of difference in both l_2- and l_∞-norm was 10^{-4} after $t = 0.75$ and order 10^{-3} in the end of simulations. For even more steep curves of viscosity ($\mu(c) = exp(-4c)$ and further), the difference was in the order of 10^{-4} after timestep $t = 0.5$ and 10^{-3} at timesteps $t = 0.75$ and $t = 1.0$.

4.2.4 Analysis of the impact of the width of the thin strip, ϵ, on flow

The simulation was run with the following values of the parameters:

$$\alpha = 1, \beta = 0,$$
$$D_{2D} = D_{1D} = 0.1 \text{ (diffusion)},$$
$$\mu(c) = exp(-c) \text{ (function of diffusion)},$$

Both the l_2- and l_∞-norm of the concentration difference and the infinite-norm of flux are measured at $t = 1.0$ (by the end of the simulation).

	1	2	3	4
ϵ	0.4	0.2	0.1	0.05
h	$3.202 \cdot 10^{-2}$	$2.693 \cdot 10^{-2}$	$2.550 \cdot 10^{-2}$	$2.513 \cdot 10^{-2}$
l_2	$1.985 \cdot 10^{-3}$	$2.763 \cdot 10^{-4}$	$8.929 \cdot 10^{-5}$	$2.347 \cdot 10^{-4}$
l_∞	$6.861 \cdot 10^{-3}$	$5.487 \cdot 10^{-4}$	$1.235 \cdot 10^{-4}$	$3.433 \cdot 10^{-4}$
$\|u\|_{l_\infty}$	$4.001 \cdot 10^{-2}$	$7.449 \cdot 10^{-3}$	$1.553 \cdot 10^{-3}$	$3.610 \cdot 10^{-4}$

ϵ: Width of the thin strip
h: Step-size (length of hypotenuse in triangles in mesh)
l_2: l_2-norm of the error
l_∞: l_∞-norm of the error

Table 4.8: The errors between the vertical-averaged 2D-model and the 1D-model and the infinity norm of the flux

4.3 Indicators of comparison of vertical-averaged and 1D

4.3.1 Without gravity

From the paper of G. Menon, F. Otto, Dynamic Scaling in Miscible Viscous Fingering [20], they propose a couple of indicators of viscous fingering. The first of these indicators is the measure of the width of fingers, which is why they define the mean perimeter as such:

$$P(t) = \fint \left|\nabla \bar{c}(x,t)\right| dx \tag{4.12}$$

where $\bar{c}(x,t)$ is the local concentration at time t and position x. The other parameters being studied are defined to by the cited paper to be: *gravitational potential energy*

$$E(t) = -\fint \left[c(x,y,t) - c_0(x)\right] x dx \tag{4.13}$$

Gravity will not be included in the models in this section, but for later use in this thesis, the indicator $E(t)$ shows how much of the domain has a different concentration, compared to the beginning (of the simulation). The higher the value, - the more of the domain has changed concentration compared to the start/beginning.
The next equations are two so called *entropy* functions. These functions catches the zone of the domain where the value for $c(x,t)$ is between 0 and 1.

$$H(t) = \fint c(1-c) dx \tag{4.14}$$

$$S(t) = -\fint \left(c\, log(c) + (1-c)\, log(1-c)\right) dx \tag{4.15}$$

The models being modelled here, are the same one as from the previous sections. The flux will be calculated with the following 2D-model

$$\underline{\mathbf{u}}(x,y,t) = -\frac{\boldsymbol{K}}{\mu(c)} \nabla p(x,y) = -\frac{1}{exp(-c(x,y,t))} \begin{bmatrix} \epsilon^\alpha & 0 \\ 0 & \epsilon^\beta \end{bmatrix} \nabla p(x,y) \tag{4.16}$$

and the corresponding flux for 1D

$$u^*(x,t) = -\epsilon^\alpha \frac{\partial_x p(x)}{exp(-c(x,t))} \tag{4.17}$$

For the 2D-model, the transport model is as follows

$$\partial_t c(x,y,t) = D\Delta c(x,y,t) - \nabla \cdot \left(\underline{\mathbf{u}}(x,y,t)\, c(x,y,t)\right) \tag{4.18}$$

and the vertical-average is defined as

$$\bar{c}(x,t) = \frac{1}{\epsilon} \int_0^\epsilon c(x,\xi,t) d\xi \tag{4.19}$$

For the 1D-model, the model reduces to

$$\partial_t c^*(x,t) = D\partial_{xx} c^*(x,t) - \partial_x \left(u^*(x,t)\, c^*(x,t)\right) \tag{4.20}$$

The magnitude of these parameters are studied for the different regimes. This is then used to compare the 1D-model with the vertical-averaged 2D-model. To emphasize the difference between the parameters, the diffusion coefficients named as D_{2D} and D_{1D}, while the concentration and the flux for the 1D-model is $c^*(x,t)$ and $u^*(x,t)$, respectively. Only the case where $\epsilon = 0.1$ is covered. If nothing else is defined, then the diffusion coefficients D_{2D}, D_{1D} will be equal to 0.1. This section is a study without turbulence, which is why the difference between them are very limited.

4.3.1.1 Results of indicator $P(t)$

Initially, the mean perimeter function is investigated. The output of this function will describe the mean perimeter of fingers created in a miscible viscous flow. As a beginning, the parameters $\alpha = \beta = 0$ are used.

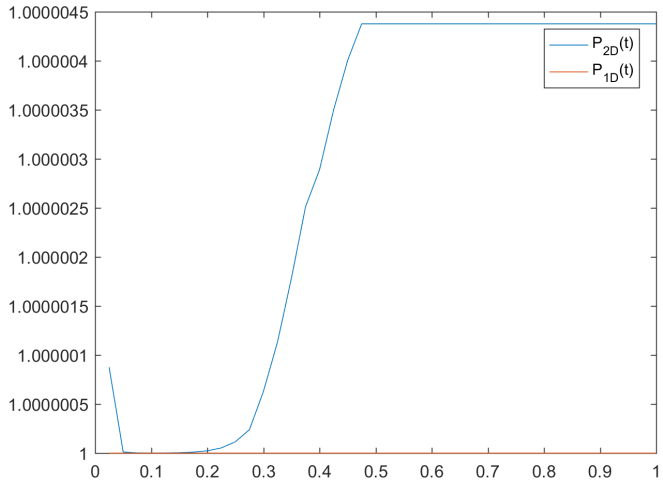

Comparing P_{2D} and P_{1D} for $\alpha = \beta = 0$

As can be seen here, when time-step t passes 0.3, P_{2D} increases to be slightly above P_{1D}. However the size of this difference is merely 10^{-6}.

Moving on to the cases, where $-1 < \alpha < 0$ - starting with $\alpha = -0.5$ and $\beta = 0$.

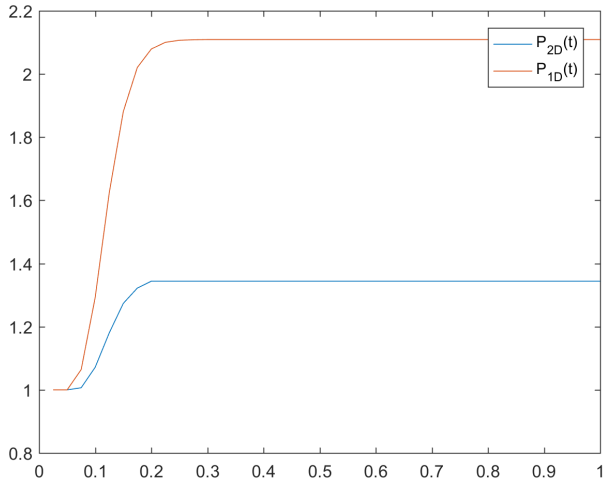

Figure 4.15: ComparingP_{2D} and P_{1D} for $\alpha = -0.5$ and $\beta = 0$

There is a significant difference between the result of the 1D-model and the vertical-averaged 2D-model. The difference in the concentration can be seen here:

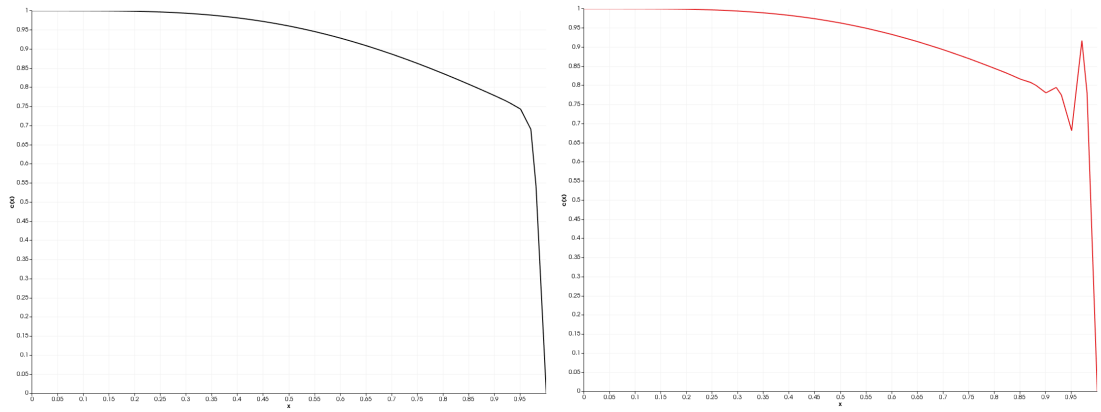

(a) $\bar{c}(x,t)$ (b) $c^*(x,t)$

Figure 4.16: Comparing $\bar{c}(x,t)$ and $c^*(x,t)$ for $\alpha = -0.5$ and $\beta = 0$ at $t = 0.125$

Trying to compensate for this difference by adjusting $D_{1D} = 0.15$ ($\|D\| =$). Which leads to the following profile

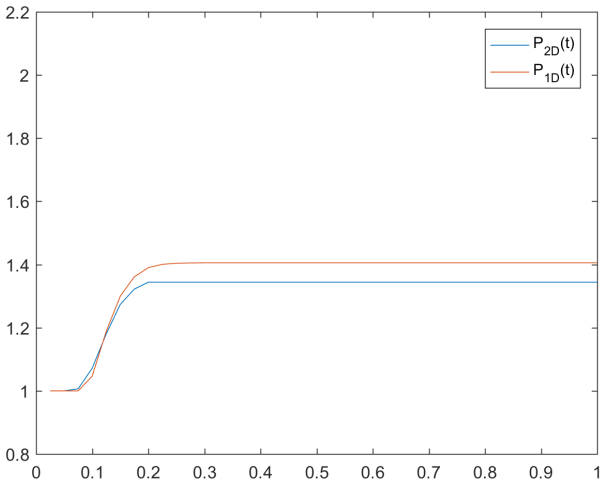

Figure 4.17: $D_{2D} = 0.1$ and $D_{1D} = 0.15$

As can be seen on fig. (4.17), the difference can be minimized by ajusting D_{1D} to 0.15.

Then $\alpha = -0.75$ and $\beta = 0$ is inspected

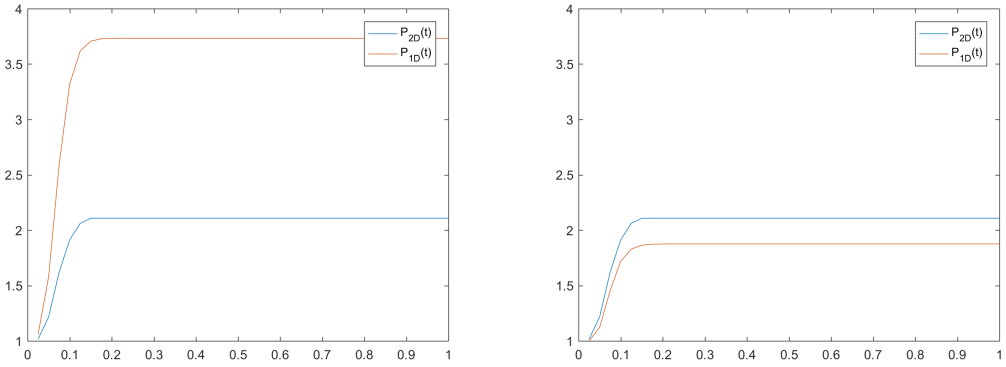

(a) $D_{2D} = D_{1D} = 0.1$ (b) $D_{2D} = 0.1$ and $D_{1D} = 0.2$

Figure 4.18: Comparing P_{2D} and P_{1D} for $\alpha = -0.75$ and $\beta = 0$

And for the last case, a simulation was performed, where $\alpha = -0.25$ and $\beta = 0$

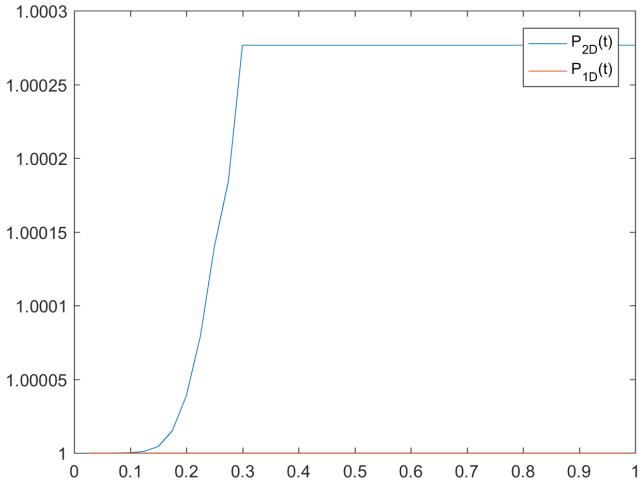

Figure 4.19: Comparing P_{2D} and P_{1D} for $\alpha = -0.25$, $\beta = 0$ and $D_{2D} = D_{1D} = 0.1$

As seen from the figures (4.19), (4.16) and (4.18): The lower the value for α, the bigger the difference will be to a diffusion of 0.1.

Continuing to the cases where $\alpha > 0$ - starting with the following values: $\alpha = 1$ and $\beta = 0$

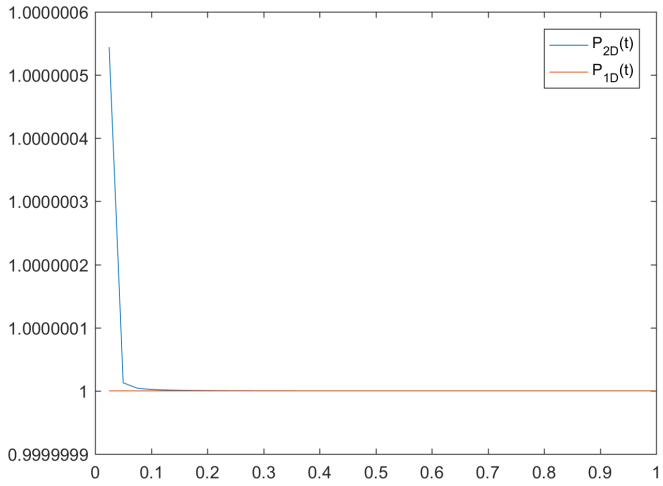

Figure 4.20: Comparing P_{2D} and P_{1D} for $\alpha = 1$ and $\beta = 0$

In this case, there is little to no difference between P_{2D} and P_{1D}, other than in the beginning where the difference is merely an order of $\mathcal{O}(10^{-7})$. There is no difference when adjusting the diffusion for 1D here, as it is the averaged 2D-model which has the highest values.

4.3.1.2 Results of indicator $H(t)$

Starting with $\alpha = \beta = 0$.

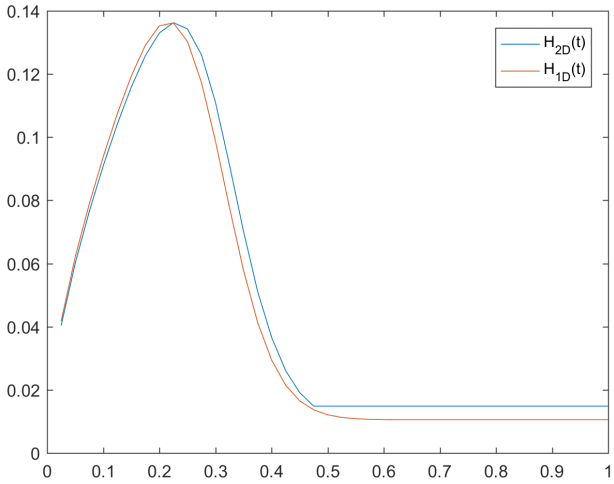

Figure 4.21: Comparing H_{2D} and H_{1D} for $\alpha = \beta = 0$

For this case the two results are already very close. So changing D_{1D} will create a bigger difference. Therefore, moving right along to the next case, which is for $\alpha = 1$ and $\beta = 0$. This results in the following plot:

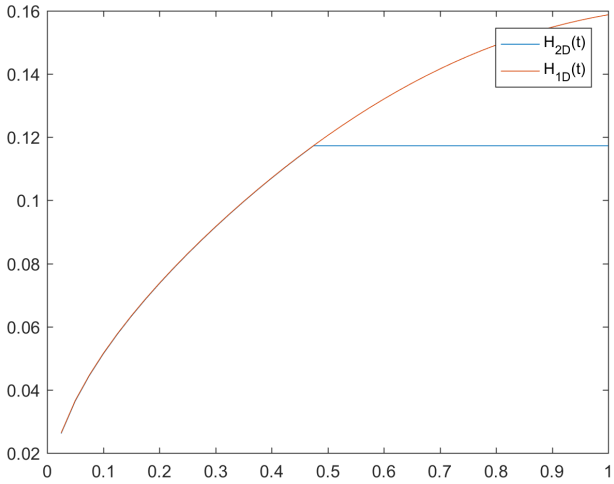

Figure 4.22: Comparing H_{2D} and H_{1D} for $\alpha = 1$ and $\beta = 0$

The two results are almost identical until $t = 0.475$, whereafter the difference increases. Here changing D_{1D} will not make a difference, because the difference will increase in a earlier timestep.

For $\alpha = -0.5$ and $\beta = 0$ the following plot can be produced

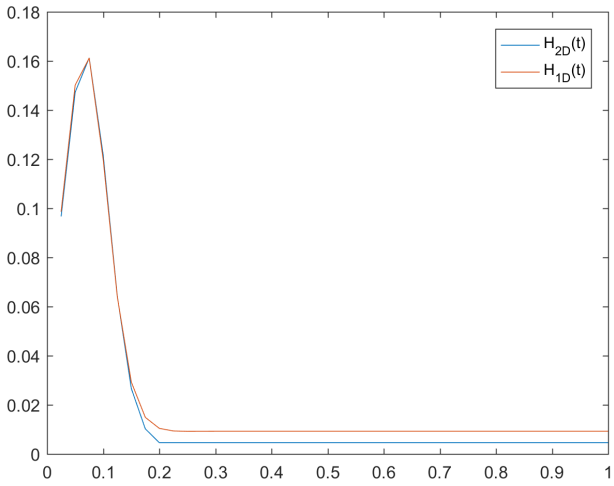

Figure 4.23: Comparing H_{2D} and H_{1D} for $\alpha = -\frac{1}{2}$ and $\beta = 0$

In conclusion, for the parameter/indicator $H(t)$: changing D_{1D} only makes the differences increase. Therefore this parameter is not very conclusive for measuring the strength of the Taylor dispersion term.

4.3.1.3 Results of indicator $S(t)$

We then move over to the the other entropy parameter, and start with $\alpha = \frac{1}{2}, \beta = 0$.

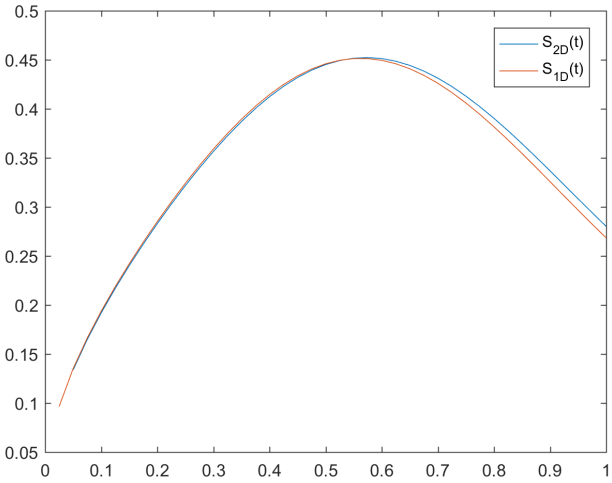

Figure 4.24: Comparing S_{2D} and S_{1D} for $\alpha = \frac{1}{2}$ and $\beta = 0$

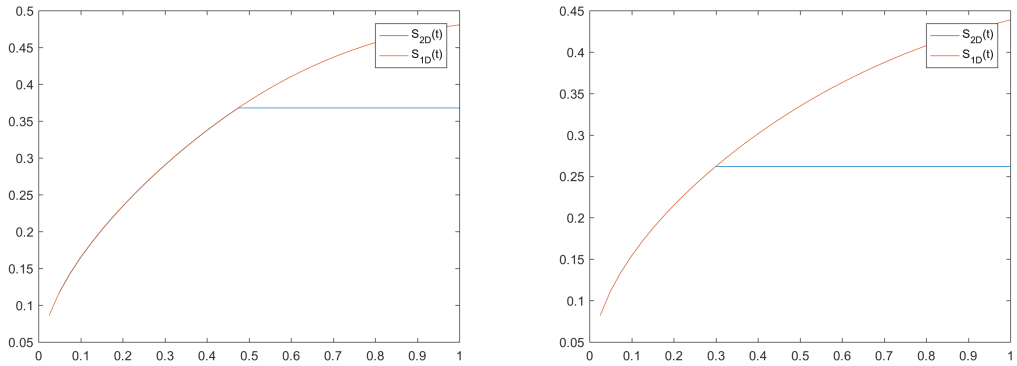

(a) $\alpha = 1$ (b) $\alpha = 2$

Figure 4.25: Comparing S_{2D} and S_{1D} for $\alpha = \{1, 2\}$ and $\beta = 0$

As can be observed on fig. (4.24) and (4.25), for $\alpha > 0$, then there is a point, whereafter the difference will increase (drastically). For larger values of α this point occurs at an earlier timestep.
Moving on to the case where $\alpha = 0$

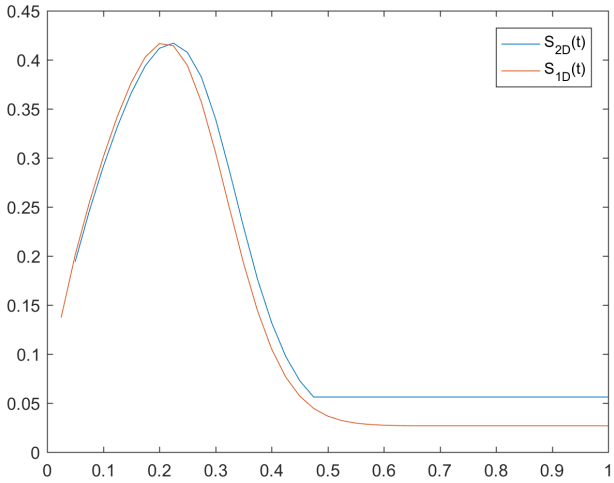

Figure 4.26: Comparing S_{2D} and S_{1D} for $\alpha = 0$ and $\beta = 0$

For $\alpha < 0$:

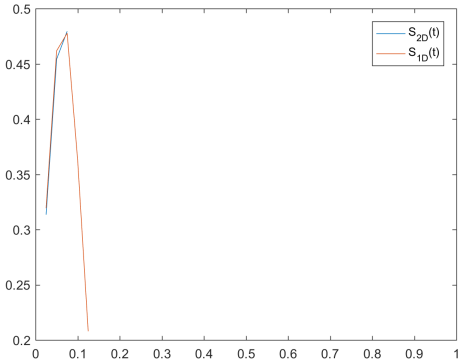

(a) $\alpha = -0.5$:

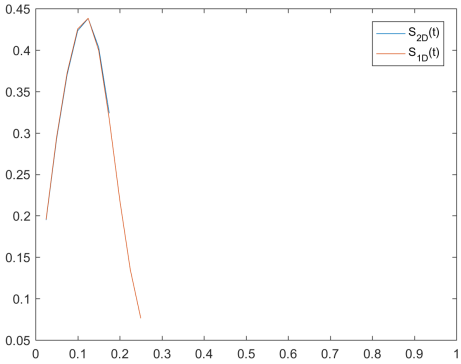

(b) $\alpha = -0.25$:

Figure 4.27: Comparing S_{2D} and S_{1D} for $\alpha = \{-0.25, -0.50\}$ and $\beta = 0$

The integrals was not bounded, which is why the plots stop. See fig. (4.28) for the concentrations for $\alpha = -0.25$ at $t = 0.275$.

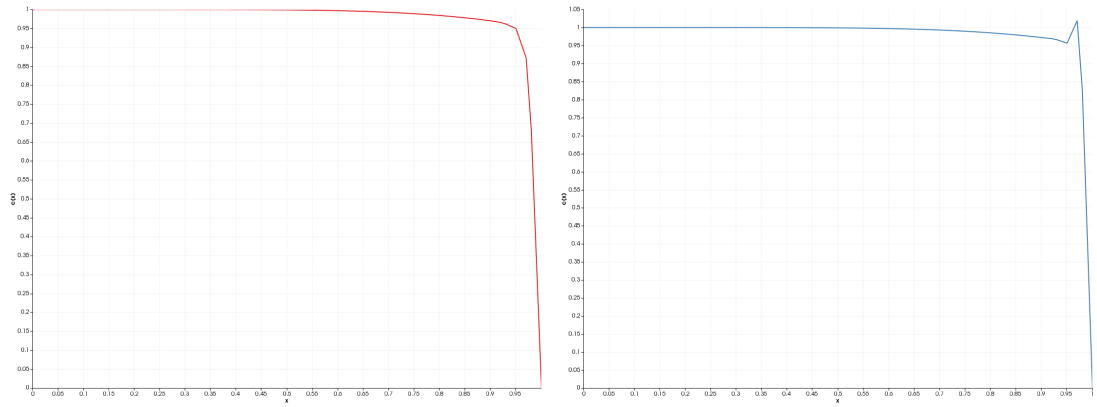

(a) $\bar{c}(x,t)$ (b) $c^*(x,t)$

Figure 4.28: Comparing $\bar{c}(x,t)$ and $c^*(x,t)$ for $\alpha = -0.25$ and $\beta = 0$

As can be seen from fig. (4.28), the concentration on the graph for the 1D-result fig. (4.28b) goes a little over 1, and therefore it tries to take the natural logarithm of a negative number (by the definition of $S(t)$). This results in NaN (not a number) and the series on both subfigures in fig. (4.27) stops suddenly.

4.3.1.4 Results of indicator $E(t)$

The last of the proposed functions to study/analyze, is the function for gravitational potential energy. Starting with the values $\alpha = -\frac{1}{2}$ and $\beta = 0$.

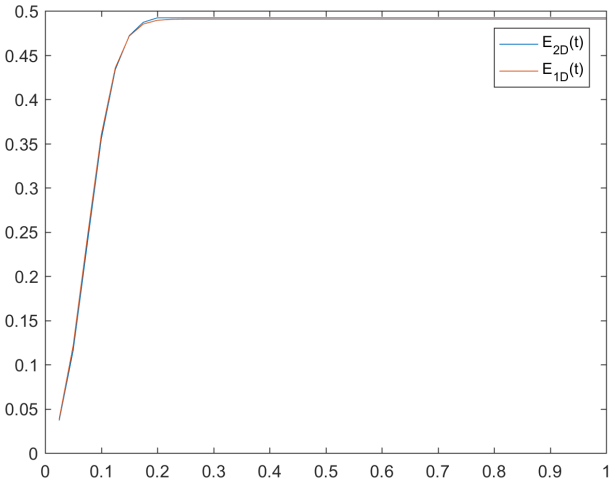

Figure 4.29: Comparing E_{2D} and E_{1D} for $\alpha = -\frac{1}{2}$ and $\beta = 0$

For $\alpha = 0$:

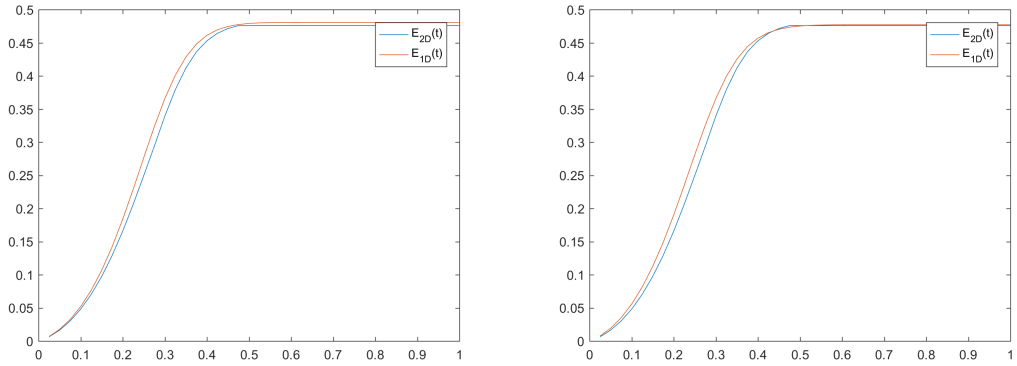

(a) $D_{2D} = D_{1D} = 0.10$ (b) $D_{2D} = 0.10$ and $D_{1D} = 0.12$

Figure 4.30: Comparing E_{2D} and E_{1D} for $\alpha = 0$ and $\beta = 0$

The result is slightly improving when D_{1D} is increased from 0.1 to 0.12.

For $\alpha > 0$:

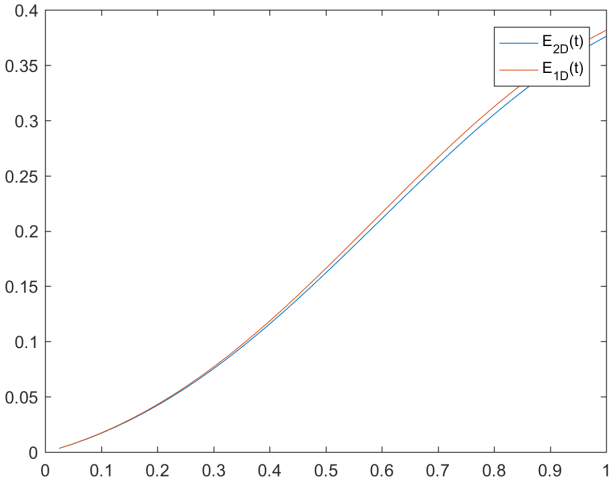

Figure 4.31: Comparing E_{2D} and E_{1D} for $\alpha = 0.5$ and $\beta = 0$

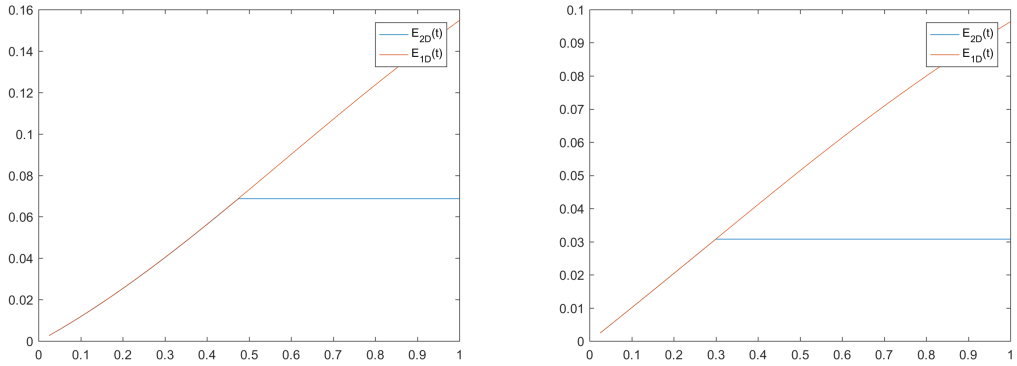

(a) $\alpha = 1$ (b) $\alpha = 2$

Figure 4.32: Comparing E_{2D} and E_{1D} for $\alpha = \{1, 2\}$ and $\beta = 0$

Which is the same results, as gotten for $S(t)$ where for $\alpha > 0$, so there is a point, whereafter the difference will increase (drastically). The larger α becomes, the earlier this point of change occurs.

4.3.1.5 Conclusion of the indicators

This section has studied and analyzed the comparisons of functions for a vertical-averaged 2D-model and a 1D-model. These functions were the functions for $P(t)$ (4.12), $E(t)$ (4.13), $H(t)$ (4.14) and $S(t)$ (4.15). Of these, it seems that $P(t)$ (4.12) was the most useful parameter for finding the correct balance between the diffusion coefficient, D_{1D}, and the Taylor dispersion term.

4.4 Indicators of comparison for a turbulent flow with gravity of vertical-averaged 2D- and 1D-model

This section will study the behaviour of the model for the presence of a turbulent flow and gravity. The turbulent flow is caused by viscosity, μ, being dependent on y-position and concentration and also the contribution of gravity is dependant on concentration. The result of this is an inhomogeneous flow where there could occur fingering. This will be studied for three different regimes.

The model used in this section will be using is the same as for the previous sections but now with an added gravity term working in the x-direction. The flux model then becomes

$$\underline{\mathbf{u}}(x,y,t) = -\frac{\boldsymbol{K}}{\mu(c)}\nabla p(x,y) = -\frac{1}{exp(-c(x,y,t))}\begin{bmatrix} \epsilon^{\alpha} & 0 \\ 0 & \epsilon^{\beta} \end{bmatrix}\nabla p(x,y) + \begin{bmatrix} \frac{1}{10}c(x,y,t)\,g \\ 0 \end{bmatrix} \quad (4.21)$$

where $g = 10$ and the corresponding result for 1D:

$$u^*(x,t) = -\epsilon^{\alpha}\frac{\partial_x p(x)}{exp(-c(x,t))} + \frac{1}{10}c(x,t)\,g \quad (4.22)$$

4.4.1 Case 1, $\alpha > 0$

The first case is studied for an anisotropic permeability. As it can be seen in the system of parameters in eq. (4.23), the parameter $\alpha = 1$. This results in a very small flux and therefore it is the diffusive part which is dominating. This is reflected in the plots where there is a smooth transition in the concentration profile and for the indicators.

$$\begin{aligned} \alpha = 1, \beta = 0, \epsilon = 0 \\ D_{2D} = 0.1, D_{1D} = 0.1, g = 9.81 \\ \mu(x, y, t) = exp\left(-1 + \frac{0.7\, y}{\epsilon} c(x, y, t)\right) \end{aligned} \tag{4.23}$$

The concentration for time $t = 0.5$ is shown in the following figure.

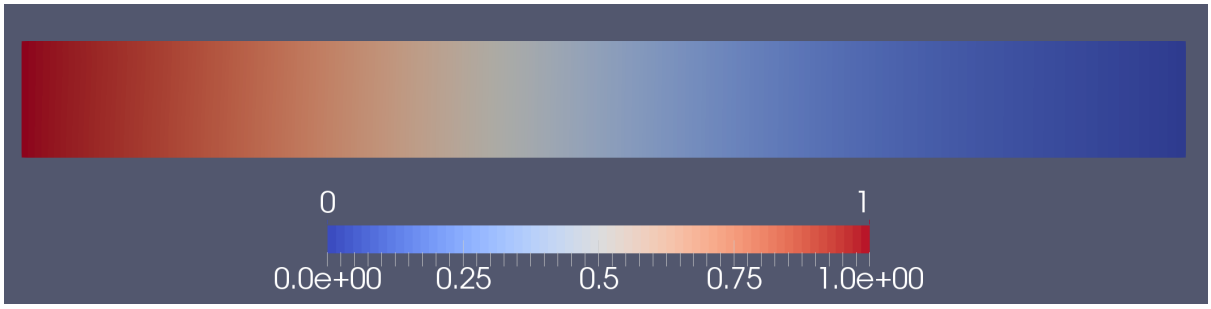

(a) Concentration distribution in 2D model for $t = 0.5$

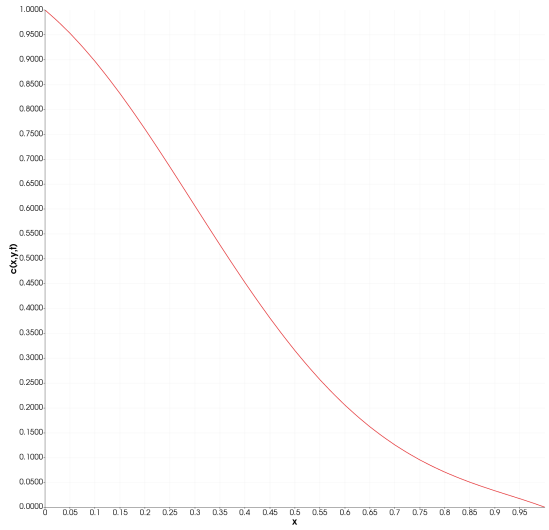

(b) $\bar{c}(x, t)$

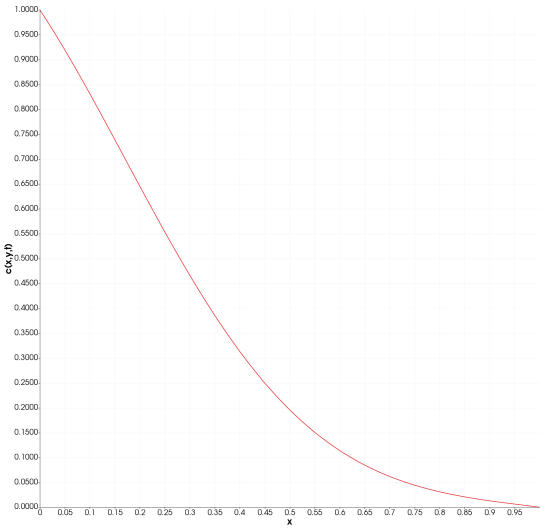

(c) $c^*(x, t)$

Figure 4.33: Comparing concentrations $\bar{c}$ (vertical-averaged 2D-model) and c^* (1D-model) for $\alpha = 1$ and $\beta = 0$ at $t = 0.5$

The dependency of y is shown in fig. (4.34), where there is a plot of the concentration in the 2D-model (vertical axis) for a given y (horizontal axis) at a fixed position $x = 0.2$.

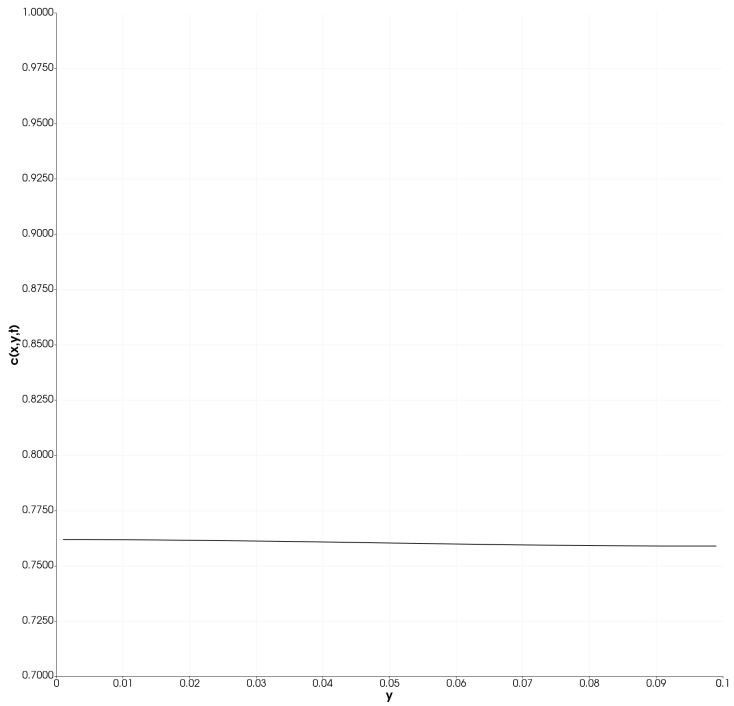

Figure 4.34: Concentration in 2D model as a function of y for $x = 0.2$ at $t = 0.5$

4.4.1.1 Indicator $P(t)$ for Case 1

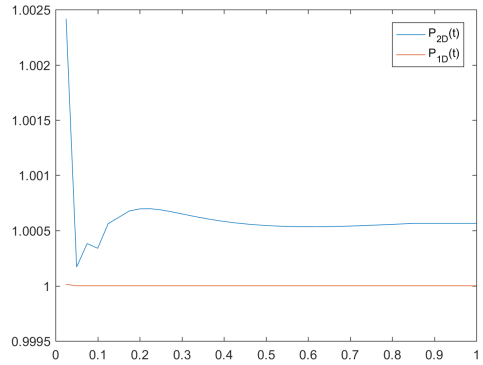

(a) $D_{2D} = D_{1D} = 0.05$

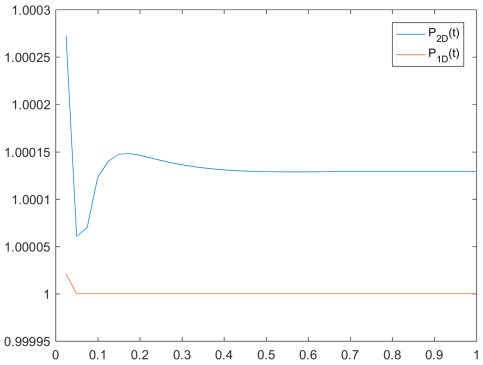

(b) $D_{2D} = D_{1D} = 0.1$

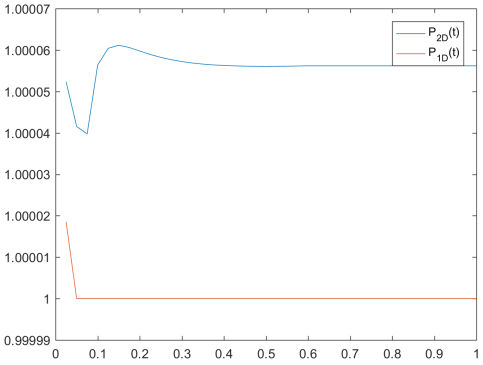

(c) $D_{2D} = D_{1D} = 0.15$

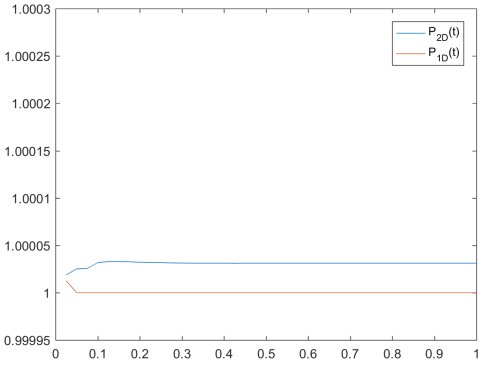

(d) $D_{2D} = D_{1D} = 0.2$

Figure 4.35: Comparing P_{2D} and P_{1D} for different diffusion coefficients with $\alpha = 1$ and $\beta = 0$

The width of the thin strip, ϵ, is then changed to $\epsilon = 0.2$ to see the effect of this parameter under these conditions.

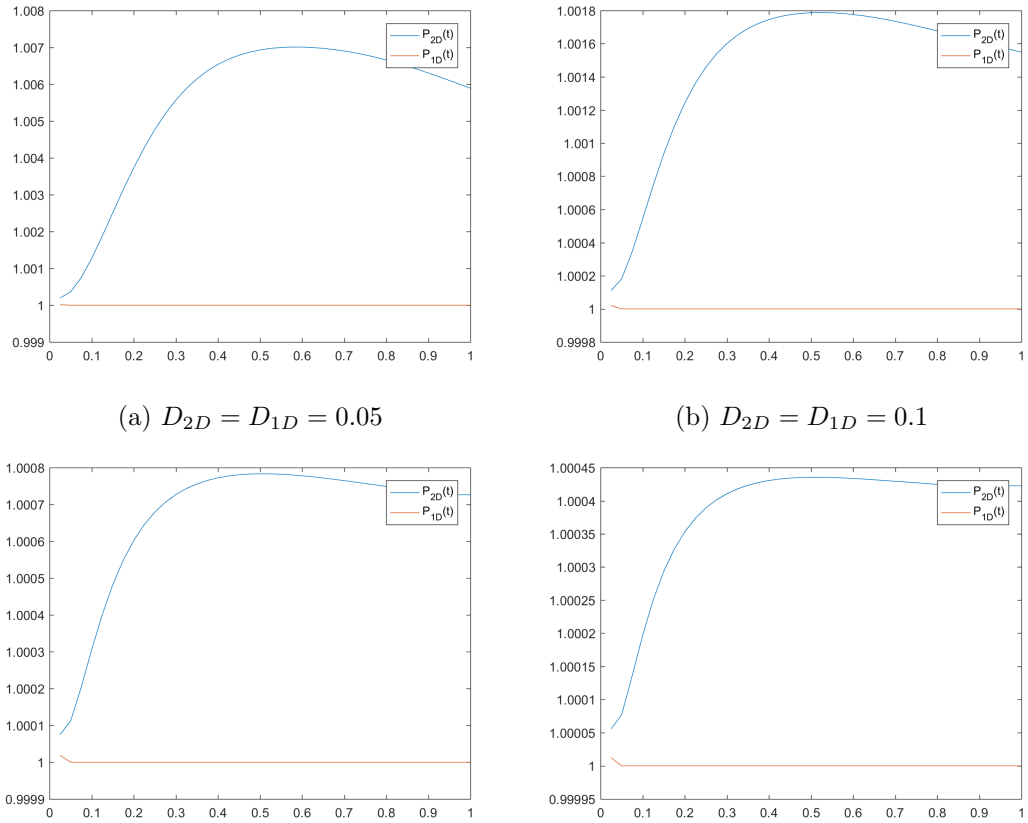

(a) $D_{2D} = D_{1D} = 0.05$

(b) $D_{2D} = D_{1D} = 0.1$

(c) $D_{2D} = D_{1D} = 0.15$

(d) $D_{2D} = D_{1D} = 0.2$

Figure 4.36: Comparing P_{2D} and P_{1D} for different diffusion coefficients with $\alpha = 1$ and $\beta = 0$

As shown in the figures above, we see that the P_{2D} shrinks when the diffusion coefficient increases. If we look at figure (4.36d) we see that the maximum, $P(t = 0.5) = 1.00045$, the distance (from 1) is almost 20 times higher than in figure (4.36a). For an increasing thickness of the thin-stip, ϵ, we see that the maximum increases. Comparing figure (4.36a) with (4.35a) we observe that the maximum distance (from 1) is 3 times higher.

4.4.1.2 Indicator $E(t)$ for Case 1

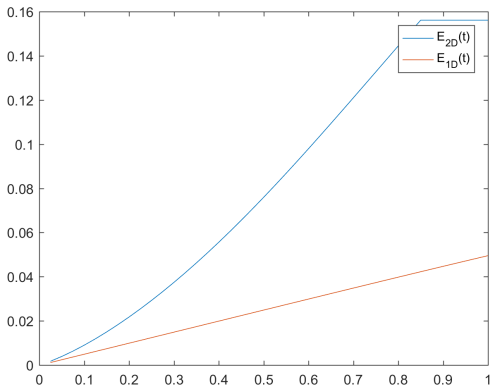

(a) $D_{2D} = D_{1D} = 0.05$

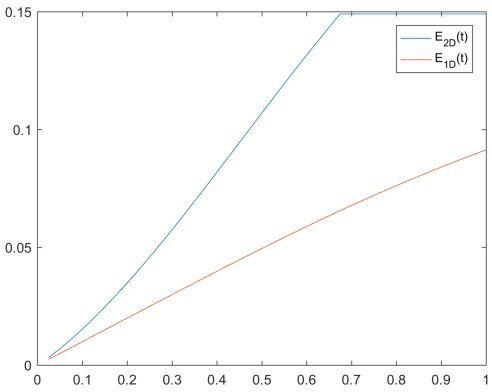

(b) $D_{2D} = D_{1D} = 0.1$

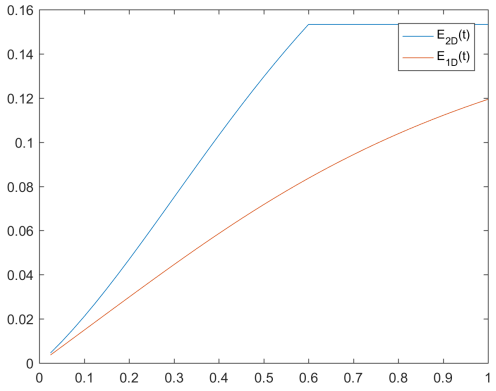

(c) $D_{2D} = D_{1D} = 0.15$

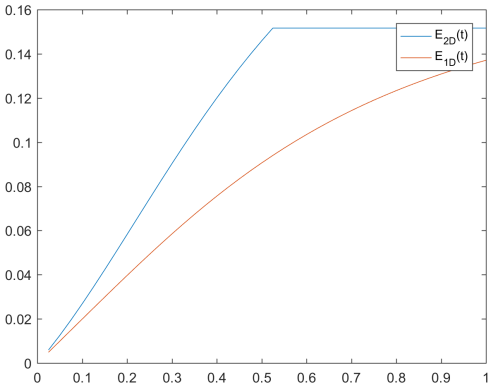

(d) $D_{2D} = D_{1D} = 0.2$

Figure 4.37: Comparing E_{2D} and E_{1D} for different diffusion coefficients with $\alpha = 1$ and $\beta = 0$

The width of the thin strip, ϵ, is then changed to $\epsilon = 0.2$ to see the effect of this parameter under these conditions.

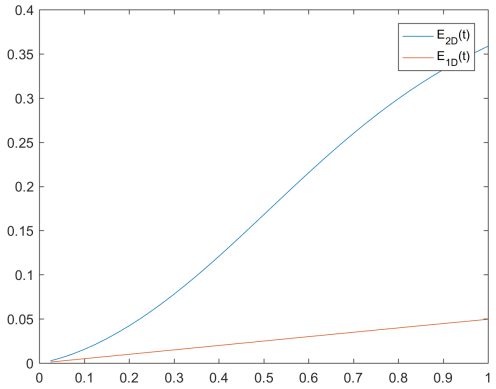

(a) $D_{2D} = D_{1D} = 0.05$

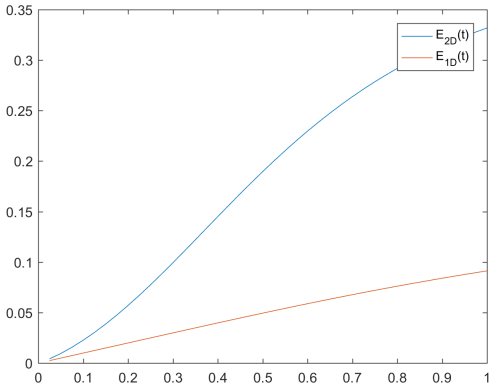

(b) $D_{2D} = D_{1D} = 0.1$

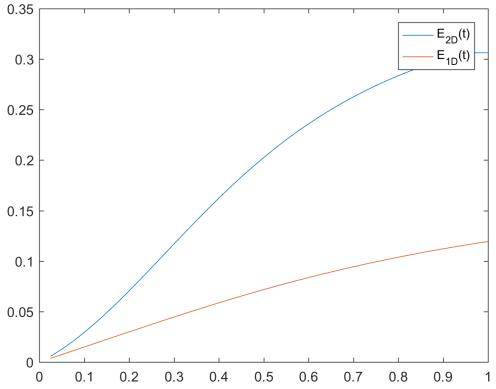

(c) $D_{2D} = D_{1D} = 0.15$

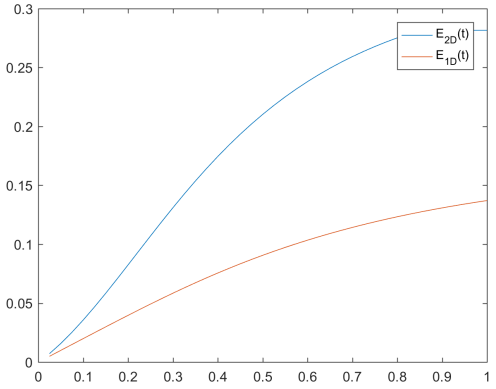

(d) $D_{2D} = D_{1D} = 0.2$

Figure 4.38: Comparing E_{2D} and E_{1D} for different diffusion coefficients with $\alpha = 1$, $\beta = 0$ and $\epsilon = 0.2$

As with the indicator $P(t)$, $E(t)$ decreases with an increasing diffusion and increases with an increasing thickness, ϵ. We also see here that in figure (4.37a) the part up to $t = 0.8$ is convex while in figure (4.37a) it is more linear. In the second part, where $\epsilon = 0.2$, in figure (4.38a) it is convex in the start and concave in the end, while in figure (4.38d) it is concave.

4.4.1.3 Indicator $S(t)$ for Case 1

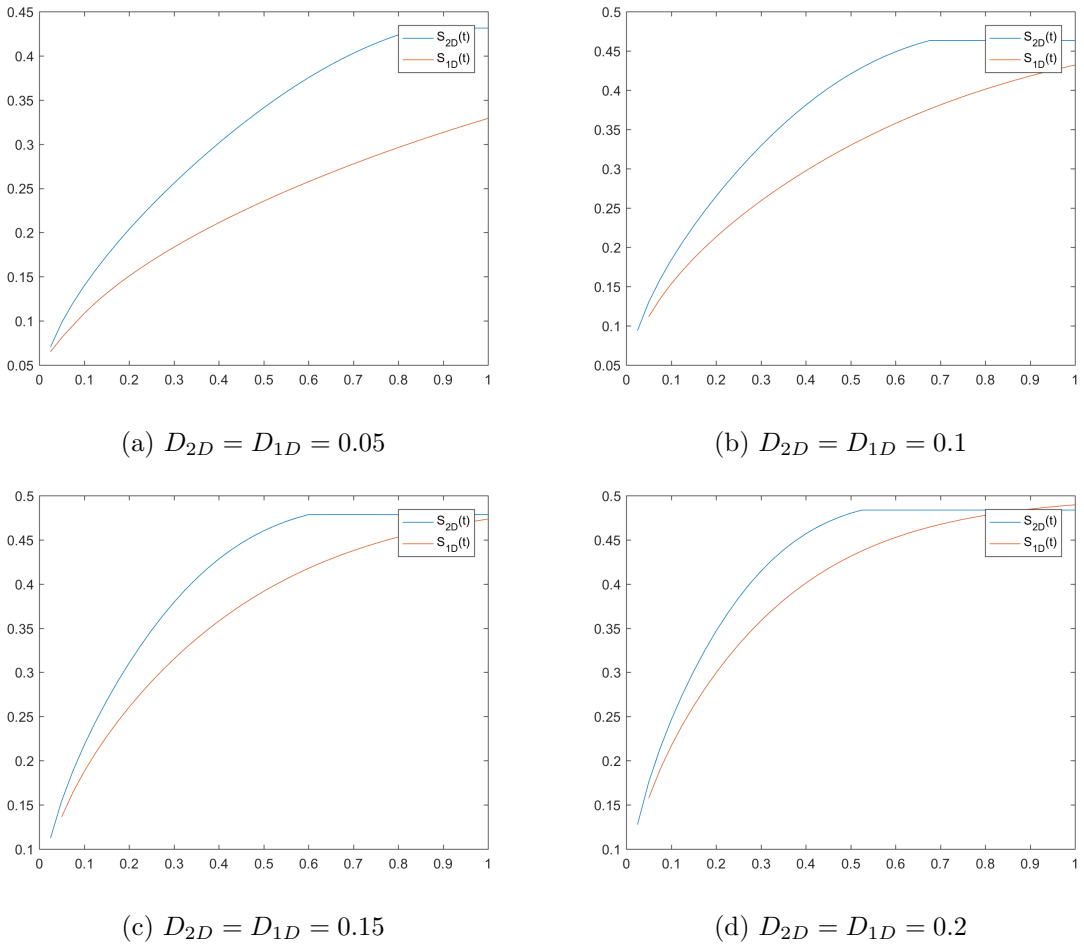

(a) $D_{2D} = D_{1D} = 0.05$ (b) $D_{2D} = D_{1D} = 0.1$

(c) $D_{2D} = D_{1D} = 0.15$ (d) $D_{2D} = D_{1D} = 0.2$

Figure 4.39: Comparing S_{2D} and S_{1D} for different diffusion coefficients with $\alpha = 1$ and $\beta = 0$

The width of the thin strip, ϵ, is then changed to $\epsilon = 0.2$ to see the effect of this parameter under these conditions.

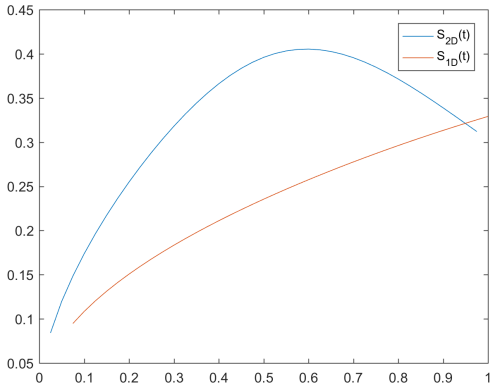

(a) $D_{2D} = D_{1D} = 0.05$

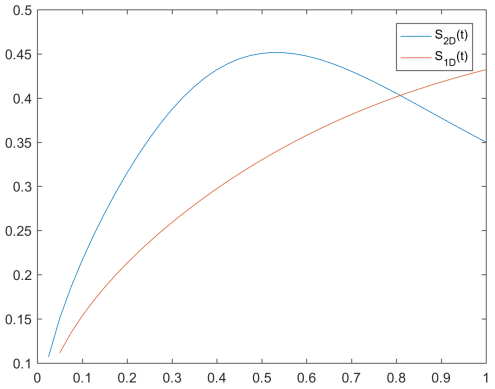

(b) $D_{2D} = D_{1D} = 0.1$

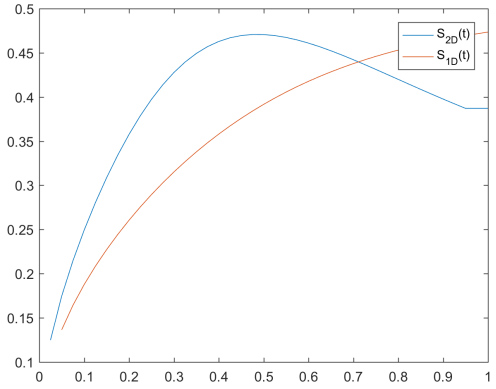

(c) $D_{2D} = D_{1D} = 0.15$

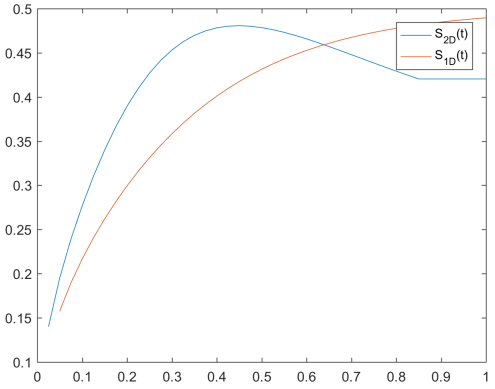

(d) $D_{2D} = D_{1D} = 0.2$

Figure 4.40: Comparing S_{2D} and S_{1D} for different diffusion coefficients with $\alpha = 1$, $\beta = 0$ and $\epsilon = 0.2$

As we can see on the figures of this indicator, for higher value of diffusion, we see a more increasing maximum value as well as it is reaching a steady-state at an earlier timestep. This is due to the boundaries of the domain has a no-flow condition, and therefore there will not be more transport after this boundary is reached. For $\epsilon = 0.2$, the velocity increases a bit, and therefore there is a more parabolic profile and get a little reduced before the boundary comes into play. It is reduced at the end because of the "mushy" zone is reduced and it has a large gradient.

4.4.1.4 Indicator $H(t)$ for Case 1

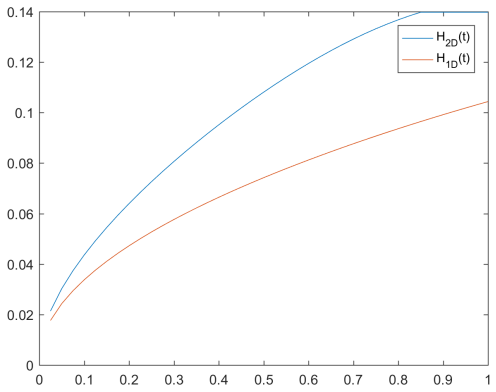

(a) $D_{2D} = D_{1D} = 0.05$

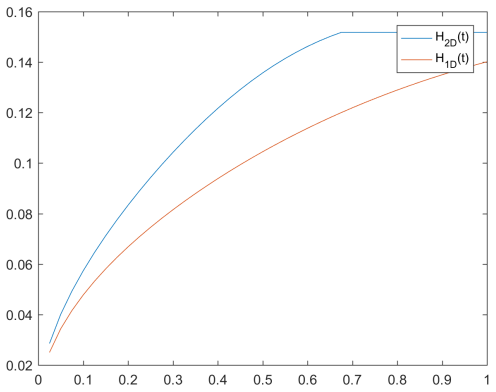

(b) $D_{2D} = D_{1D} = 0.1$

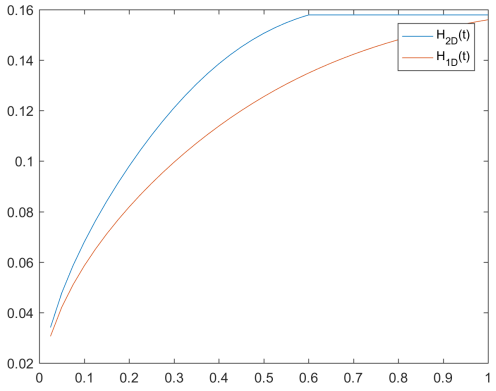

(c) $D_{2D} = D_{1D} = 0.15$

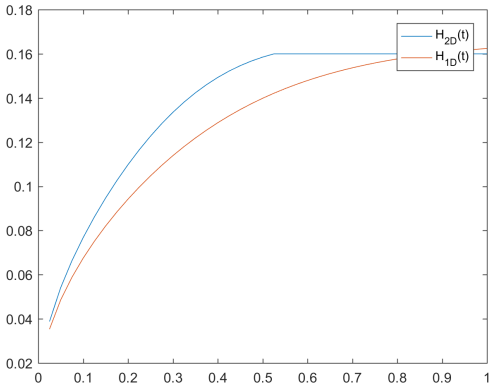

(d) $D_{2D} = D_{1D} = 0.2$

Figure 4.41: Comparing H_{2D} and H_{1D} for different diffusion coefficients with $\alpha = 1$ and $\beta = 0$

The width of the thin strip, ϵ, is then changed to $\epsilon = 0.2$ to see the effect of this parameter under these conditions.

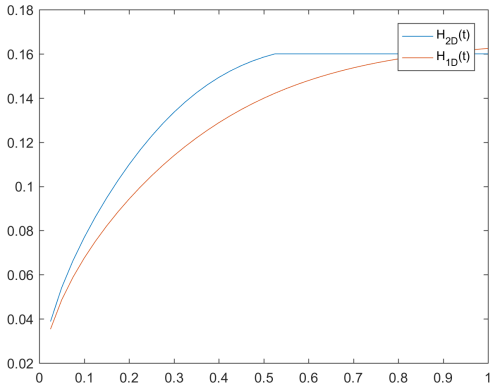

(a) $D_{2D} = D_{1D} = 0.05$

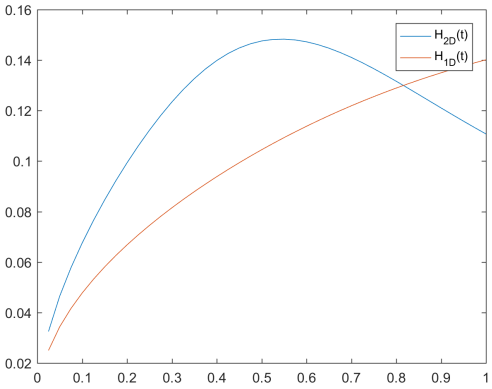

(b) $D_{2D} = D_{1D} = 0.1$

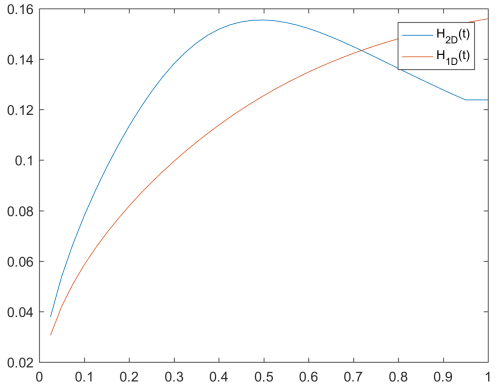

(c) $D_{2D} = D_{1D} = 0.15$

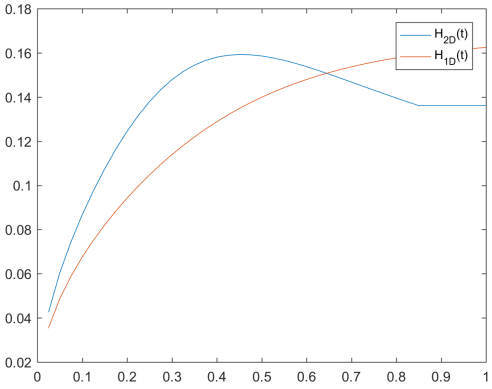

(d) $D_{2D} = D_{1D} = 0.2$

Figure 4.42: Comparing H_{2D} and H_{1D} for different diffusion coefficients with $\alpha = 1$, $\beta = 0$ and $\epsilon = 0.2$

For $H(t)$, the story is very similar to $S(t)$, for $\epsilon = 0.1$ it is monotonic increasing until it reaches the boundary at $x = 1$, where the transport stops. For a increasing diffusion, that happens earlier. For $\epsilon = 0.2$, we have a more parabolic profile which also has a negative gradient at the end. This is because of the flow being more dominant than in the other case.

4.4.2 Case 2, $\alpha = 0$

The second case studies the indicators for an isotropic permeability. As it can be seen in the system of parameters in eq. (4.24), the parameter $\alpha = 0$. This results in a higher flux than in the previous case and here there is the flux which is dominating. This is reflected in the plots where there is a less smooth transition, than in case 1, in the concentration profile and for the indicators.

$$\begin{aligned} \alpha = 0, \beta = 0, \epsilon = 0 \\ D_{2D} = 0.1, D_{1D} = 0.1, g = 9.81 \\ \mu(x, y, t) = exp\left(-1 + \frac{0.7\, y}{\epsilon} c(x, y, t)\right) \end{aligned} \tag{4.24}$$

The concentration for time $t = 0.1$ is shown in the following figure.

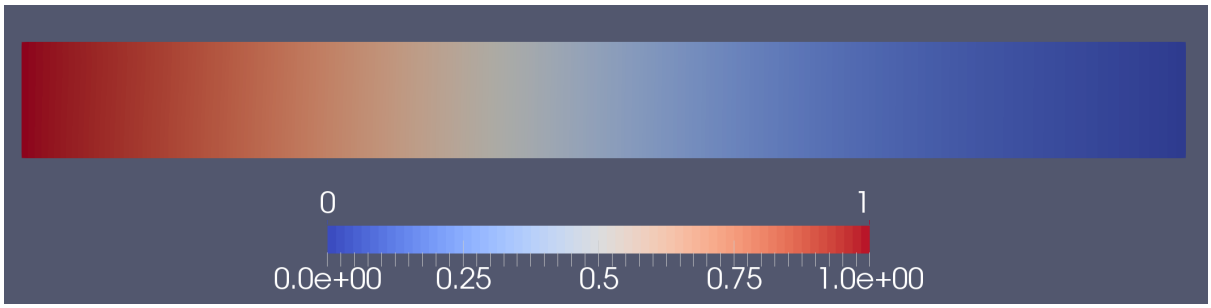

(a) Concentration distribution in 2D model for $t = 0.1$

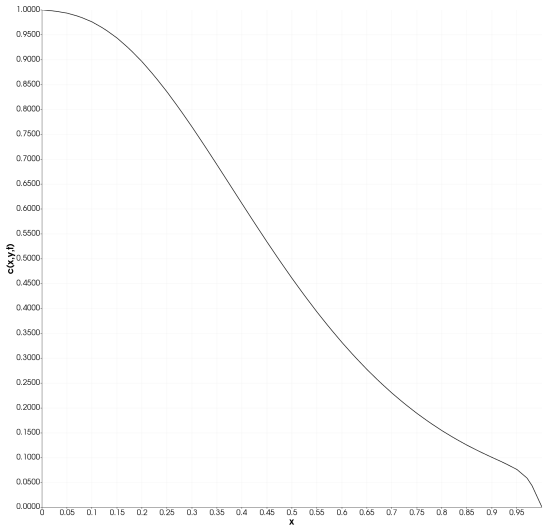

(b) $\bar{c}(x, t)$

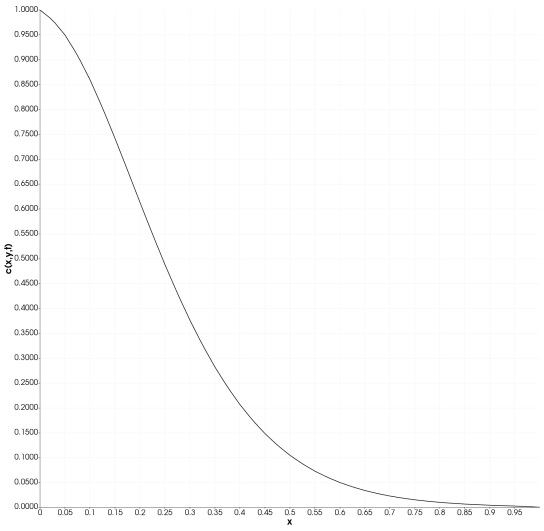

(c) $c^*(x, t)$

Figure 4.43: Comparison plots of concentrations for $\alpha = 1$ and $\beta = 0$ at $t = 0.1$

The dependency of y is shown in fig. (4.44), where there is a plot of the concentration in the 2D-model (vertical axis) for a given y (horizontal axis) at a fixed position $x = 0.2$.

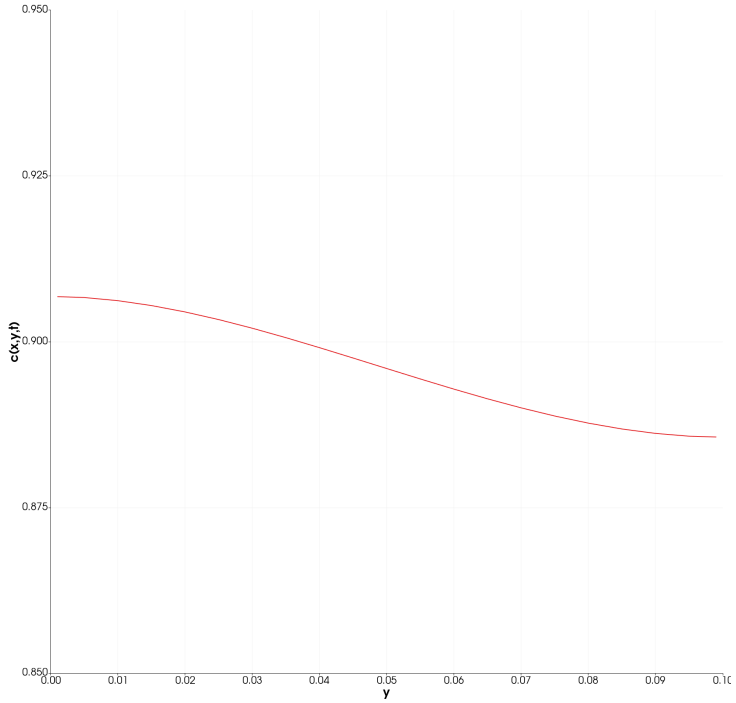

Figure 4.44: Concentration in 2D model as a function of y for $x = 0.2$ at $t = 0.1$

4.4.2.1 Indicator $P(t)$ for Case 2

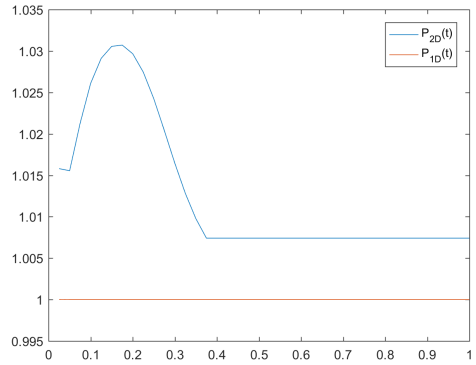

(a) $D_{2D} = D_{1D} = 0.05$

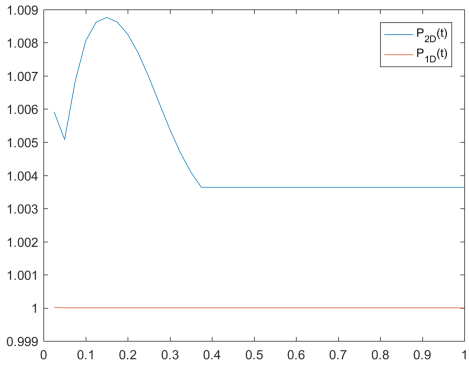

(b) $D_{2D} = D_{1D} = 0.1$

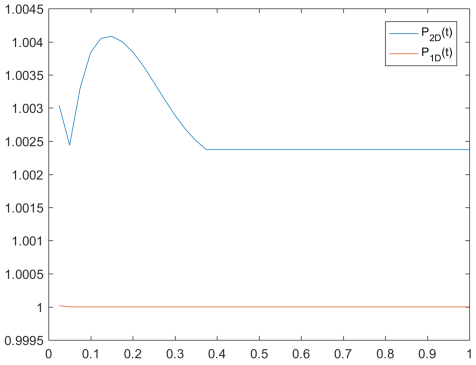

(c) $D_{2D} = D_{1D} = 0.15$

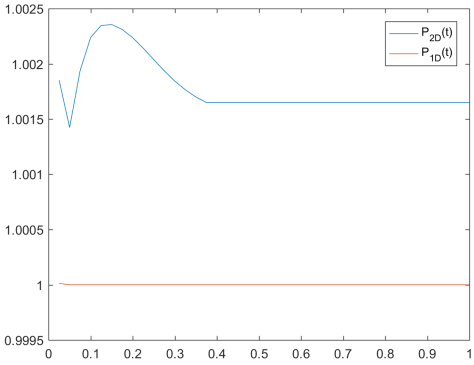

(d) $D_{2D} = D_{1D} = 0.2$

Figure 4.45: Comparing P_{2D} and P_{1D} for different diffusion coefficients with $\alpha = 0$ and $\beta = 0$

The width of the thin strip, ϵ, is then changed to $\epsilon = 0.2$ to see the effect of this parameter under these conditions.

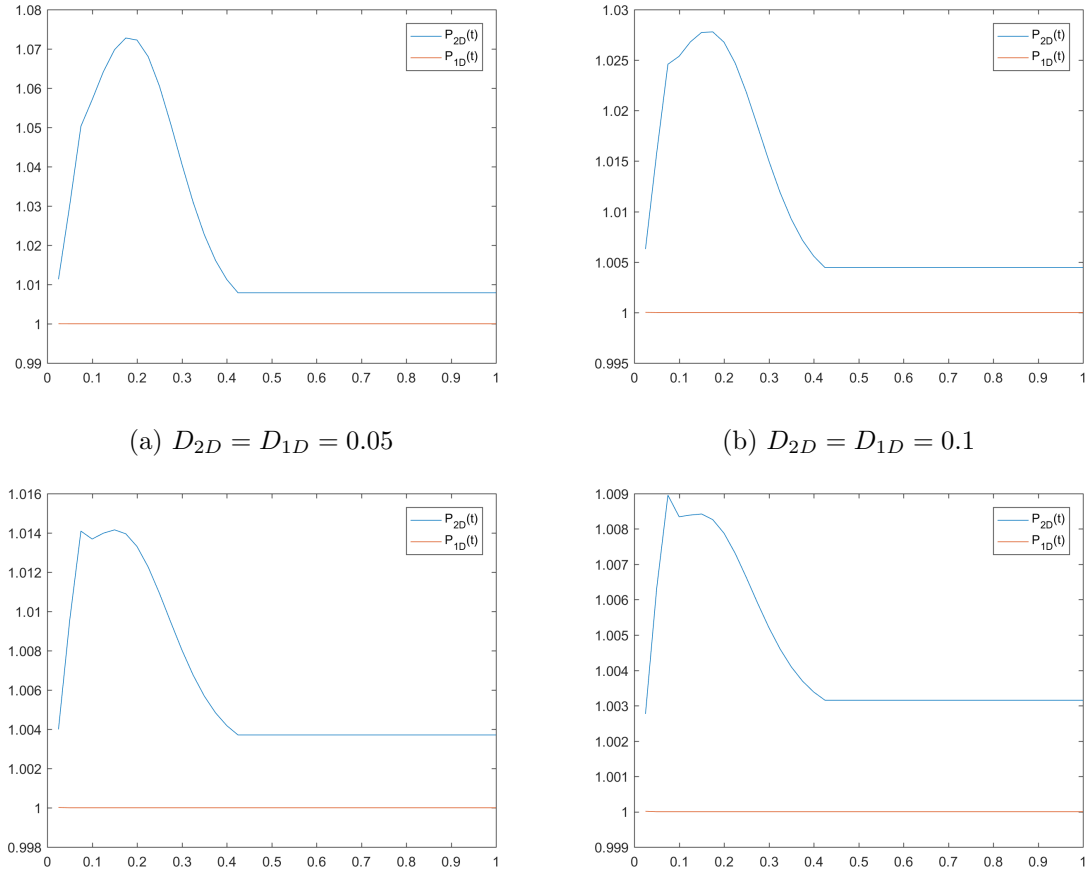

(a) $D_{2D} = D_{1D} = 0.05$

(b) $D_{2D} = D_{1D} = 0.1$

(c) $D_{2D} = D_{1D} = 0.15$

(d) $D_{2D} = D_{1D} = 0.2$

Figure 4.46: Comparing P_{2D} and P_{1D} for different diffusion coefficients with $\alpha = 0$, $\beta = 0$ and $\epsilon = 0.2$

At these plots, we see that the maximum is decreased for an increasing diffusion and increased for an increasing ϵ. All of these plots has a rise from the start, reaches a maximum and then goes down to the same as start level for $\epsilon = 0.1$ and goes beyond that for $\epsilon = 0.2$. This is not due to the ϵ present in the flow equation as $\alpha = 0$, but rather there being a bigger difference of concentration due to the flow being stronger in some parts of the domain as the viscosity being dependent on the y-coordinate. And since the domain is larger, the viscosity has a larger spans than for $\epsilon = 0.1$.

4.4.2.2 Indicator $H(t)$ for Case 2

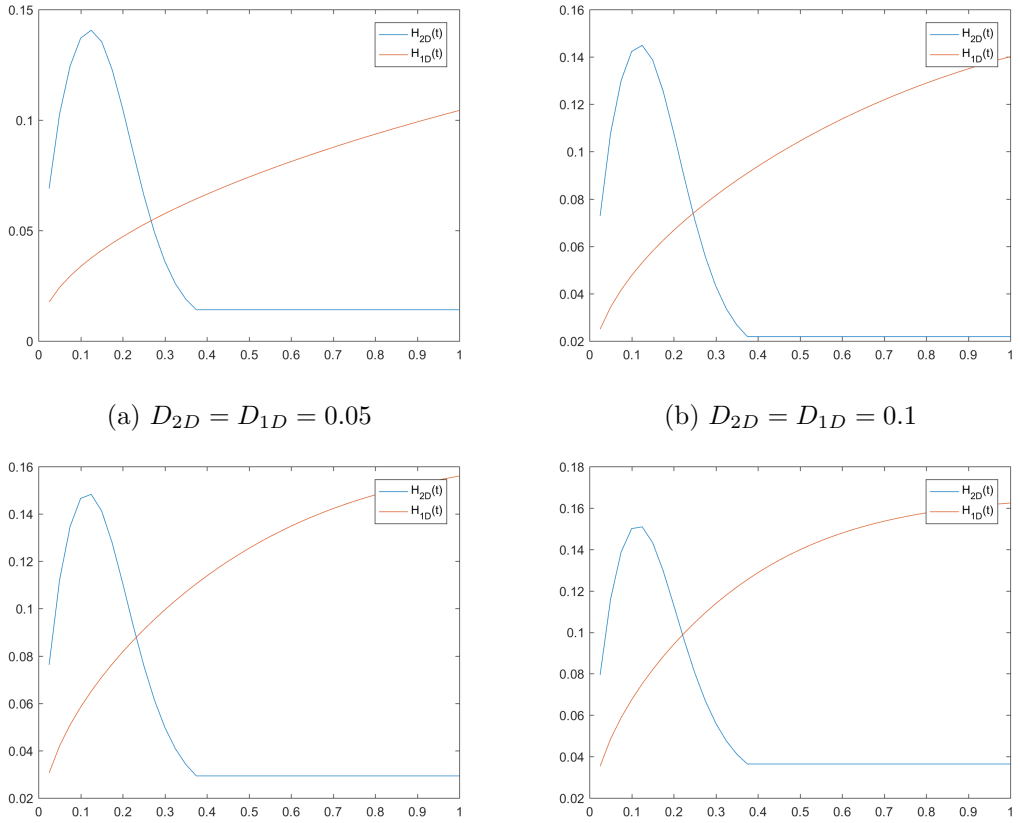

(a) $D_{2D} = D_{1D} = 0.05$ (b) $D_{2D} = D_{1D} = 0.1$

(c) $D_{2D} = D_{1D} = 0.15$ (d) $D_{2D} = D_{1D} = 0.2$

Figure 4.47: Comparing H_{2D} and H_{1D} for different diffusion coefficients with $\alpha = 0$ and $\beta = 0$

The width of the thin strip, ϵ, is then changed to $\epsilon = 0.2$ to see the effect of this parameter under these conditions.

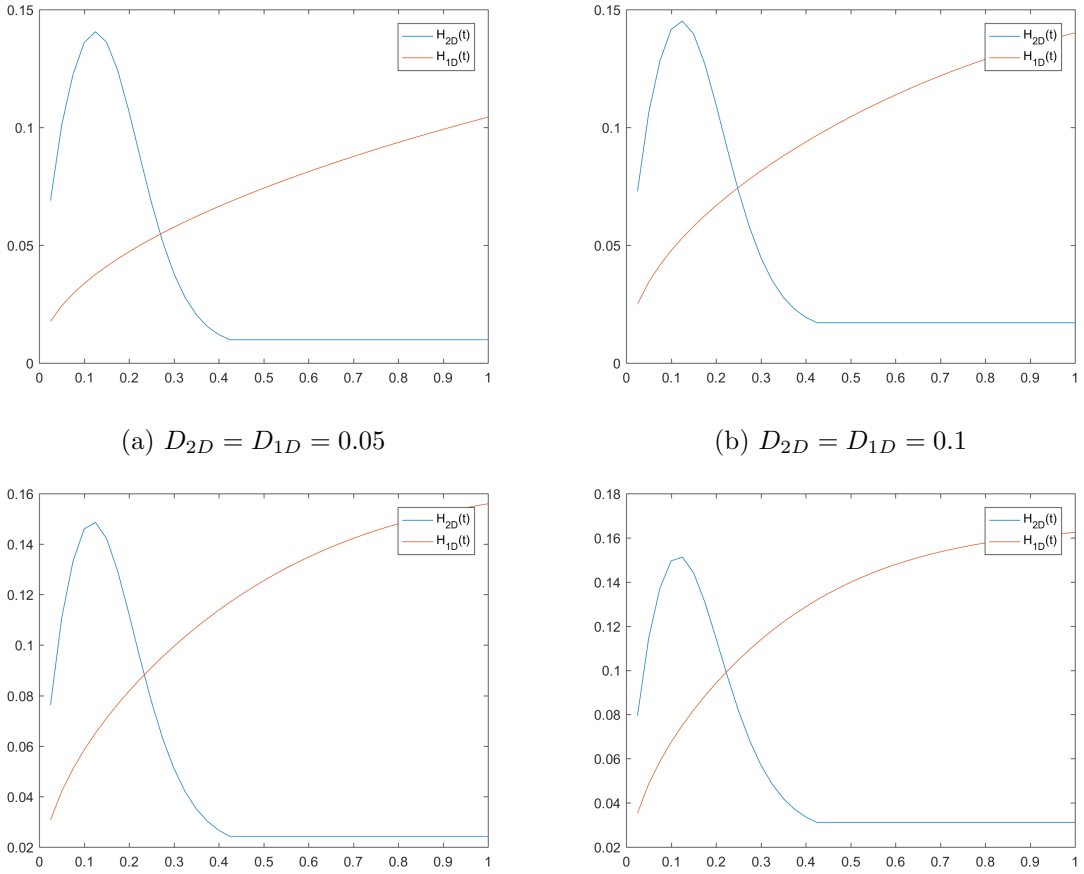

(a) $D_{2D} = D_{1D} = 0.05$

(b) $D_{2D} = D_{1D} = 0.1$

(c) $D_{2D} = D_{1D} = 0.15$

(d) $D_{2D} = D_{1D} = 0.2$

Figure 4.48: Comparing H_{2D} and H_{1D} for different diffusion coefficients with $\alpha = 0$, $\beta = 0$ and $\epsilon = 0.2$

For indicator $H(t)$ we have that for a increasing diffusion the value at the start increases, the maximum stays very similar but the minimum value increases. That is because a stronger diffusion leads to a distribution over larger area and therefore the minimum value increases. The results are the same for $\epsilon = 0.1$ and $\epsilon = 0.2$, as the flow rate is very similar in both cases but a slightly different profile due to a y-dependency in viscosity.

4.4.2.3 Indicator $S(t)$ for Case 2

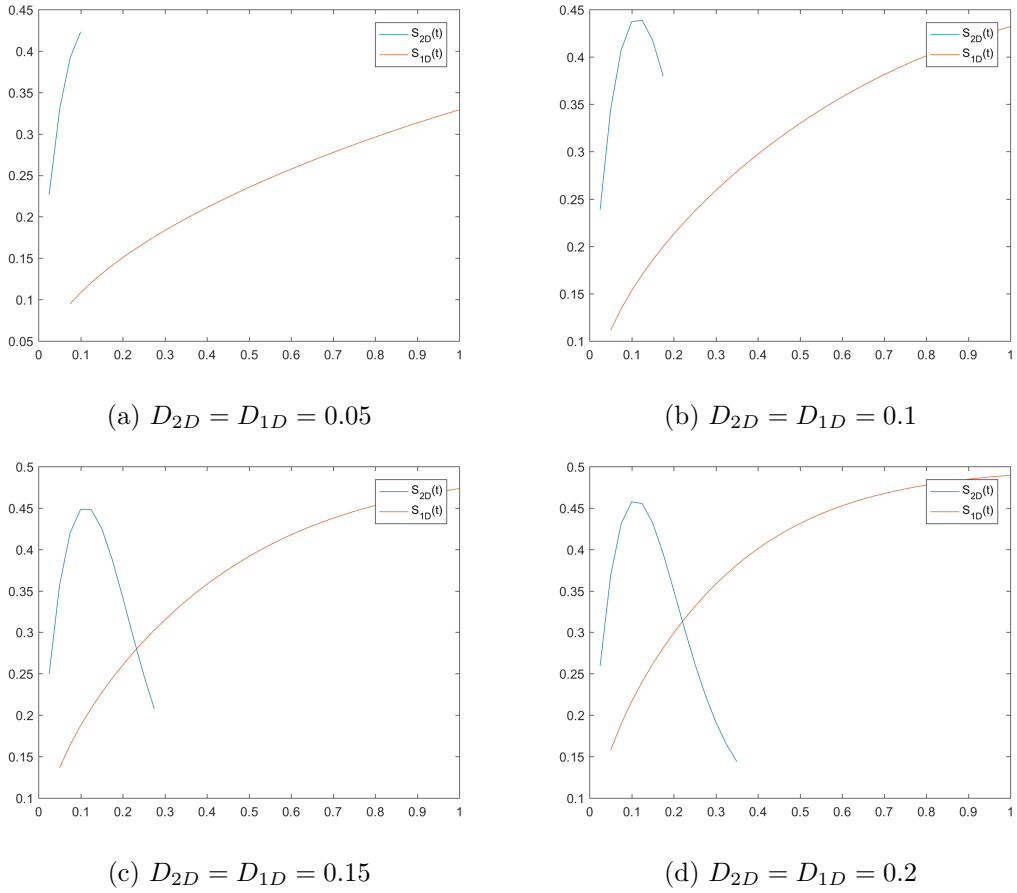

(a) $D_{2D} = D_{1D} = 0.05$ (b) $D_{2D} = D_{1D} = 0.1$

(c) $D_{2D} = D_{1D} = 0.15$ (d) $D_{2D} = D_{1D} = 0.2$

Figure 4.49: Comparing S_{2D} and S_{1D} for different diffusion coefficients with $\alpha = 0$ and $\beta = 0$

The width of the thin strip, ϵ, is then changed to $\epsilon = 0.2$ to see the effect of this parameter under these conditions.

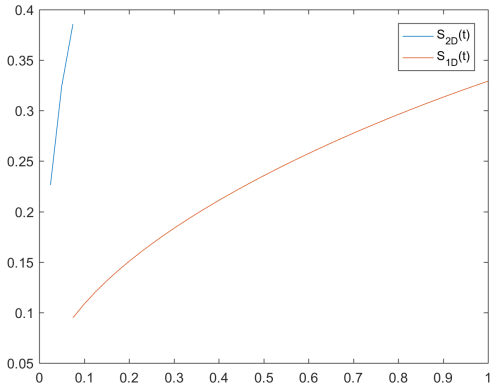

(a) $D_{2D} = D_{1D} = 0.05$

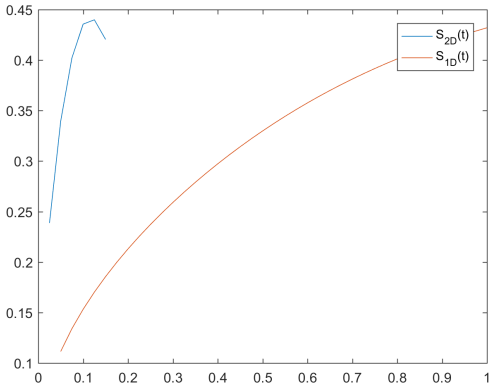

(b) $D_{2D} = D_{1D} = 0.1$

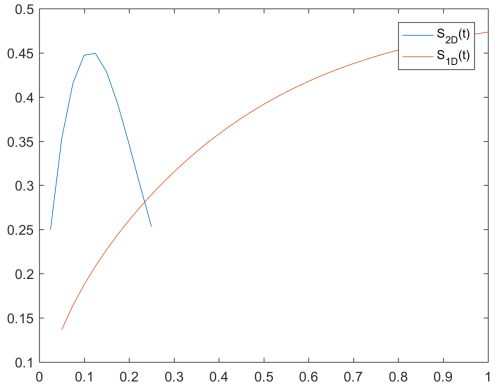

(c) $D_{2D} = D_{1D} = 0.15$

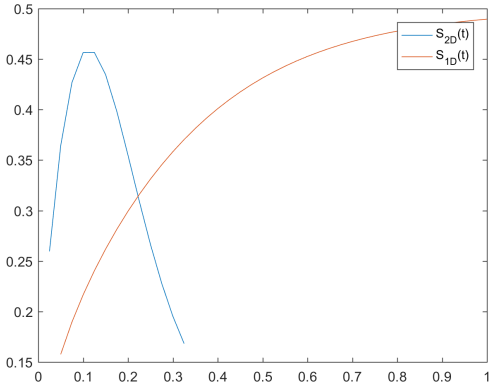

(d) $D_{2D} = D_{1D} = 0.2$

Figure 4.50: Comparing S_{2D} and S_{1D} for different diffusion coefficients with $\alpha = 0$, $\beta = 0$ and $\epsilon = 0.2$

For a small diffusion there is a larger difference of concentration and here the concentration at some areas has a value very close to $c = 1$ and/or $c = 0$. This causes the natural logarithm-terms to go to minus infinity, and therefore this did not converge longer than the line shows in the figures above. It also seams that a larger ϵ results in the terms going to infinity at a timestep or two earlier.

4.4.2.4 Indicator $E(t)$ for Case 2

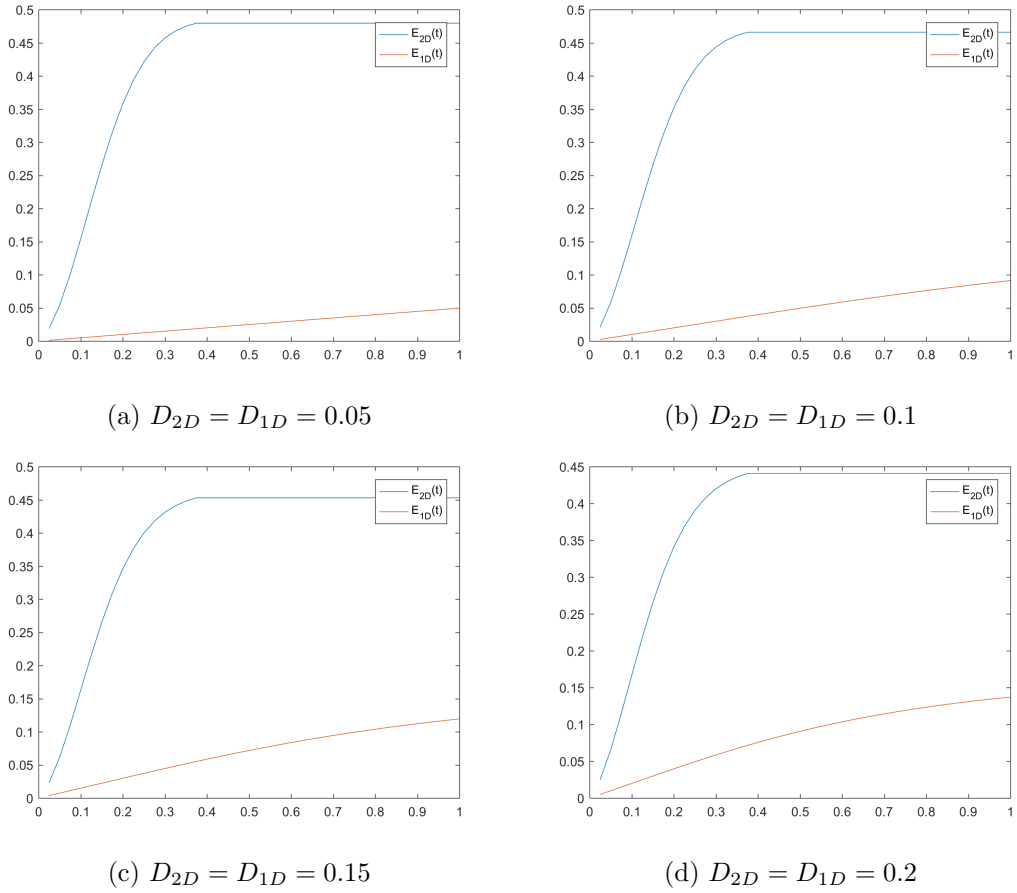

(a) $D_{2D} = D_{1D} = 0.05$ (b) $D_{2D} = D_{1D} = 0.1$

(c) $D_{2D} = D_{1D} = 0.15$ (d) $D_{2D} = D_{1D} = 0.2$

Figure 4.51: Comparing E_{2D} and E_{1D} for different diffusion coefficients with $\alpha = 0$ and $\beta = 0$

The width of the thin strip, ϵ, is then changed to $\epsilon = 0.2$ to see the effect of this parameter under these conditions.

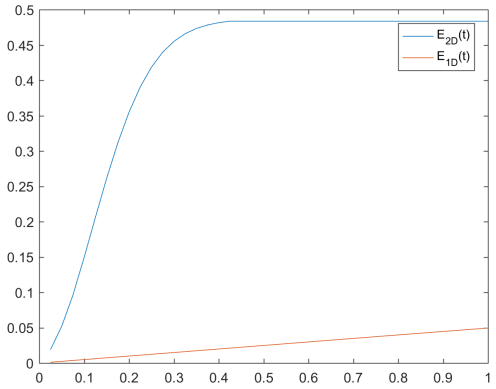

(a) $D_{2D} = D_{1D} = 0.05$

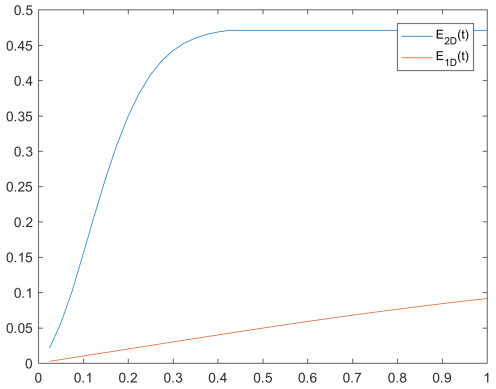

(b) $D_{2D} = D_{1D} = 0.1$

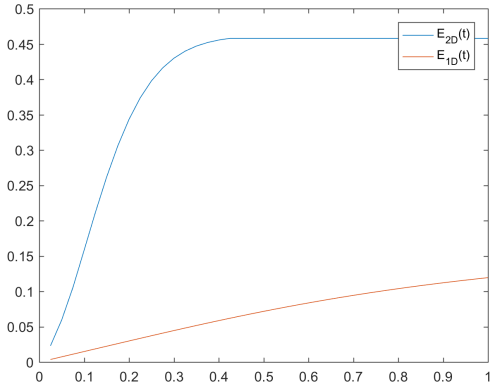

(c) $D_{2D} = D_{1D} = 0.15$

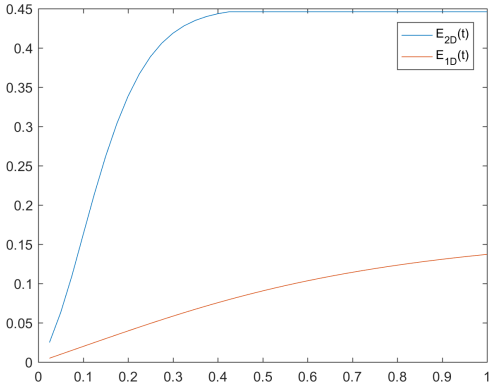

(d) $D_{2D} = D_{1D} = 0.2$

Figure 4.52: Comparing E_{2D} and E_{1D} for different diffusion coefficients with $\alpha = 0$, $\beta = 0$ and $\epsilon = 0.2$

We observe that for a larger diffusion the maximum value is reduced while a larger ϵ results in a slightly increased maximum, but it reaches its maximum value at a later timestep. However, as we see here, the impact of diffusion and ϵ is limited.

4.4.3 Case 3, $-1 < \alpha < 0$

$$\alpha = -0.5, \beta = 0, \epsilon = 0.1$$

$$D_{2D} = 0.1, D_{1D} = 0.1, g = 9.81$$

$$\mu(x, y, t) = exp\left(-1 + \frac{0.7\, y}{\epsilon} c(x, y, t)\right)$$

The concentration for time $t = 0.05$ is shown in the following figure.

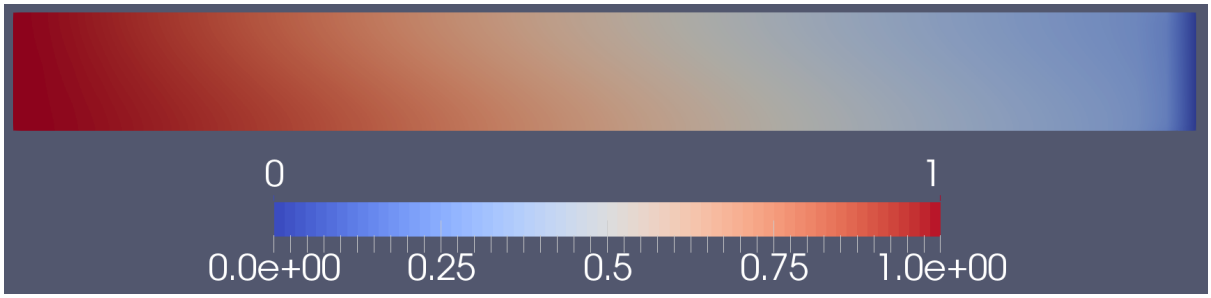

(a) Concentration distribution in 2D model for $t = 0.05$

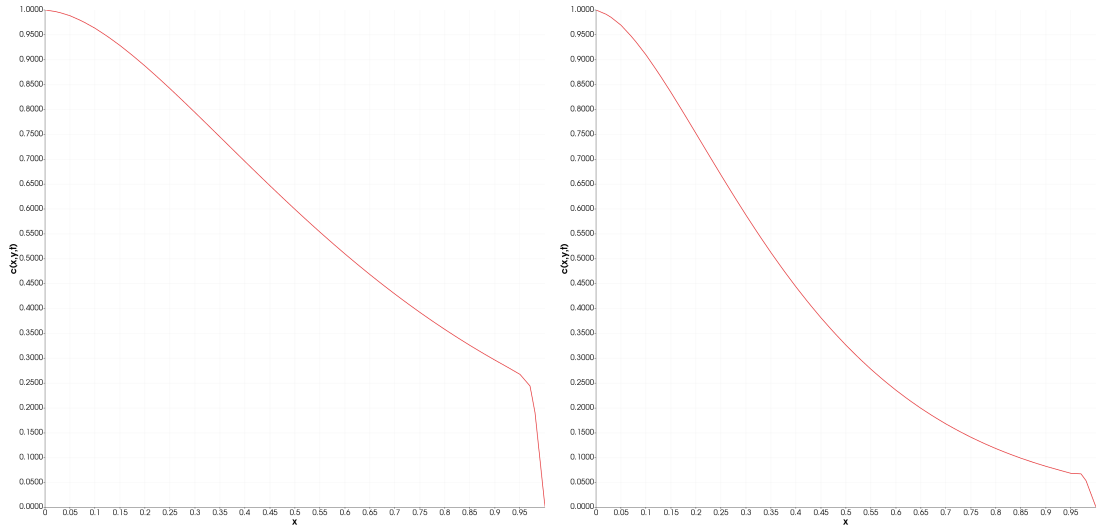

(b) $\bar{c}(x, t)$ (c) $c^*(x, t)$

Figure 4.53: Comparison plots of concentrations for $\alpha = 1$ and $\beta = 0$ at $t = 0.05$

The dependency of y is shown in fig. (4.54), where there is a plot of the concentration in the 2D-model (vertical axis) for a given y (horizontal axis) at a fixed position $x = 0.2$.

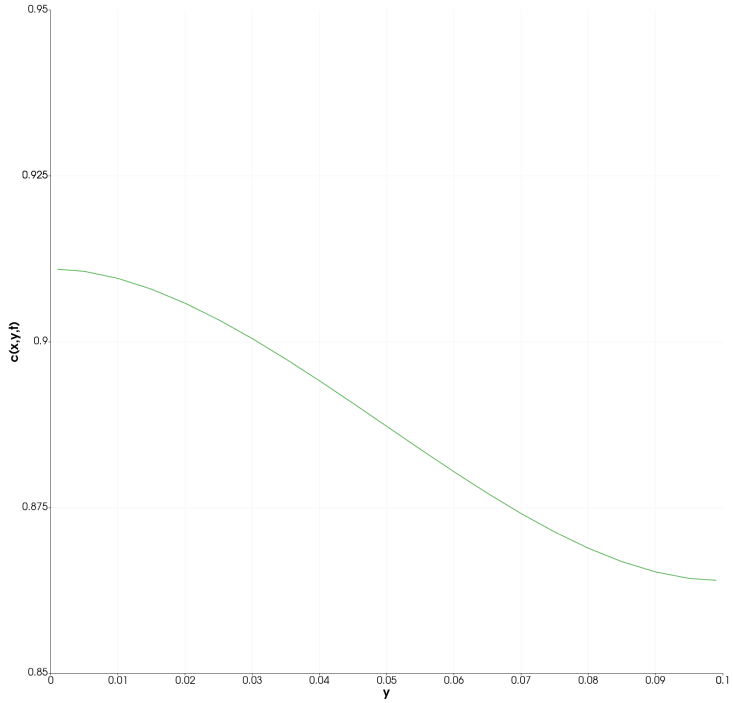

Figure 4.54: Concentration in 2D model as a function of y for $x = 0.2$ at $t = 0.05$

4.4.3.1 Indicator $P(t)$ for Case 3

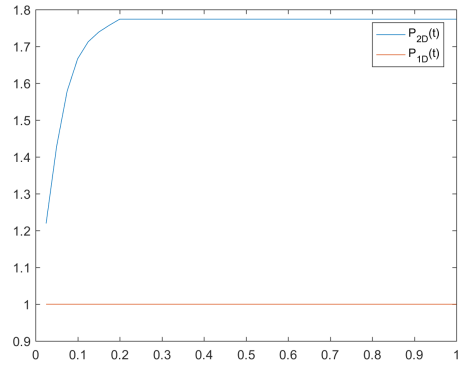

(a) $D_{2D} = D_{1D} = 0.05$

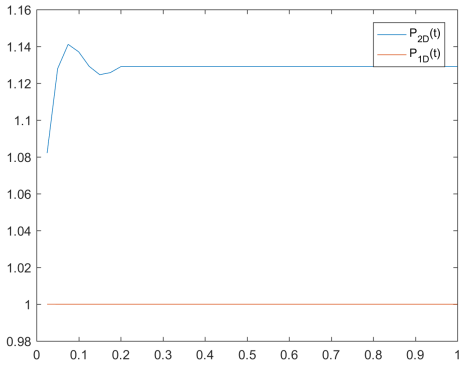

(b) $D_{2D} = D_{1D} = 0.1$

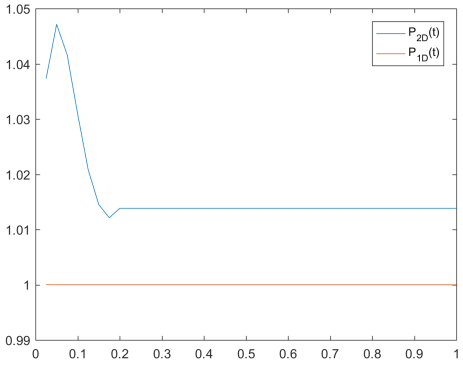

(c) $D_{2D} = D_{1D} = 0.15$

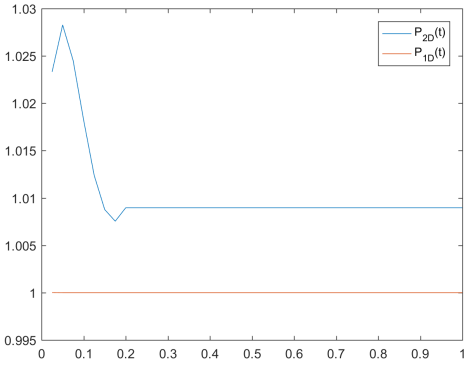

(d) $D_{2D} = D_{1D} = 0.2$

Figure 4.55: Comparing P_{2D} and P_{1D} for different diffusion coefficients with $\alpha = -0.5$ and $\beta = 0$

The width of the thin strip, ϵ, is then changed to $\epsilon = 0.2$ to see the effect of this parameter under these conditions.

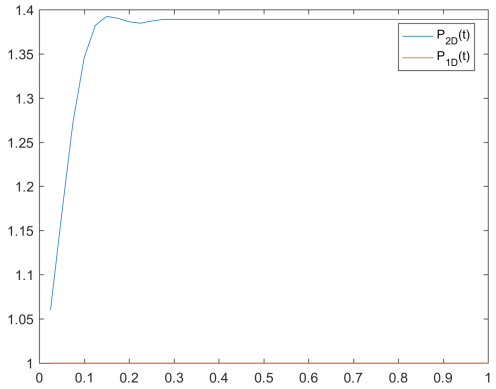

(a) $D_{2D} = D_{1D} = 0.05$

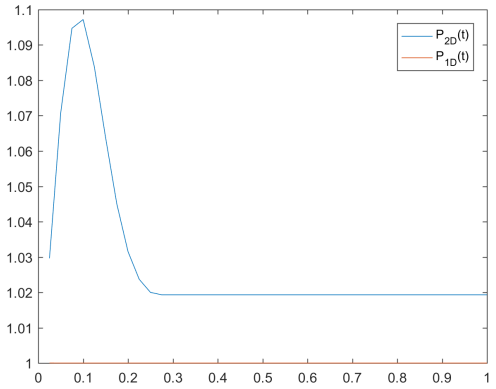

(b) $D_{2D} = D_{1D} = 0.1$

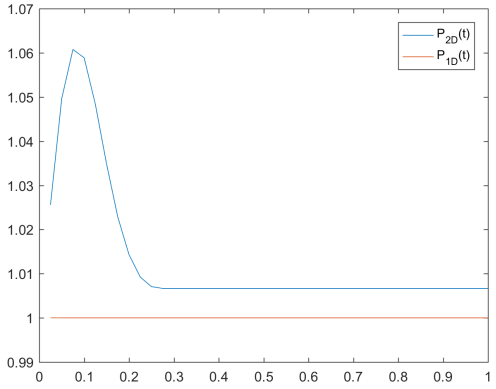

(c) $D_{2D} = D_{1D} = 0.15$

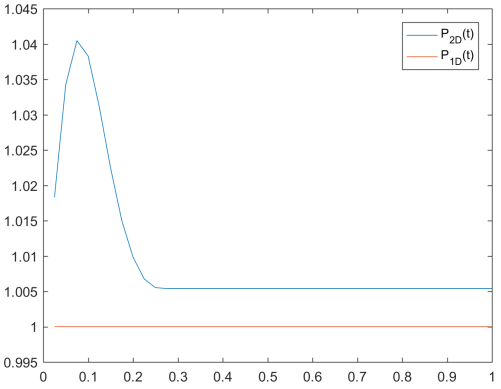

(d) $D_{2D} = D_{1D} = 0.2$

Figure 4.56: Comparing P_{2D} and P_{1D} for different diffusion coefficients with $\alpha = -0.5$, $\beta = 0$ and $\epsilon = 0.2$

Here we observe that for a diffusion coefficient of 0.05, $P(t)$ reaches its maximum and stays constant for the rest of the simulation, but for a larger diffusion, the value goes down after the maximum. For diffusions larger than 0.1 it goes down to a value very close to 1. For $\epsilon = 0.2$, this threshold goes for diffusions larger than 0.05. This could be due to the flow-rate being higher than for $\epsilon = 0.1$. We also observe that for a diffusion larger than 0.1, the plots for $\epsilon = 0.2$ shows a higher maximum value and a lower maximum for diffusions of 0.1 and lower.

4.4.3.2 Indicator $H(t)$ for Case 3

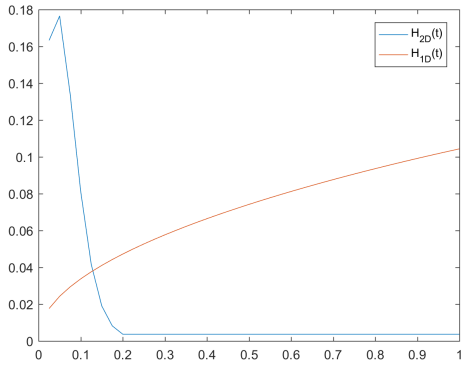

(a) $D_{2D} = D_{1D} = 0.05$

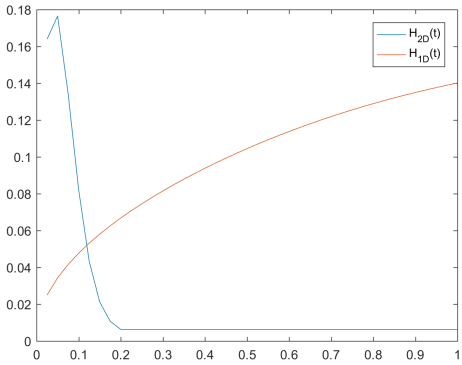

(b) $D_{2D} = D_{1D} = 0.1$

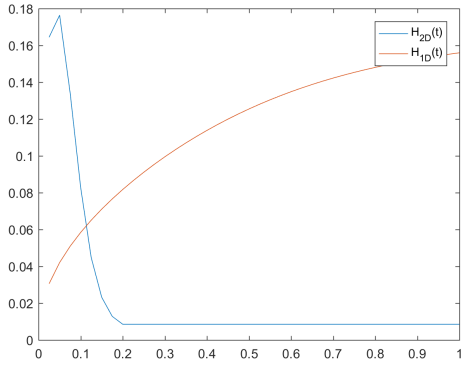

(c) $D_{2D} = D_{1D} = 0.15$

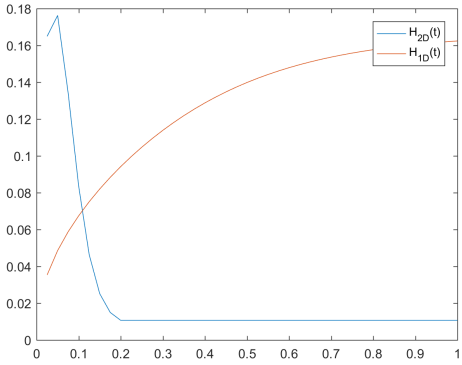

(d) $D_{2D} = D_{1D} = 0.2$

Figure 4.57: Comparing H_{2D} and H_{1D} for different diffusion coefficients with $\alpha = -0.5$ and $\beta = 0$

The width of the thin strip, ϵ, is then changed to $\epsilon = 0.2$ to see the effect of this parameter under these conditions.

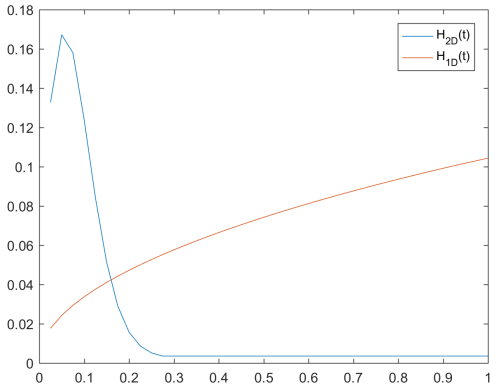

(a) $D_{2D} = D_{1D} = 0.05$

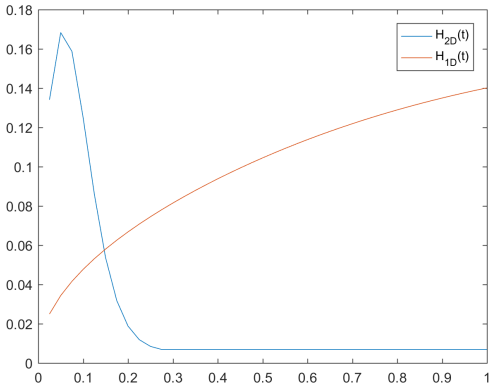

(b) $D_{2D} = D_{1D} = 0.1$

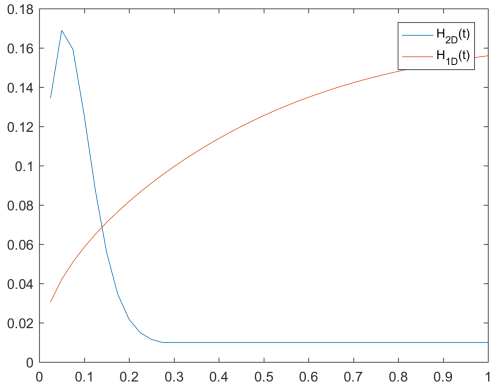

(c) $D_{2D} = D_{1D} = 0.15$

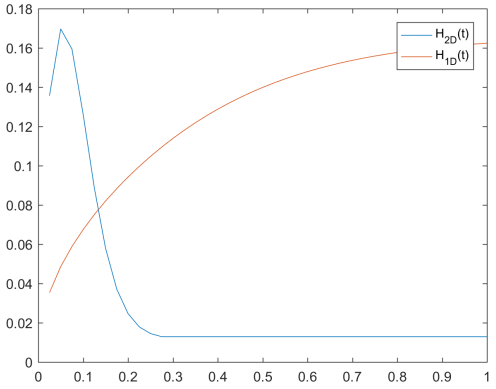

(d) $D_{2D} = D_{1D} = 0.2$

Figure 4.58: Comparing H_{2D} and H_{1D} for different diffusion coefficients with $\alpha = -0.5$, $\beta = 0$ and $\epsilon = 0.2$

For this indicator we observe that the plot for P_{2D} does not change noticeable with a bigger diffusion other than the minimum value increases a bit and the same goes for an increase in ϵ. This is what we expected with an increase in flow rate, then the diffusion does not impact the solutions as much as for the other cases.

4.4.3.3 Indicator $S(t)$ for Case 3

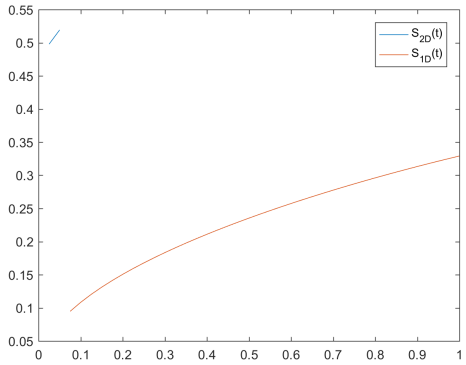

(a) $D_{2D} = D_{1D} = 0.05$

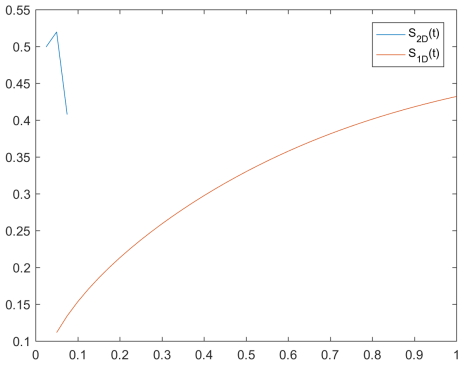

(b) $D_{2D} = D_{1D} = 0.1$

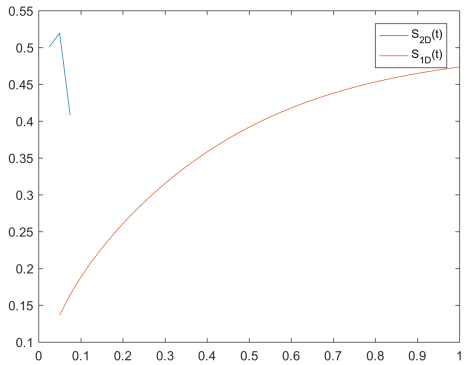

(c) $D_{2D} = D_{1D} = 0.15$

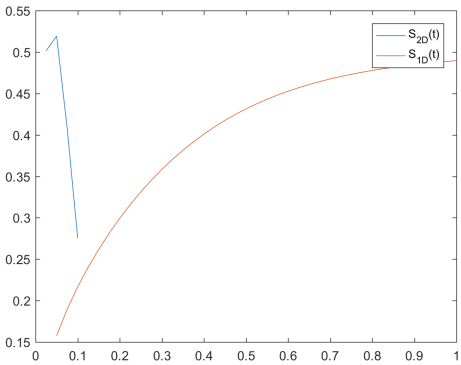

(d) $D_{2D} = D_{1D} = 0.2$

Figure 4.59: Comparing S_{2D} and S_{1D} for different diffusion coefficients with $\alpha = -0.5$ and $\beta = 0$

The width of the thin strip, ϵ, is then changed to $\epsilon = 0.2$ to see the effect of this parameter under these conditions.

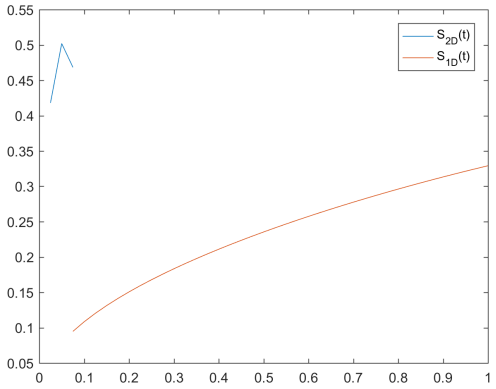

(a) $D_{2D} = D_{1D} = 0.05$

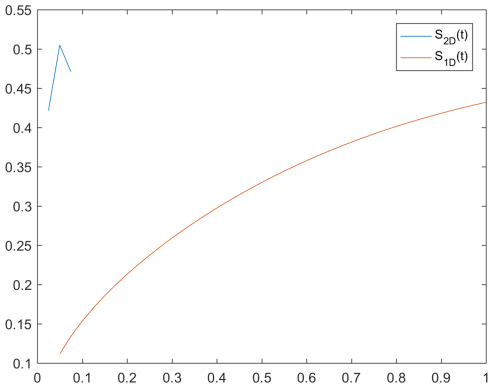

(b) $D_{2D} = D_{1D} = 0.1$

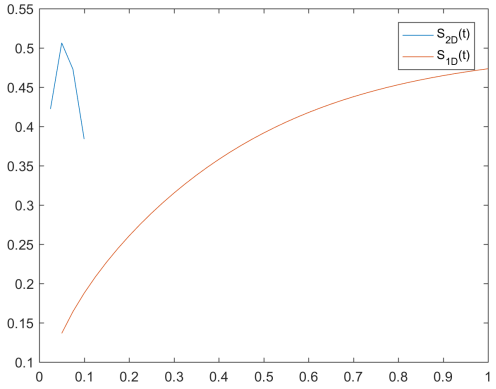

(c) $D_{2D} = D_{1D} = 0.15$

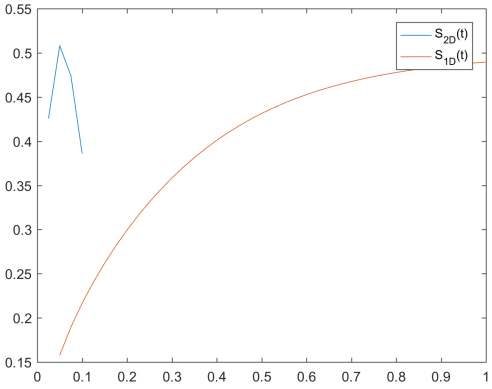

(d) $D_{2D} = D_{1D} = 0.2$

Figure 4.60: Comparing S_{2D} and S_{1D} for different diffusion coefficients with $\alpha = -0.5$, $\beta = 0$ and $\epsilon = 0.2$

As for Case 2, there is not a very conclusive results. For a larger diffusion, we get a result of the integration for more timesteps and longer into the simulation. As described in the previous case, it goes to infinity when the c is very close to 0 or 1. Like in the other case, a larger ϵ results in the terms going to infinity at a timestep or two earlier

4.4.3.4 Indicator $E(t)$ for Case 3

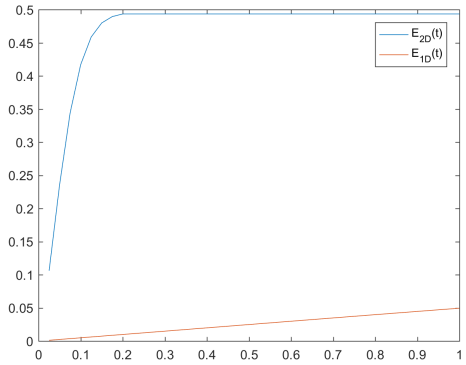

(a) $D_{2D} = D_{1D} = 0.05$

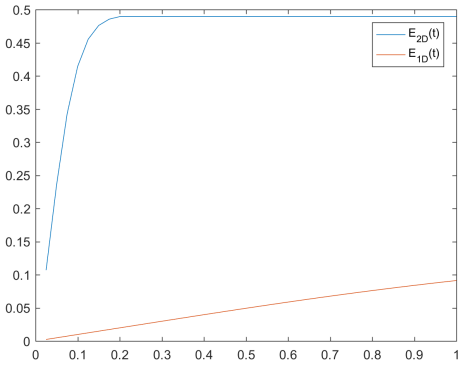

(b) $D_{2D} = D_{1D} = 0.1$

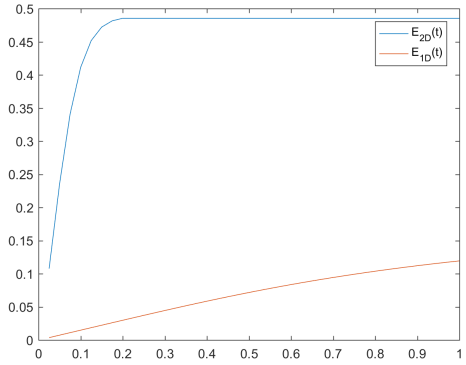

(c) $D_{2D} = D_{1D} = 0.15$

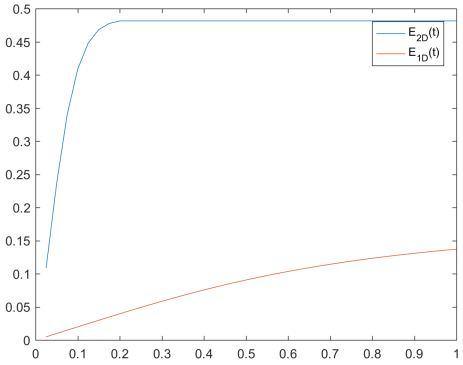

(d) $D_{2D} = D_{1D} = 0.2$

Figure 4.61: Comparing E_{2D} and E_{1D} for different diffusion coefficients with $\alpha = -0.5$ and $\beta = 0$

The width of the thin strip, ϵ, is then changed to $\epsilon = 0.2$ to see the effect of this parameter under these conditions.

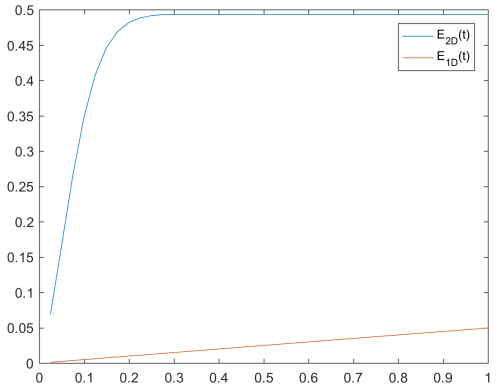

(a) $D_{2D} = D_{1D} = 0.05$

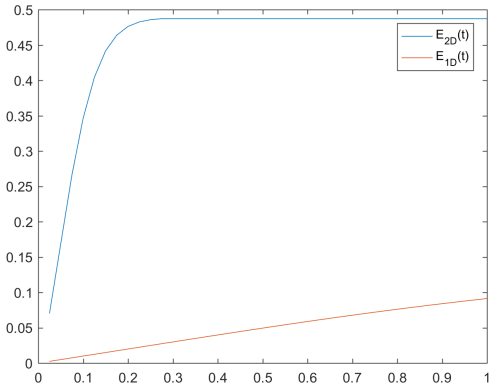

(b) $D_{2D} = D_{1D} = 0.1$

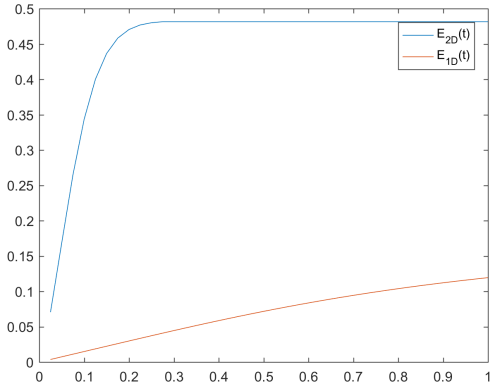

(c) $D_{2D} = D_{1D} = 0.15$

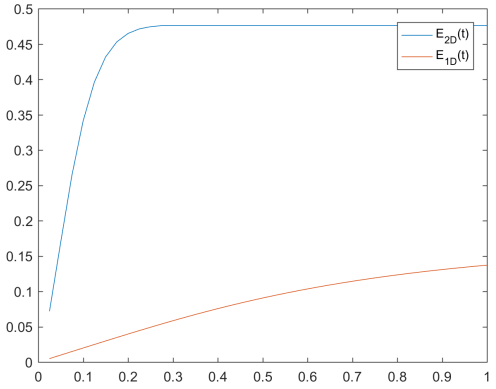

(d) $D_{2D} = D_{1D} = 0.2$

Figure 4.62: Comparing E_{2D} and E_{1D} for different diffusion coefficients with $\alpha = -0.5$, $\beta = 0$ and $\epsilon = 0.2$

We observe that for a larger diffusion the maximum value is a bit reduced, but the change is less than in the previous cases. This is in hand with the derivations of the indicators in Chapter 3. A larger ϵ results in a more curved increase to the same maximum value. However, as we see here and in previous case, the impact of diffusion and ϵ is very limited.

Chapter 5

Conclusion

Throughout this thesis we have rigorously derived a 1D-model from taking the vertical average of a 2D-model. Under this derivation, we have shown the convergence and boundedness for different regimes of α and β. The thesis also provides a formal derivation of an effective 1D-model from a vertical-averaged model. Later we also have shown with numerical results the same kind of results, where we have shown the convergence in the different regimes of α and β. We also have also tested our scheme against an analytical solution where the different convergence rates and sizes of error has been presented. The whole thesis has also focused on the coupling of the Darcy equation for flow and the convectiondiffusion equation for transport.

This coupling has been handled with an iterative scheme, where the flux has been calculated by using the concentration from the previous time-step, then calculating concentration before iterating between the two until convergence. The scheme for the flux calculations was using a dual-mixed formulation, which meant that the flux and pressure was calculated in a mixed function space where both the pressure and flux lied.

Furthermore, we saw that the models used performed good with high convergence rates within the validity range of α and β. For $-1 < \alpha, \beta < 3$ the solutions behaved smoothly in most cases. For the cases where the viscosity function had very large fluctuations, the validity range was smaller.

As shown in section (4.4), the purposed 1D model for $\bar{c}(x,t)$, a vertical-averaged value for $c(x,y,t)$, does not capture all the geometry that the indicators mentioned in the section measures. This is especially the case when we have a high flow-rate and an inhomogeneous flow. For the last part where we consider $\alpha < 0$ we see that there is more turbulence happening due to larger flux differences and therefore the indicators fluctuate more than for the other cases. This is not being captured in the 1D-model which do not show turbulence. From this we can conclude that with the models today, we do not have a good 1D-model that captures the different geometries that is caused by a turbulent flow in a 2D-model. There is a need for new and better 1D-models in this field.

From our study we can conclude that the models will have to make use of these indicators of geometrical properties which has to be reflected / compensated for in the 1D-model.

5.1 Further work

The thesis deals with upscaling of a single-phase flow coupled to transport of a chemical species in an anisotropic permeability field. Our attempts are in deriving and testing upscaled 1D-model that captures sufficient details of the 2D thin strip model. Several extensions of this work are possible and are left for future works.

1. We have only performed the upscaling for a single-phase flow model. Extending it to a two-phase flow model is important both from the theoretical and applications point of view. The carbon sequestration problem involves multiple phases and high fidelity upscaled models are quite important there. However, challenges remain in performing this upscaling for the different scalings of the transport properties. From a theoretical perspective, getting a control on the gradients of saturation in a two-phase flow model is quite complex.

2. We believe that there is a link between non-monotone saturation profiles in a 1D sand column experiments and the experimental speed of the viscous fingering transition zone. It turns out that the experimental speed of the viscous fingering in the transition phase is half of what is predicted by entropy solutions that are rarefaction. Otto and Menon and later Yortsos have proved that the experimentally observed speed is explained by considering shock solutions that are moving at different speeds. In the work of Pop, van Duijn, and Peletier[33], non-monotone saturation profiles for Buckeley Leverett equation are explained by considering a regularization of the form that consists of time derivative of Laplacian. One of the equilibrium solutions as obtained by travelling wave solutions is two shock profiles moving at different speeds. We expect a similar situation here where a different regularization of the transport equation (of the form of time derivative of Laplacian) will explain the apparent contradiction arising from the entropy solution not being the observed one. This work remains incomplete in our thesis.

3. Even though we have provided indicators based on the geometric properties for the comparison of 1D model and 2D model, we have not been able to use this to provide a better 1D model in the case when the fingering is present. It is interesting that the quantity called Perimeter measures the width of the fingers, however, we have a differential inequality rather than an equation for this quantity that can be used to construct a better 1D model. It would be interesting to formulate a 1D model based on the quantities that are introduced in this thesis.

4. The main challenge in the upscaling of transport equation is the control of gradient of the concentration in the vertical direction. This situation is comparable to the turbulent flow model in a pipe. In a pipe flow, the equation that describes the turbulence is described in terms of a coupled mean flow model with an equation modelling turbulence. The situation in our case is quite similar with the mean flow model representing the average concentration and the turbulence denoting the perturbation from the average concentration. We can profitably adopt some of the models of turbulence in our case to provide a better 1D model.

References

[1] Dietrich Braess. *Finite Elements*. Cambridge University Press, second edition, 2001. Translated from the German by Larry L. Schumaker.

[2] C. Bringedal, I. Berre, I. S. Pop, and F. A. Radu. Upscaling of nonisothermal reactive porous media flow under dominant pclet number: The effect of changing porosity. *Multiscale Modeling & Simulation*, 14(1):502–533, 2016.

[3] Min Chen, William Rossen, and Yannis C. Yortsos. The flow and displacement in porous media of fluids with yield stress. *Chemical Engineering Science*, 60(15):4183 – 4202, 2005.

[4] Catherine Choquet and Andro Mikelić. Laplace transform approach to the rigorous upscaling of the infinite adsorption rate reactive flow under dominant Peclet number through a pore. *Appl. Anal.*, 87(12):1373–1395, 2008.

[5] Catherine Choquet and Andro Mikelić. Rigorous upscaling of the reactive flow with finite kinetics and under dominant Péclet number. *Contin. Mech. Thermodyn.*, 21(2):125–140, 2009.

[6] S. E. Gasda, J. M. Nordbotten, and M. A. Celia. Vertical equilibrium with sub-scale analytical methods for geological co2 sequestration. *Computational Geosciences*, 13(4):469, Apr 2009.

[7] S. E. Gasda, J. M. Nordbotten, and M. A. Celia. Vertically averaged approaches for co2 migration with solubility trapping. *Water Resources Research*, 47(5):n/a–n/a, 2011. W05528.

[8] Sarah E. Gasda, Jan M. Nordbotten, and Michael A. Celia. Application of simplified models to co2 migration and immobilization in large-scale geological systems. *International Journal of Greenhouse Gas Control*, 9(Supplement C):72 – 84, 2012.

[9] S.E. Gasda, A.F. Stephansen, I. Aavatsmark, and H.K. Dahle. Upscaled modeling of co2 injection and migration with coupled thermal processes. *Energy Procedia*, 40(Supplement C):384 – 391, 2013. European Geosciences Union General Assembly 2013, EGUDivision Energy, Resources & the Environment, ERE.

[10] Vivette Girault, Kundan Kumar, and Mary F. Wheeler. Convergence of iterative coupling of geomechanics with flow in a fractured poroelastic medium. *Computational Geosciences*, 20(5):997–1011, Oct 2016.

[11] G. M. Homsy. Viscous fingering in porous media. *Fluid Mechanics*, 19:271–311, 1987.

[12] Tanveer Iqbal and Arnold Neumaier. Worst case error bounds for the solution of uncertain poisson equations with mixed boundary conditions. *Journal of Computational and Applied Mathematics*, 303(Supplement C):40 – 55, 2016.

[13] Claes Johnson. *Numerical solution of partial differential equations by the finite element method*. Cambridge University Press, 1987.

[14] T. L. van Noorden K. Kumar and I. S. Pop. Effective dispersion equations for reactive flows involving free boundaries at the microscale. *Multiscale Model. Simul.*, 9:53–57, 2011.

[15] K. Kumar, M. Neuss-Radu, and I. S. Pop. Homogenization of a pore scale model for precipitation and dissolution in porous media. *IMA Journal of Applied Mathematics*, 81(5):877–897, 2016.

[16] K. Kumar, I. S. Pop, and F. A. Radu. Convergence analysis of mixed numerical schemes for reactive flow in a porous medium. *SIAM Journal on Numerical Analysis*, 51(4):2283–2308, 2013.

[17] K. Kumar, I. S. Pop, and F. A. Radu. Convergence analysis for a conformal discretization of a model for precipitation and dissolution in porous media. *Numerische Mathematik*, 127(4):715–749, Aug 2014.

[18] Shuangcai Li and Christopher J. Duffy. Fully-coupled modeling of shallow water flow and pollutant transport on unstructured grids. *Procedia Environmental Sciences*, 13(Supplement C):2098 – 2121, 2012. 18th Biennial ISEM Conference on Ecological Modelling for Global Change and Coupled Human and Natural System.

[19] Jan M. Nordbotten and Michael A. Celia. *Geological Storage of CO: Modeling Approaches for Large-Scale Simulation*. John Wiley & Sons, Inc., 11 2011.

[20] G. Menon and F. Otto. Dynamic scaling in miscible viscous fingering. *Communications in Mathematical Physics*, 257(2):303–317, Jul 2005.

[21] Andro Mikelić, Vincent Devigne, and C. J. van Duijn. Rigorous upscaling of the reactive flow through a pore, under dominant Peclet and Damkohler numbers. *SIAM J. Math. Anal.*, 38(4):1262–1287, 2006.

[22] Andro Mikelić and C. J. van Duijn. Rigorous derivation of a hyperbolic model for Taylor dispersion. *Math. Models Methods Appl. Sci.*, 21(5):1095–1120, 2011.

[23] Jude L. Musuuza, Florin A. Radu, and Sabine Attinger. The effect of dispersion on the stability of density-driven flows in saturated homogeneous porous media. *Advances in Water Resources*, 34(3):417 – 432, 2011.

[24] Jude L. Musuuza, Florin A. Radu, and Sabine Attinger. The stability of density-driven flows in saturated heterogeneous porous media. *Advances in Water Resources*, 34(11):1464 – 1482, 2011.

[25] J. M. Nordbotten and H. K. Dahle. Impact of the capillary fringe in vertically integrated models for co2 storage. *Water Resources Research*, 47(2):n/a–n/a, 2011. W02537.

[26] Jan Martin Nordbotten, Michael A. Celia, and Stefan Bachu. Injection and storage of co2 in deep saline aquifers: Analytical solution for co2 plume evolution during injection. *Transport in Porous Media*, 58(3):339–360, Mar 2005.

[27] Lars Onsager. Reciprocal relations in irreversible processes. i. *Phys. Rev.*, 37:405–426, Feb 1931.

[28] FEniCS Project. Dual-mixed formulation for poisson equation. `https://fenicsproject.org/olddocs/dolfin/1.4.0/python/demo/documented/mixed-poisson-dual/python/documentation.html`.

[29] F.A. Radu, N. Suciu, J. Hoffmann, A. Vogel, O. Kolditz, C.-H. Park, and S. Attinger. Accuracy of numerical simulations of contaminant transport in heterogeneous aquifers: A comparative study. *Advances in Water Resources*, 34(1):47 – 61, 2011.

[30] Hongxing Rui and Jingyuan Zhang. A stabilized mixed finite element method for coupled stokes and darcy flows with transport. *Computer Methods in Applied Mechanics and Engineering*, 315(Supplement C):169 – 189, 2017.

[31] K. Shankar and Yanis C. Yortsos. Asymptotic analysis of single pore gas-solid reactions. *Chemical Engineering Science*, 38(8):1159 – 1165, 1983.

[32] C. J. van Duijn, X. Cao, and I. S. Pop. Two-phase flow in porous media: Dynamic capillarity and heterogeneous media. *Transport in Porous Media*, 114(2):283–308, Sep 2016.

[33] C. J. van Duijn, L. A. Peletier, and I. S. Pop. A new class of entropy solutions of the buckleyleverett equation. *SIAM Journal on Mathematical Analysis*, 39(2):507–536, 2007.

[34] C.J. van Duijn, Y. Fan, L.A. Peletier, and I.S. Pop. Travelling wave solutions for degenerate pseudo-parabolic equations modelling two-phase flow in porous media. *Nonlinear Analysis: Real World Applications*, 14(3):1361 – 1383, 2013.

[35] D Chandra Mohan Vyas, Sumit Kumar, and Atul Srivastava. Porous media based bio-heat transfer analysis on counter-current artery vein tissue phantoms: Applications in photo thermal therapy. *International Journal of Heat and Mass Transfer*, 99(Supplement C):122 – 140, 2016.

[36] Adam Z. Webera. A critical review of modeling transport phenomena in polymer-electrolyte fuel cells. *Journal of Electrochemestry Society*, 161(19):1254 – 1299, 2014.

[37] Z.M. Yang, Y.C. Yortsos, and Dominique Salin. Asymptotic regimes in unstable miscible displacements in random porous media. *Advances in Water Resources*, 25(8):885 – 898, 2002.

[38] A.G Yiotis, A.K Stubos, A.G Boudouvis, and Y.C Yortsos. A 2-d pore-network model of the drying of single-component liquids in porous media. *Advances in Water Resources*, 24(3):439 – 460, 2001. Pore Scale Modeling.

[39] Y. C. Yortsos and D. Salin. On the selection principle for viscous fingering in porous media. *Journal of Fluid Mechanics*, 557:225–236, 2006.

[40] Y.Q. Zu. Modelling of migration of co2 in porous media under conditions of saline aquifers using lattice boltzmann method. *Procedia Engineering*, 126(Supplement C):471 – 475, 2015. Frontiers in Fluid Mechanics Research.

Appendices

Appendix A

Main program for reference solution

The code is based on Python 2, running in the FEniCS docker container.

```
# Imports the necessary functions and packages for the calculations to work.
from __future__ import print_function
from dolfin import *
import numpy as np

# Variables for time-stepping
T = 5.0
num_steps = 20
dt = T / num_steps
t = 0.0

delta = 5
eps = 1

# Mesh settings
x0 = 0
x1 = 5
y0 = 0
y1 = 1

# Grid cells in each direction
nx = 10
ny = 2

# Model settings
element_pressure = "CG"
element_pressure_deg = 3
element_flux = "DRT"
element_flux_deg = 2
element_concentration = "P"
element_concentration_deg = 2

mesh = RectangleMesh( Point( x0, y0 ), Point( x1, y1 ), nx, ny )

# Define variational problem for transport
V_c = FunctionSpace( mesh, element_concentration, element_concentration_deg )

# Construction of finite element space
v1 = FiniteElement( element_pressure, mesh.ufl_cell(), element_pressure_deg )
v2 = FiniteElement( element_flux, mesh.ufl_cell(), element_flux_deg )
V = FunctionSpace( mesh, v1 * v2 )
```

```
# Define Dirichlet BC
def boundary( x, on_boundary ):
   return on_boundary

def transport_boundary( x, on_boundary ):
   return ( x[0] > 5 - DOLFIN_EPS or x[0] < DOLFIN_EPS or x[1] < DOLFIN_EPS or x[1] >
       1 - DOLFIN_EPS ) and on_boundary

# Analytical solutions, can be used to calculate convergence and errors as well.
p_a_expr = Expression( "x[0] * ( 5 - x[0] ) * x[1] * ( 1 - x[1] )", degree = 2 )

u_a_expr = Expression(
   (
      "2 * ( 5 - 2 * x[0] ) * x[1] * ( x[1] - 1 )",
      "    ( 1 - 2 * x[1] ) * x[0] * ( x[0] - 5 )"
   ),
   degree = 2
)

c_a_expr = Expression( "( 5 - x[0] ) * x[1] * ( 1 - x[1] ) * t", t = t, degree = 2 )

bc = DirichletBC( V.sub( 0 ), p_a_expr, boundary )
bc_t = DirichletBC( V_c, c_a_expr, boundary )

# Define functions for flux and pressure and analytic functions
( p, u ) = TrialFunctions( V )
( v, w ) = TestFunctions( V )

# Define function used in the function space.
z = Function( V )

# Permeability tensor
k = Constant( ( ( 2, 0 ), ( 0, 1 ) ) )

# function f from div( u ) = f
f = Expression(
   '- 4 * x[1] * ( x[1] - 1 ) - 2 * x[0] * ( x[0] - 5 )',
   degree = 2
)

# Define dual-mixed variational form used to calculate flux and pressure.
a = ( dot( u, w ) + dot( k * grad( p ), w ) - dot( u, grad( v ) ) ) * dx
L = f * v * dx

# Split up functions
(p, u) = z.split()

# Compute the mixed formulation
solve( a == L, z, bc )

# Split the mixed solution using deepcopy
# (needed for further computation on coefficient vector)
( p, u ) = z.split( True )

# Define trial function, functions and test function in function space for transport
    eq.
c = Function( V_c )
c_n = Function( V_c )
```

```
q = TestFunction( V_c )

# Impose analytic solution as previous step
c_a = interpolate( c_a_expr, V_c )
c_n.assign( c_a )

f_c_1 = Expression( "( 5 - x[0] ) * x[1] * ( 1 - x[1] )", degree = 2 )
f_c_2 = Expression( "- 2 * eps * ( x[0] - 5 ) * t", degree = 1, t = t, eps = delta )
f_c_3_1 = Expression(
   "pow( x[1], 2 ) * ( 1 - x[1] ) * ( x[1] - 1 ) * t * ( - 4 * ( 5 - x[0] ) - 2 * ( 5
      - 2 * x[0] ) )", degree = 3,
   t = t )
f_c_3_2 = Expression( "( 5 - x[0] ) * x[0] * ( x[0] - 5 ) * t * ( - 6 * x[1] + 6 *
    pow( x[1], 2 ) + 1 )", degree = 3, t = t )

f_c = f_c_1 + f_c_2 + f_c_3_1 + f_c_3_2

d = Constant( dt )
delta = Constant( delta )

F = ((c - c_n) / d) * q * dx + delta * dot( grad( c ), grad( q ) ) * dx + div( c * u
    ) * q * dx - f_c * q * dx

# Time-stepping
for n in range( num_steps ):
   # Update current time and in boundary in concentration
   t += dt

   f_c_2.t = t
   f_c_3_1.t = t
   f_c_3_2.t = t
   c_a_expr.t = t

   print()
   print( 't = ', t )

   # Compute the mixed formulation
   solve( a == L, z, bc )

   # Split the mixed solution using deepcopy
   # (needed for further computation on coefficient vector)
   (p, u) = z.split( True )

   # Transport equation
   solve( F == 0, c, bc_t )

   # Update previous solution
   c_n.assign( c )
```

Appendix B

FEniCS snippets

Here is some snippets from the FEniCS code used.

B.1 Vertical-average

This is used on for example a domain, Ω

$$\Omega = \Omega(x, y) = (0, 1) \times (0, 1)$$

If this should be averaged over the y-coordinate, it can be done in the following way:

1. f(x,y) - Function to average over
2. nx - Cells in the x-direction
3. ny - Cells in the y-direction

Steps to do before using this:

1. Create a Unit Interval mesh → mesh = UnitIntervalMesh(nx)
2. Create a function space using mesh above → V = FunctionSpace(mesh, 1, 'P')
3. Create a function used to save the average to → f_avg = Function(V)

```
f_avg_array = f_avg.vector().array()

for i in range( nx + 1 ):
   value = 0

   for j in range( ny + 1 ):
      value += f( x0 + x1 * (i / nx), y0 + y1 * (j / ny) )

   value /= (ny + 1)

   f_avg_array[ nx - i ] = value

f_avg.vector().set_local( f_avg_array )
```

B.2 Integrate functions over whole domain

This is used on for example a domain, Ω

$$\Omega = \Omega(x, y) = (0, 1) \times (0, 1)$$

Given a function $f(x, y, t)$ in FEniCS and it should be integrated over the x- and y-coordinate, where the equation is the following

$$F(t) = \oint \left| \nabla f(x, y, t) \right| = \int_0^1 \int_0^1 \sqrt{(\partial_x f)^2 + \left(\partial_y f\right)^2}\, dx\, dy \tag{B.1}$$

Then the code needed is only the following:

```
f_t = assemble( sqrt( dot( grad( f ), grad( f ) ) ) * dx )
```

Remember if it is not an unit domain and it shall be compared for different mesh sizes, this has to be manually added to the calculations like,

$$\Omega = \Omega(x, y) = (a, b) \times (c, d)$$

Then the code becomes

```
f_t = assemble( ( 1 / ( b - a ) ) * ( ( 1 / ( d - c ) ) * sqrt( dot( grad(f),
    grad(f) ) ) * dx )
```